

**INVESTIGATION INTO THE ENHANCED ACTIVATION OF THE ARE
AND THE CORRELATIONS BETWEEN NRF2 AND OTHER
CYTOPROTECTIVE PATHWAYS SUCH AS AHR, HSP AND
APOPTOSIS**

A Dissertation

Presented to the Faculty of the Graduate School

of Liberty University

In Partial Fulfillment of the Requirements for the Degree of

Doctor of Philosophy

by

Jonathon Joseph Odom

November 2022



**INVESTIGATION INTO THE ENHANCED ACTIVATION OF THE ARE
AND THE CORRELATIONS BETWEEN NRF2 AND OTHER
CYTOPROTECTIVE PATHWAYS SUCH AS AHR, HSP AND
APOPTOSIS**

By Jonathon Joseph Odom

A Dissertation Approved for the Department of Biology and Chemistry

Approved By:

Gregory Raner, Ph.D. (Committee Chair)

Gary Isaacs, Ph.D. (Committee Member)

Jeremiah Winter, Ph.D. (Committee Member)

© 2022 Jonathon Joseph Odom

**INVESTIGATION INTO THE ENHANCED ACTIVATION OF THE ARE
AND THE CORRELATIONS BETWEEN NRF2 AND OTHER
CYTOPROTECTIVE PATHWAYS**

Jonathon Odom, Ph.D.

Liberty University 2022

Oxidative damage is a cellular threat that is responsible for many pathologic conditions such as Alzheimer's disease, Parkinson's disease, chronic obstructive pulmonary disease (COPD), cancer, and many more. The primary cytoprotective pathway within the cell that is responsible for mitigating the harmful effects of oxidative stress is the antioxidant system. The master regulator of the antioxidant system is the transcription factor, nuclear factor erythroid 2-related factor 2 (NRF2) which operates by binding to the antioxidant response element (ARE) and inducing the production of many antioxidant genes. It is known that the early response of NRF2 is regulated by electrophilic interaction with Kelch-like ECH-associated protein 1 (Keap1) and the delayed response is regulated by glycogen synthase kinase 3 beta (GSK-3 β). There have been many antioxidant natural products reported, including, but not limited to, broccoli, Cinnamomum cassia oil, turmeric powder, sulforaphane, cinnamaldehyde, and curcumin. Many of these function through interactions with Keap1 in the early response. This study identified two novel inducers of ARE activity: sabinene and tetrafluorohydroquinone. Further, Kenpaullone, is another compound that has been identified to have effects on the delayed response, as it is a known inhibitor of GSK-3 β . Many studies have investigated the effects of these compounds on the induction of NRF2, however, in this study, the effect of a dual-targeted treatment of HepG2 cells was investigated in attempts to regulate the NRF2 pathway through both the early and the

delayed response. This study showed that across multiple combinations of early response inducers in combination with kenpaullone HepG2/NRF2 cells had an enhanced activity of the ARE that was much greater than any compound or natural product could induce individually. This suggests that enhanced activation of the ARE can occur through a dual-targeted treatment.

Further, the antioxidant pathway has been shown to have correlations to other cytoprotective pathways such as xenobiotic metabolism and heat shock proteins. For example, since many reactive oxygen species (ROS) are produced in the process of xenobiotic metabolism, the antioxidant system and xenobiotic system are typically activated simultaneously. Likewise, oxidative stress cannot only induce the antioxidant pathway but it can cause damage to proteins as well, and therefore activate heat shock proteins. In light of the correlations between NRF2 and other cytoprotective pathways, it would be logical to assume that enhanced activation of the antioxidant pathway could lead to the activation of other protective mechanisms. Therefore, this study also investigated the activation of xenobiotic metabolism and heat shock proteins in response to the NRF2 activators mentioned previously. Interestingly, the results indicate a novel activity of KP as an inducer of the xenobiotic response, as indicated by cytochrome P450, family 1 subfamily a, polypeptide 1 (CYP1A1), a classic marker for the activation of the xenobiotic response element (XRE) by the aromatic hydrocarbon receptor (AHR).

Not only did the results of this study indicate that enhanced activation of the ARE could be achieved through a dual-targeting treatment, but also that attenuation of the activation occurred at high concentrations, suggesting that a negative-feedback mechanism was responsible for the inactivation of the antioxidant pathway. It has been well reported that the over-activation of cytoprotective pathways can induce programmed cell death, therefore experimentation was

done to evaluate the potential activation of apoptosis at high concentrations of dual-targeted treatment. However, using qPCR assessment the treatment concentrations used did not seem to indicate attenuation of the NADPH quinone oxidoreductase-1 (NQO1), a classical marker of ARE activation. Rather, p53 upregulated modulator of apoptosis (PUMA) expression seemed to be reduced, and therefore the activation of apoptosis was not observed. In light of elevated NQO1 expression, PUMA expression would not be expected to be elevated as these results are consistent with the literature and are consistent with a relationship between cytoprotective pathways and programmed cell death.

To my wife, Victoria Odom, who encouraged me to follow my passion, gifting,
and ultimately – God’s calling.

ACKNOWLEDGEMENTS

Victoria Odom & Isaiah Odom

Dr. Raner

Dr. Isaacs

Dr. Winter

Dr. Kalu

Dr. Leonard

Jennifer McGlaufflin

Dr. Sellers

Jessica Supernatant

Stacy Johnson

Robbe Sisson

TABLE OF CONTENTS

| | |
|---|------|
| ABSTRACT..... | iv |
| DEDICATION..... | vii |
| ACKNOWLEDGEMENTS..... | viii |
| TABLE OF CONTENTS..... | ix |
| LIST OF SCHEMATICS..... | xi |
| LIST OF FIGURES..... | xii |
| LIST OF TABLES..... | xvi |
| LIST OF ABBREVIATIONS..... | xvii |
| | |
| CHAPTER 1: Enhanced Activation of the Antioxidant Response Element through coordinated targeting of the NRF2 Pathway | |
| INTRODUCTION..... | 2 |
| MATERIALS AND METHODS..... | 10 |
| RESULTS AND DISCUSSION..... | 13 |
| CONCLUSION..... | 43 |
| | |
| CHAPTER 2: Activation of Aromatic Hydrocarbon Receptor by Kenpaullone | |
| INTRODUCTION..... | 46 |
| MATERIALS AND METHODS..... | 52 |
| RESULTS AND DISCUSSION..... | 55 |

| | |
|--|----|
| CONCLUSION..... | 63 |
| CHAPTER 3: Potential Cross-talk between NRF2 and other Cytoprotective Pathways | |
| INTRODUCTION..... | 65 |
| MATERIALS AND METHODS..... | 74 |
| RESULTS AND DISCUSSION..... | 77 |
| CONCLUSION..... | 91 |
| REFERENCES..... | 93 |

LIST OF SCHEMATICS

Schematic 1. NRF2-Keap1 Complex and the NRF2 degradation process under basal conditions.

Schematic 2. Depiction of NRF2 activation in the early response.

Schematic 3. Depiction of the delayed response mediating NRF2 export from the nucleus and consequent downregulation of ARE-dependent transcription.

Schematic 4. Proposed mechanism of enhanced activation by Keap1 activators combined with the GSK-3 β inhibitor, KP.

Schematic 5. Proposed mechanism by which coordinated treatment leads to enhanced ARE activation in the HepG2/NRF2 reporter system.

Schematic 6. Model showing the general mechanism associated with AHR activation by aromatic hydrocarbons.

Schematic 7. Regulation of hsp70 and its ability to modulate protein folding.

Schematic 8. Effect of siRNA knockdown of NRF2 and the resulting activation of apoptosis.

Schematic 9. GSK-3 β Regulation of Apoptosis.

Schematic 10. Three mechanisms by which JNK can induce apoptosis.

Schematic 11. The extrinsic and intrinsic model for caspase-3 activation and ultimately apoptosis.

LIST OF FIGURES

Figure 1.1 In vitro activity of GSK-3 β in the presence of 50 μ M kenpaullone (KP)

Figure 1.2 Molecular structure of SFN.

Figure 1.3 Luciferase activity in HepG2/NRF2 cells in response to increasing sulforaphane.

Figure 1.4 Luciferase activity in HepG2/NRF2 cells in response to increasing kenpaullone.

Figure 1.5 Luminescence dose-response of HepG2/NRF2 cells to SFN & KP at 20hrs.

Figure 1.6 RTqPCR fold-induction of HepG2 cell treatment with SFN and KP and analysis of NQO1 induction.

Figure 1.7 Luciferase activity in HepG2/NRF2 cells in response to the increasing balm of Gilead oil.

Figure 1.8 Molecular structure of Sab.

Figure 1.9 Luminescence assay demonstrates the pattern of NRF2 induction with varying concentrations of Sab and KP.

Figure 1.10 Molecular structure of TFHQ.

Figure 1.11 A) Luminescence Dose-response of HepG2/NRF2 cells to TFHQ represented as fold-induction on the Y-axis and increasing concentration of TFHQ on the X-axis. B)

Luminescence assay demonstrates the pattern of NRF2 induction with varying concentrations of TFHQ and KP.

Figure 1.12 Luminescence assay of NRF2 induction based on the treatment of SFN, TFHQ, and both compounds combined.

Figure 1.13 The molecular structures of CIN, T2D, and CURC.

Figure 1.14 Luminescence assay demonstrates the pattern of NRF2 induction with varying concentrations of T2D and KP.

Figure 1.15 Luminescence assay demonstrates the pattern of NRF2 induction with varying concentrations of CIN and KP.

Figure 1.16 Luminescence assay demonstrates the pattern of NRF2 induction with varying concentrations of CURC and KP.

Figure 1.17 Luminescence assay demonstrates the pattern of NRF2 induction with varying concentrations of BROC and KP.

Figure 1.18 Luminescence assay demonstrates the pattern of NRF2 induction with varying concentrations of CIL and KP.

Figure 1.19 Luminescence assay demonstrates the pattern of NRF2 induction with varying concentrations of CAS and KP.

Figure 1.20 Luminescence assay demonstrates NRF2 induction based on the treatment of crude extracts.

Figure 1.21 Luminescence assay demonstrates the pattern of NRF2 induction with varying concentrations of TURPD and KP.

Figure 2.1 RTqPCR fold-induction of HepG2 cell treatment with SFN and KP and analysis of CYP1A1 induction.

Figure 2.2 1.5% Agarose gel electrophoresis of mRNA RT-PCR analysis of GAPDH and CYP1A1 with various treatment concentrations of SFN and KP.

Figure 2.3 Chemical structure of KP.

Figure 2.4 Luminescence assay indicating fold-induction of CYP1A1 activity in HepG2 cells treated with KP.

Figure 2.5 Molecular structure of β NF.

Figure 2.6 Luminescence assay indicating fold-induction of CYP1A1 activity in HepG2 cells

treated with β NF.

Figure 2.7 Luminescence assay indicating fold-induction of CYP1A1 activity in HepG2 cells treated with β NF and KP.

Figure 3.1 Luminescence dose-response of HepG2/NRF2 cells to SFN & KP.

Figure 3.2 RTqPCR fold-induction of HepG2 cell treatment with SFN and KP and analysis of NQO1 and PUMA1 induction.

Figure 3.3 RTqPCR fold-induction of HepG2/NRF2 cell treatment with SFN and KP and analysis of NQO1 and PUMA1 induction.

Figure 3.4 RT-PCR of HepG2/NRF2 cell treatment with SFN and KP and analysis of GAPDH, NQO1, and PUMA1 induction. Abbreviations used are as follows, G: GAPDH; N: NQO1; P: PUMA1.

Figure 3.5 RT-PCR of HepG2/NRF2 cell treatment with Sab and KP and analysis of GAPDH, NQO1, and PUMA1 induction.

Figure 3.6 Caspase luminescence assay demonstrates the pattern of ARE induction with varying concentrations of SFN and KP.

Figure 3.7 Luminescence assay demonstrates the pattern of NRF2 induction with varying concentrations of BRUS and KP.

Figure 3.8 RTqPCR fold-induction of HepG2/NRF2 cell treatment with BRUS and KP and analysis of ACTB, NQO1, PUMA1, and PUMA2 induction.

Figure 3.9 Caspase Luminescence assay demonstrates the pattern of ARE induction with varying concentrations of BRUS and KP.

Figure 3.10 LDH assay assessing necrosis prevalence with various treatment combinations of SFN, BRUS, and KP

LIST OF TABLES

Table 1. A partial list of the enzymes upregulated by NRF2.

LIST OF ABBREVIATIONS

2,3,7,8-tetrachlorodibenzop-dioxin (TCDD)

Adenosine triphosphate (ATP)

Aldehyde dehydrogenase 3a1 (Aldh3a1)

Antioxidant response element (ARE)

Aryl hydrocarbon receptor (AHR)

Aryl hydrocarbon receptor nuclear translocator (ARNT)

Balm of Gilead (BOG)

B-cell lymphoma-2 (Bcl-2)

B-cell lymphoma-extra large (Bcl-xL)

Beta-Naphthoflavone (β NF)

Broccoli (BROC)

Brusatol (BRUS)

cAMP response element binding protein (CREB)

Carbonyl reductase 3(CBR3)

Chronic obstructive pulmonary disease (COPD)

Cilantro (CIL)

Cinnamaldehyde (CIN)

Cinnamomum cassia oil (CAS)

c-Jun N-terminal kinase (JNK)

Cullin3 (Cul3)

Curcumin (CURC)

Cyclooxygenase-2 (COX-2)

Cytochrome P450, family 1 subfamily a, polypeptide 1 (CYP1A1)

Fas ligand (FASL)

Gas chromatography/mass spectrometry (GC/MS)

Glyceraldehyde 3-phosphate dehydrogenase (GAPDH)

Glycogen synthase kinase 3 beta (GSK-3 β)

Gst alpha 1 (Gsta1)

Halogenated aromatic hydrocarbons (HAH)

Heat shock elements (HSEs)

Heat shock factor 1 (HSF1)

Heat shock protein 90 (hsp90)

Heme oxygenase-1 (HO-1)

Hsp 70 kDa (hsp70)

Immunophilin-like X-associated protein 2 (XAP2)

Inhibitor of NRF2 (INrf2)

Kelch-like ECH-associated protein1 (Keap1)

Kenpaullone (KP)

Lactate dehydrogenase (LDH)

Mammalian target of rapamycin (mTOR)

Murine double minute 2 homolog (MDM2)

NADPH:quinone oxidoreductase-1 (NQO1)

Nuclear factor erythroid 2-related factor 2 (NRF2)

Polycyclic aromatic hydrocarbons (PAH)

Protein kinase C (PKC)

Reactive oxygen species (ROS)

RING-box protein 1 (Rbx1)

Sabinene (Sab)

Small Maf proteins (sMaf)

Sulforaphane (SFN)

Superoxide dismutase (SOD)

Tetrafluorohydroquinone (TFHQ)

Trans-2-decenal (T2D)

Transcription (txn)

Turmeric powder (TURPD)

Ubiquitin ligase complex E3 (E3)

UDP-glucuronosyltransferase 1a6 (Ugt1a6)

Xenobiotic response element (XRE)

Chapter 1 – Enhanced Activation of the Antioxidant Response Element through coordinated targeting of the NRF2 Pathway

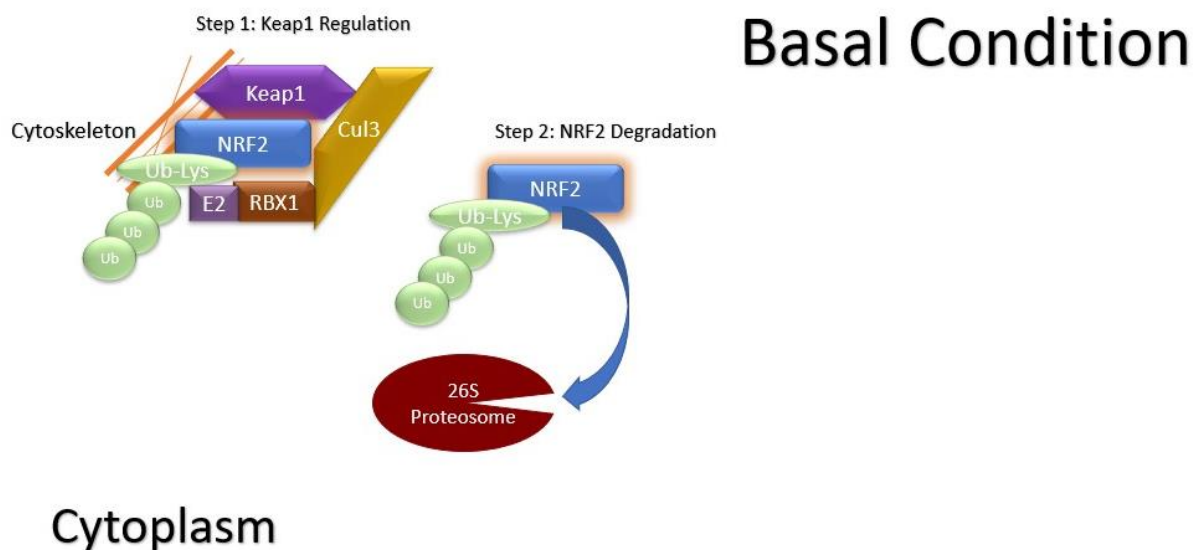
Introduction

The antioxidant pathway is highly studied due to the many clinical implications that are correlated with this pathway. For example, cancer is the second leading cause of death in the United States and physiologically, the antioxidant system is meant to protect the body against the development of harmful cell conditions, which can be carcinogenic (Heron, 2021). However, in the context of cancer, the antioxidant system can actually become hijacked and instead of protecting the cell, it increases oncogenic cell survival allowing for the evasion of cell death as well as resistance to chemotherapy (Sporn & Liby, 2012). Furthermore, the protection from oxidative damage by the antioxidant system can help prevent the pathogenesis of many other disease conditions such as diabetes, Alzheimer's disease, Parkinson's disease, hypertension chronic obstructive pulmonary disease (COPD), and the aging process itself (Griendling et al., 2021; Gureev, Popov, & Starkov, 2020; Oh & Jun, 2017; Percário et al., 2020; Sporn & Liby, 2012; Xu, Liu, & Song, 2020). Due to the vast implications regarding this pathway understanding the detailed mechanistic aspects of its induction and attenuation would be very useful. It is well understood that of the endogenous antioxidants produced, nuclear factor erythroid 2-related factor 2 (NRF2), is considered the master regulator of cellular antioxidant pathways (Jain & Jaiswal, 2007a).

NRF2 functions as a transcription factor that binds to an antioxidant response element (ARE) (consensus sequence: 5'-RTKAYnnnGCR-3'), found in the promoter region of target genes, and regulates the production of a large number of antioxidant enzymes (Erickson, Nevarea, Gipp, & Mulcahy, 2002). Under basal conditions, NRF2 activity is mediated by Kelch-like ECH-associated protein1 (Keap1) also known as an inhibitor of NRF2 (INrf2) (Schematic. 1) (Oh & Jun, 2017). Keap1 is anchored to the cytoskeleton sequestering the Keap1-NRF2 complex, preventing it from initiating transcriptional activation. Keap1 is an adaptor protein that facilitates

the interaction of NRF2 with Cullin3 (Cul3) containing ubiquitin ligase complex E3 (E3). Along with the Cul3 and E3, RING-box protein 1 (Rbx1) is present in the complex and is needed for the ubiquitination of NRF2 (Gureev et al., 2020; Oh & Jun, 2017; Zenkov et al., 2017).

Ubiquitination of NRF2 occurs at lysine residues and leads to its degradation by the 26S proteasome (Jaramillo & Zhang, 2013). In this way, the cell can be maintained in a “ready” state so the production of reactive oxygen species can be rapidly addressed without the need to generate NRF2 *de novo*.

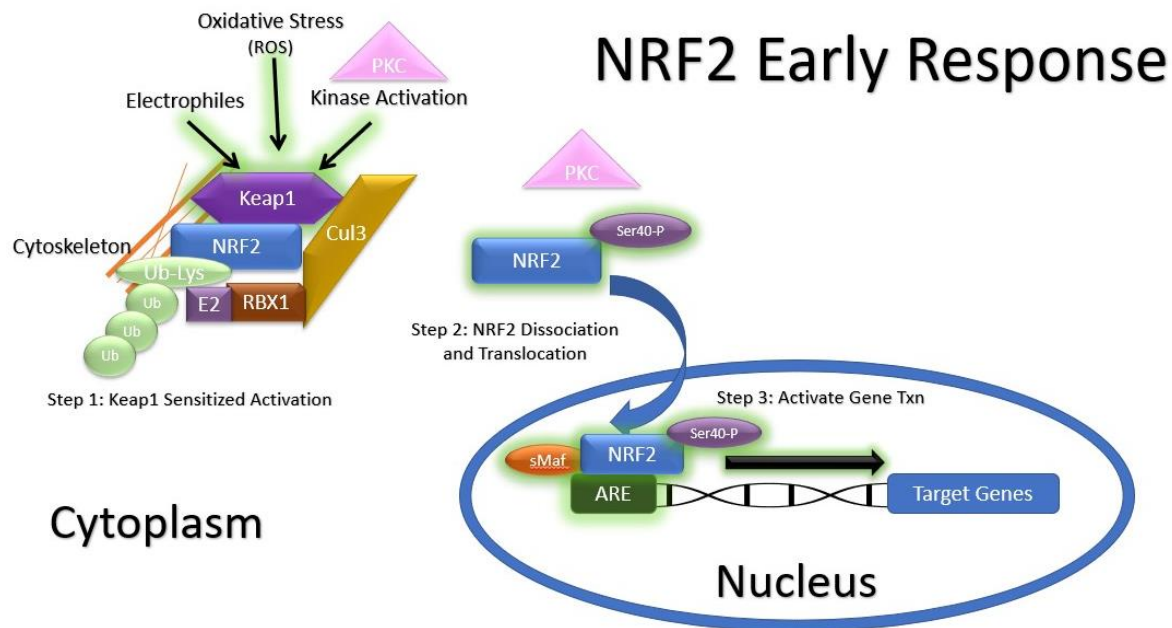


Schematic 1. This figure illustrates the NRF2-Keap1 Complex and the NRF2 degradation process under basal conditions. Keap1 sequesters NRF2 to the cytoskeleton, allowing other proteins to associate and form a heterodimer, in which E2 tags the lysine residue of NRF2 with ubiquitin, signaling NRF2 for degradation via the 26S proteasome.

Prior to its proteasomal degradation, NRF2 can be enlisted for duty in transcriptional activation when cellular conditions dictate. This is done via Keap1 modification. Keap1 is essential for monitoring the redox status of the cell and is part of the response system for detecting conditions where NRF2 activity is needed for cytoprotective functions. Keap1 has 25 cysteines that function as sensors for a wide variety of compounds that can affect the stability of

the Keap1-NRF2 complex. In the presence of ROS or electrophilic modification of the thiol groups on the cysteine residues of Keap1, the sequestering function of this protein will be neutralized and allow for NRF2 to dissociate from the complex (Schematic 2) (Li, R., Jia, & Zhu, 2019; Oh & Jun, 2017; Tonelli, Chio, & Tuveson, 2018; Zenkov et al., 2017).

Another factor that influences NRF2 activation is protein kinase C (PKC). Serine/threonine PKC phosphorylates Ser40 on NRF2, therefore weakening the interaction with Keap1, increasing its stability and nuclear import (Zenkov et al., 2017). PKC will also phosphorylate glycogen synthase kinase 3 beta (GSK-3 β) at Ser9, causing GSK-3 β to be inactive (Schematic 2) (Jain & Jaiswal, 2007b). Once NRF2 is translocated inside the nucleus, it will then form heterodimers with small Maf proteins (sMaf) and bind to the ARE in the promoter region of NRF2 target genes (Oh & Jun, 2017; Tonelli et al., 2018). The NRF2-sMaf will then increase the transcription of genes that provide protection from ROS or other chemically reactive compounds (Tonelli et al., 2018). Some of the enzymes upregulated by the NRF2/sMaf complex include superoxide dismutase (SOD), NADPH: quinone oxidoreductase-1 (NQO1), heme oxygenase-1 (HO-1), carbonyl reductase 3 (CBR3), and heat shock factor 1 (HSF1) (for a more extensive list see Table 1) (Cornejo, Vargas, & Videla, 2013; Ebert, Kisiela, Malátková, El-Hawari, & Maser, 2010; Hayes, Dinkova-Kostova, & McMahon, 2009; Huang et al., 2014; Oh & Jun, 2017; Paul, Ghosh, Mandal, Sau, & Pal, 2018).



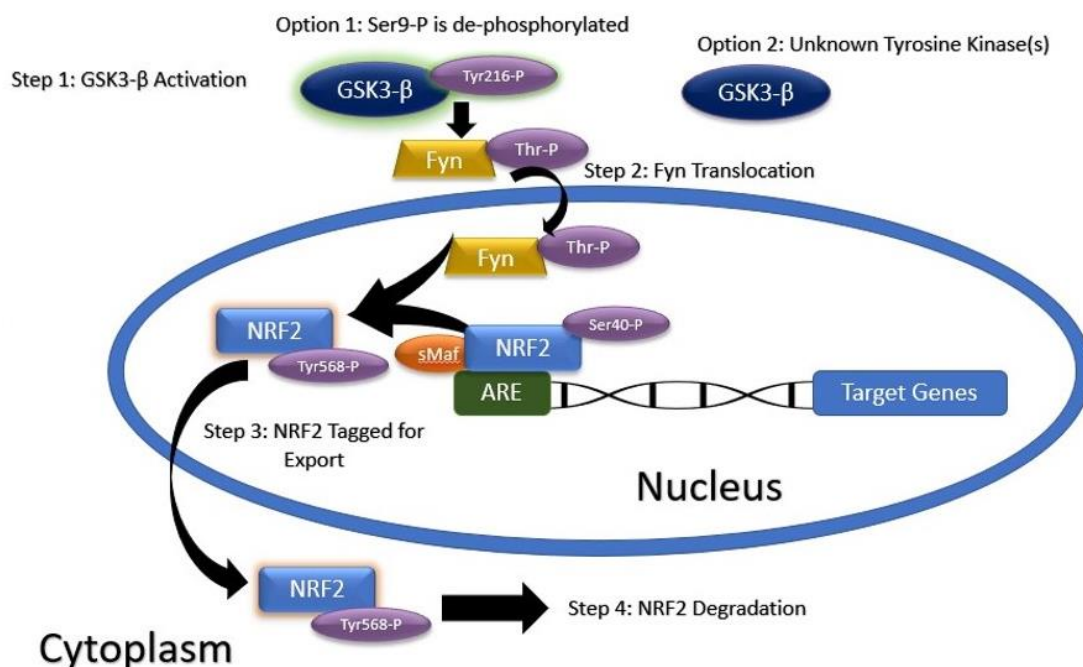
Schematic 2. Depiction of NRF2 activation in the early response. Oxidative stress, electrophiles, and PKC can interact with the cysteine residues of Keap1; causing NRF2 to dissociate from the complex. Once free in the cytosol, NRF2 is available for the phosphorylation of Ser40, which can occur via PKC. Upon phosphorylation, NRF2 will translocate into the nucleus where it associates with sMaf and binds to the ARE to activate the transcription of antioxidant genes.

| Enzymes upregulated by NRF2: | Abbreviations: |
|--------------------------------|----------------|
| Superoxide dismutase | SOD |
| Catalase | CAT |
| Glutathione peroxidase | GPx |
| Thioredoxin peroxidase | TPx |
| Thioredoxin reductase | TrxRs |
| Sulfiredoxin | Srx |
| Peroxiredoxin | Prx |
| NADPH:quinone oxidoreductase-1 | NQO1 |
| Heme oxygenase-1 | HO-1 |
| Glutathione reductase | GR |
| Glutaredoxin | Grx |
| Glutamate cysteine ligase | GCL |
| Glutathione S-transferase Ya | GST Ya |
| Glutathione S-transferase Yp | GST Yp |
| UDP-glucuronosyltransferase | UGT |
| Sulfotransferase | SULT |
| Carbonyl reductase 3 | CBR3 |
| Heat shock factor 1 | HSF1 |
| Manganese superoxide dismutase | MnSOD |

Table 1. A partial list of the enzymes upregulated by NRF2.

The nuclear export of NRF2 is the delayed response of cells used to attenuate the oxidative or electrophilic stress response. In other words, as the stress is relieved, the system resets by exporting NRF2 from the nucleus thereby turning off the antioxidant response. This pathway is mainly regulated by GSK-3 β (Schematic. 3). There are two components that play a role in the activation of GSK-3 β . The first is having the Ser9 position de-phosphorylated and the second is having the Tyr216 position phosphorylated by an unknown tyrosine kinase (Jacobs et al., 2012; Jain & Jaiswal, 2007). Once GSK-3 β is activated it will then phosphorylate Fyn, a tyrosine kinase, at a threonine residue. Once this occurs, Fyn will be translocated inside the nucleus where it will accumulate and eventually phosphorylate NRF2 on tyrosine 568. Phosphorylated NRF2 will then bind to Crm1 and be exported from the nucleus where it will undergo degradation (Jain & Jaiswal, 2007). Consequently, increases in GSK-3 β lead to overall decreases in NRF2 concentrations (Jain & Jaiswal, 2007; Lu et al., 2019).

NRF2 Delayed Response



Schematic 3. Depiction of the delayed response mediating NRF2 export from the nucleus and consequent downregulation of ARE-dependent transcription. Once activated GSK-3 β will phosphorylate a Fyn, which then translocates into the nucleus to phosphorylate the Tyr568 of NRF2, which tags it for nuclear export and subsequent degradation.

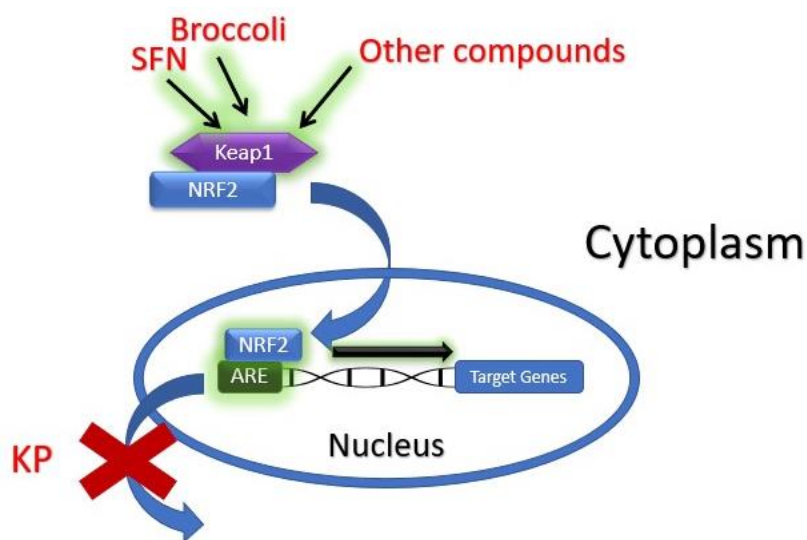
Clinically, GSK-3 β is significant because of its correlations with Alzheimer's disease, Parkinson's disease, and other neurodegenerative disorders. Each of these conditions have been demonstrated to have increased GSK-3 β activity. Due to these implications, the modulation of GSK-3 β is well-studied (Demuro, Di Martino, Ortega, & Cavalli, 2021; Percário et al., 2020). Of the many compounds researched, kenpaullone (KP) has emerged as a high-affinity inhibitor of GSK-3 β (Demuro et al., 2021; Guieu et al., 2021). The literature indicates that the IC₅₀ for KP inhibition of GSK-3 β is 0.023 μ M (Demuro et al., 2021; Leost et al., 2000). While many studies discuss the inhibitory activity of KP on GSK-3 β , there have not been any direct correlations between KP and NRF2. However, due to the role of GSK-3 β in the delayed response, and the

interaction of KP with GSK-3 β , KP treatment would likely help induce the antioxidant system (Demuro et al., 2021; Kitabayashi et al., 2019; Leost et al., 2000).

Not only is it possible that KP could lead to increased NRF2 activity, but there are likely many other compounds that could potentially lead to a targeted enhancement of the antioxidant system given its regulation by Keap1 and GSK-3 β . For example, many natural products such as broccoli (BROC), cassia oil (CAS), and turmeric powder (TURPD), contain key compounds such as sulforaphane (SFN), cinnamaldehyde (CIN), and curcumin (CURC) respectively. These are also known to have antioxidant effects (Boo, 2020; Fahey et al., ; Gamet-Payrastre et al., 2000; Tastan, Ario, & Genc, 2017; Tayyem, Heath, Al-Delaimy, & Rock, 2006). Within each of these natural products are many natural compounds that have various mechanisms of inducing antioxidant activity. For instance, BROC contains sulforaphane (SFN), while TURPD contains curcumin (CURC), both of these compounds are electrophilic and therefore have the potential to induce NRF2 activity through modulation of Keap1 (Nandini, Rao, Deepak, & Reddy, 2020; Tastan et al., 2017; Tayyem et al., 2006). While the main mechanism of SFN induction of NRF2 is thought to primarily be the result of its interactions with Keap1, it has also been shown to increase NRF2 through the epigenetic modification of the first 5 CpGs in the promotor region of the NRF2 gene in TRAMP C1 cells (Baird & Yamamoto, 2020; Yang, Palliyaguru, & Kensler, 2015; Yin, Wang, Qing, Lin, & Wu, 2016; Zhang, Su, Khor, Shu, & Kong, 2013). Another source of antioxidant induction is cinnamaldehyde (CIN), a major component of Cinnamomum cassia (CAS), which has been demonstrated to induce NRF2 and alleviate ROS production in human epidermal keratinocytes (Boo, 2020; Uchi, Hiroshi, MD, PhD, Yasumatsu, Morino-Koga, Mitoma, Chikage, MD, PhD, & Furue, Masutaka, MD, PhD, 2016). A very similar

compound, cinnamic acid, has been shown to interact with the NRF2 and Keap1 complex and increase nuclear translocation through ROS and PKC signaling cascades (Hseu et al., 2018).

Due to the ability of these natural products and compounds to initiate induction of NRF2 via the early response, and KP's ability to operate as a GSK-3 β inhibitor of the delayed response, this led to the hypothesis that targeted combination treatment could lead to enhanced activation of the ARE. To illustrate this hypothesis, schematic 4, depicts the proposed mechanism of action for our rationale. This data suggests that mechanistic enhancement of ARE activation does occur through a targeted approach.



Schematic 4. Proposed mechanism of enhanced activation by Keap1 activators combined with the GSK-3 β inhibitor, KP. It is hypothesized that through a coordinated approach that leads to activation of the early response and inhibition of the delayed response the NRF2 activation of the ARE would be enhanced through a combination treatment.

Materials and Methods

NRF2 ARE Luminescence Protocol

The HepG2/NFR2 cell line is a HepG2 ARE reporter cell line (NRF2 Antioxidant Pathway) and was obtained from BPS Bioscience (Catalog #60513). This cell line contains a firefly luciferase gene under the control of an antioxidant response element (ARE). HepG2/NRF2 cells were cultured at 37°C under 5% CO₂ in a complemented (10% FBS, pen-strep1X, 0.01% geneticin) coming EMEM media. Cells were grown in a clear T-25 to about 70% confluency and then transferred to an SPL Life Sciences Co., Ltd. DNase/RNase/DNA free (ISO 13485) white bottom 96-well plate. Cells were then administered the appropriate treatment in groups of four following incubation of 20h at 37°C under 5% CO₂. Growth media was aspirated and replaced with 25ul of pure EMEM. To assess NRF2 activity, 25ul of a luciferase glo assay substrate (Promega, USA) was added to each well. The 96-well plate was then placed on a shaker at 300-500rpm for at least 10min. A TECAN infinite M200 Pro plate reader was then used to measure luminescence for each well. Quadruplicate values were then averaged and used to determine the fold induction in comparison with the control. The standard deviation was also calculated for all replicate samples to fall within 10% of the average value.

GSK3β Glo Assay

To measure the GSK3β activity, an *in vitro* assay was developed using recombinant GSK3β (Millipore), Glycogen synthase peptide 2 from PC scientific as a substrate, ATP (Sigma), and Kinase-Glo assay kit (Promega) to monitor ATP utilization. Reaction mixtures contained 20mM tris-HCl (pH 7.5), 10mM MgCl₂, 5mM DTT, 25μM substrate peptide, 2μM ATP, and 10ng GSK3β in a total volume of 40mL. The reaction was carried out for 29min at 30°C and quenched

via the addition of 40ul Kinase-Glo reagent. After 10min, 1ml of deionized water was added, and the luminescence intensity was recorded. A standard curve for ATP concentrations between 0.5-2 μ M was also prepared using the same protocol. To measure inhibition, the identical reaction was carried out in the presence of 50nM kenpaullone, and the amount of ATP consumed in the control vs. inhibited reactions was determined using the standard curve. All reactions were carried out in duplicate. Duplicated values were then averaged and used to determine the fold induction in comparison with the control. The standard deviation was also calculated to be within 10% of the plotted values.

RTqPCR Protocol

HepG2/NRF2 cells were grown to 70% confluency at 37°C under 5% CO₂ in a T-25. Once confluency was reached, complemented EMEM was replaced and treated in a clear T-25 with the appropriate SFN/KP concentration. A simple dose-response treatment was administered for each compound as well as combination treatment groups. The cells were then allowed to incubate under these conditions for 20h. Upon completion, RNA isolation was performed using 1ml of TRIzol reagent (per T-25) and transferred to a 1.5ml conical tube following the Invitrogen protocol. RNA concentration was then determined using a Thermo Scientific NanoDrop 2000 spectrophotometer. To prepare each sample, 2ug of RNA, 16 μ l of nuclease-free water, and 4 μ l of RT reverse transcriptase Supermix (Invitrogen, Carlsbad, CA) were combined in a PCR tube. The thermal cycler was set for 5min priming at 25°C, 20min reverse transcription at 46°C, and 1min RT inactivation at 95°C. To prepare each sample, 2 μ l of cDNA, 6 μ l RNase free water, 10 μ l SYBR Green, and 2 μ l 10X Primer master mix were combined in a PCR tube. Each sample was then placed into the thermal cycler and subjected to 40 cycles of PCR. The thermal cycler was set to begin with 3min at 95°C and then cycled through intervals of 10sec at 95°C, 10sec at

60°C, 10sec at 72°C, ending with 5sec at 65°C and 95°C. Primers used were as seen in Table 2. These were designed using the DNA sequence based on exons shared by all isoforms (if possible) of the gene. Primer3 (<https://bioinfo.ut.ee/primer3-0.4.0/>) was then used to generate primers that had a product size ranging between 80-140bps. The T_m was set to 60°C, a GC clamp was added, and the GC content range was set to 40-60%.

| Gene | Forward primer | Reverse Primer |
|--|-----------------------------|-------------------------------|
| GAPDH | 5'-AGCGAGATCCCTCCAAAATC-3' | 5'-GCAGAGATGATGACCCCTTTTG-3' |
| ACTB | 5'-ACCCAGATCATGTTTGAGACC-3' | 5'-CCAGAGGCGTACAGGGATAG-3' |
| NQO1 | 5'-GTGGAGTCGGACCTCTATGC-3' | 5'-AGTTCGACAGGGCTCTCAG-3' |
| CYP1A1 | 5'-ATGAACCCAGGGTACAGAG-3' | 5'-GAGTGTCCGGAAGGTCTCCAG-3' |
| Hsp70/HSPA8 | 5'-AACCTGATGAAGCTGTTGC-3' | 5'-TCCACCAGCAGTTTCAATACC-3' |
| HMOX1 | 5'-ACTTTCAGAAGGGCCAGGTG-3' | 5'-GTAGACAGGGGCGAAGACTG-3' |
| PUMA/BBC3 (version 1 – designed for 3 of 4 isoforms) | 5'-ACCTCAACGCACAGTACGAG-3' | 5'-GAGATTGTACAGGACCCCTCCAG-3' |
| PUMA/BBC3 (version 2 – designed for 1 of 4 isoforms) | 5'-AATTGGCATGGGGTCTG-3' | 5'-AGATTGTACAGGACCCCTCCAG-3' |

Table 2. PCR Primers.

Compound/Natural Product Extraction and Dilution

To obtain a crude extract from natural products we developed a protocol to partition into various concentrations for the treatment of HepG2/NRF2 cells. Broccoli (BROC) and cilantro (CIL) were purchased from Walmart[®]. TURPD was purchased from Dwarka Organics. CAS 100% pure essential oil obtained from Majestic Pure[™] Cosmeceuticals. Trans-2-decenal (T2D) was obtained from Tokyo Chemical Industry (TCI) Co. LTD. Curcumin (CURC)100mg (LOT: 3819205) from EMD Millipore Corp. (USA). 98+% Cinnamaldehyde (CIN) obtained from Thermo Fisher Scientific. A mass of 1g of each natural product was weighed, crushed with mortar and pestle, and diluted 1:2 in nuclease-free water. Each aliquot was then centrifuged at 5,000rpm for 5min. The supernatant was then isolated and used for serial dilution in DI water.

Results and Discussion

Glycogen Synthase Kinase 3 β (GSK3 β) Inhibition by KP

KP inhibition of GSK-3 β is a well-documented phenomenon in the literature (Demuro et al., 2021; Kitabayashi et al., 2019; Li, Y., Zhang, Wan, Liu, & Sun, 2020). Fig 1.1 depicts the results of an *in vitro* analysis of GSK-3 β activity using a kinase glo assay. Here activity of the enzyme was monitored by measuring ATP consumption in the presence of the peptide substrate for GSK-3 β . This figure shows an 80% reduction in the amount of ATP consumed in the enzymatic reaction when 50nM KP was present. This demonstrates the inhibitory effect of KP on GSK-3 β at nanomolar concentrations.

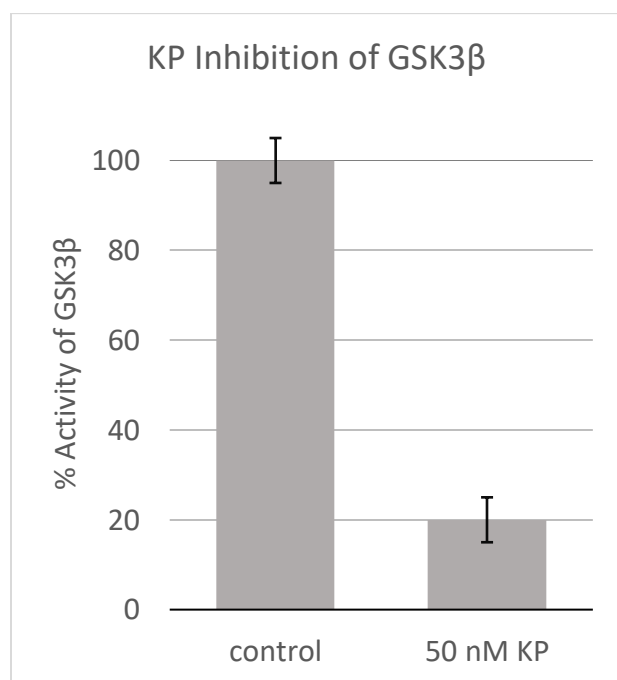
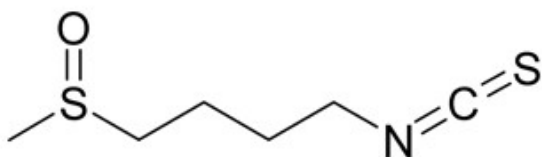


Figure 1.1 *In vitro* activity of GSK-3 β in the presence of 50 μ M kenpaullone (KP). Reactions were carried out for 10min and activity was determined by ATP consumption. The data points represented in this figure are the average of two individual samples for each group. P-value equal to 0.02.

Dose-Response Behavior of SFN and KP in Reporter Cells

As shown in Fig. 1.3, SFN (structure seen in Fig. 1.2) is a potent inducer of NRF2 activity in HepG2/NRF2 cells resulting in a concentration-dependent increase in the ARE activation over the range of 1 μ M to 25 μ M. At 25 μ M the activation appeared to be reaching saturation, which is consistent with data in the literature suggesting the maximum effects are in this range and that concentrations above this begin to have a negative impact on cell viability and lead to induction of apoptosis (Andelová, Rudolf, & Cervinka, 2007; Clarke et al., 2011; Wang et al., 2012). Fig 1.3 indicated roughly a maximum 12-fold induction of NRF2 with the 25 μ M treatment of SFN within this cell reporter system (p-value < 0.001).



Sulforaphane

Figure 1.2 Molecular structure of SFN.

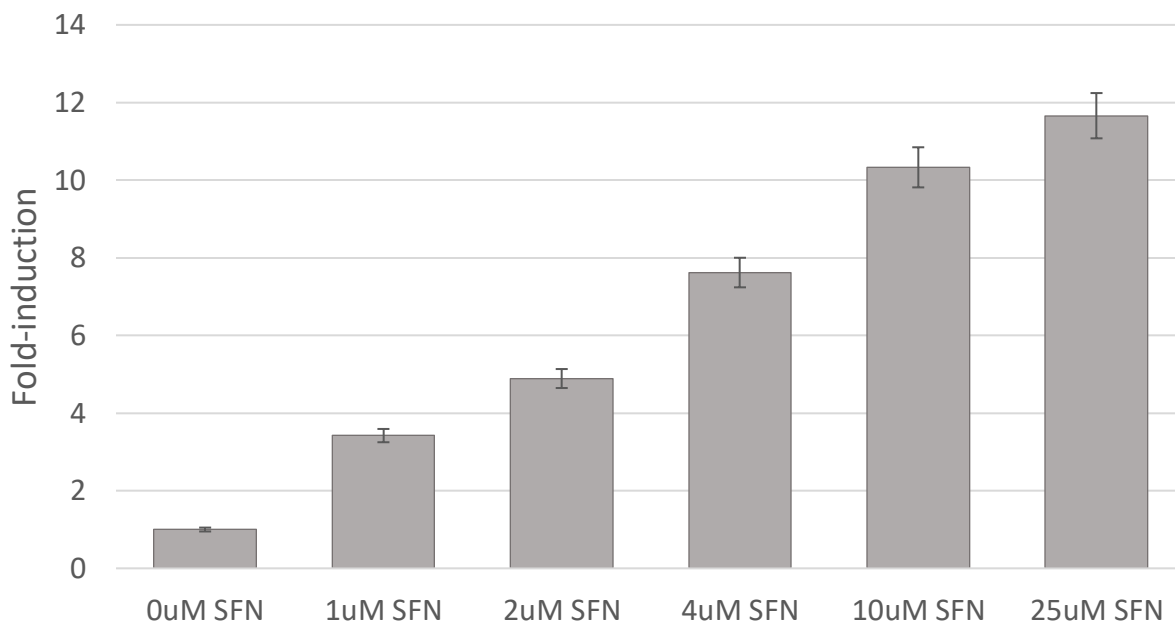


Figure 1.3 Luciferase activity in HepG2/NRF2 cells in response to increasing sulforaphane. Values plotted on the Y-axis corresponds to the fold increase in luminescence compared to the untreated samples. The standard deviation is based on four individual samples and is within 10% of the plotted values. These results were statistically significant with a p-value <0.001.

As shown in Fig. 1.4, KP is a strong inducer of NRF2 in HepG2/NRF2 cells, with a maximum threshold of induction between 7 and 8-fold which occurred around 5 μ M KP. Beyond 20 μ M KP induction decreased, potentially due to toxicity (p-value <0.01). This data suggests that saturation began to occur around 5 μ M with no additional activation at higher concentrations. This is consistent with the literature, as many of the effective doses ranges for various cell types range from 0.5 μ M to 10 μ M and do not exceed 24h for 1 μ M and 2h for 10 μ M (Joo et al., 2018; Kitabayashi et al., 2019; Yeo et al., 2021). The data shown in Fig. 1.3 and 1.4 confirm that in the reporter system used in the current study, both SFN and KP are effective ARE inducers that demonstrated saturation behavior consistent with observed induction characteristics seen using other reporters. However, since the proposed molecular mechanisms for activation by these two compounds differ, with one activating the early response and the other preventing the delayed

response, the combined dose-response behavior of these compounds may be expected to produce altered saturation patterns.

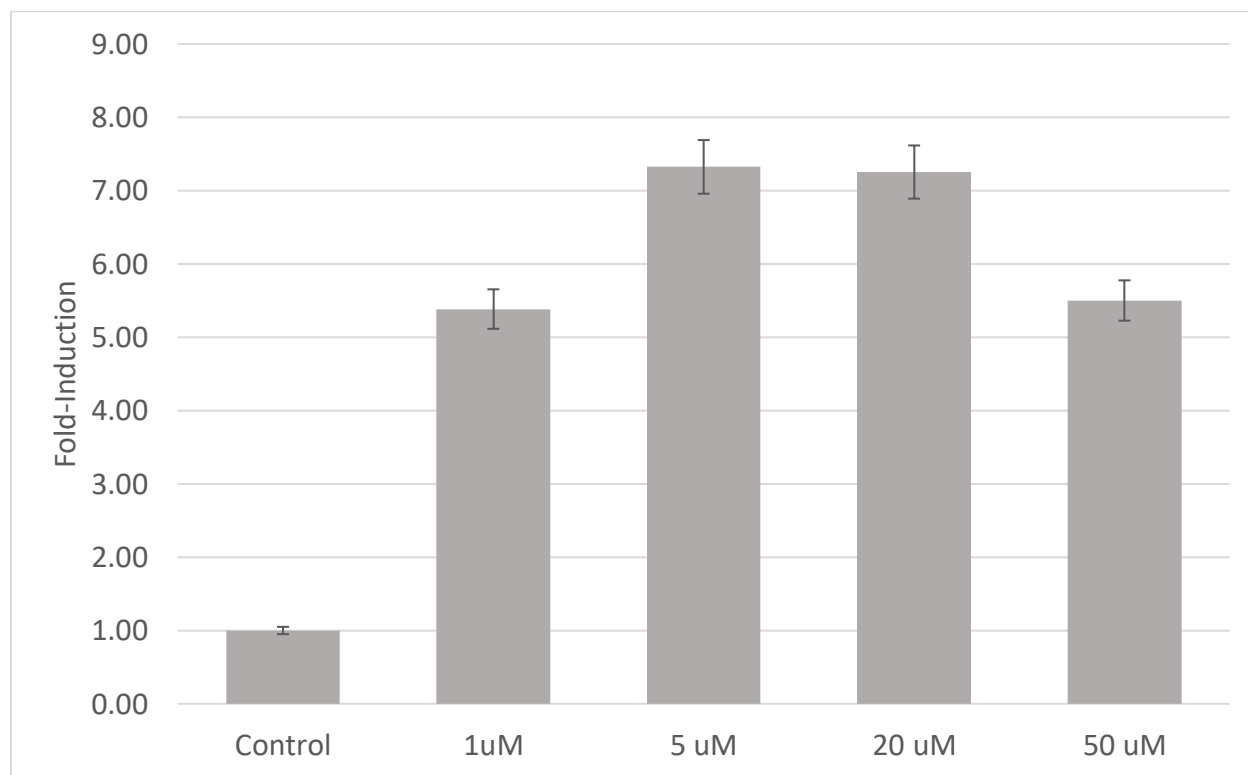


Figure 1.4 Luciferase activity in HepG2/NRF2 cells in response to increasing kenpaullone. Values plotted on the Y-axis corresponds to the fold increase in luminescence compared to the untreated samples. The standard deviation is based on four individual samples and is within 10% of the plotted values. The results were statistically significant with a p-value <0.01.

Dose-Response Behavior of Combined SFN and KP in Reporter Cells

Figure 1.5 shows the combined effect of varying concentrations of SFN and KP on ARE activation. Alone, SFN 25 μ M SFN and 0 μ M KP treatment produced the maximum 12-fold induction, consistent with data previously presented in the literature (p-value <0.001) (Andelová et al., 2007; Clarke et al., 2011; Wang et al., 2012). Conversely, 0 μ M SNF with 5 μ M KP resulted in a 13-fold induction, which was saturating for KP (p-value equal to 0.001). However, combined at 4 μ M SFN and 5 μ M KP these compounds generated a 32-fold induction of

luciferase activity in this ARE reporter system (p-value <0.001). This enhanced activation is 2-3 times higher than either compound could produce individually under saturating conditions. These results suggest that by targeting both the activation and deactivation stages of induction a much greater induction effect is achievable. Interestingly, the treatment containing 25 μ M SFN and 5 μ M KP resulted in a dramatic decrease in NRF2 activity. This is intriguing because individually neither compound is cytotoxic. There are several potential explanations for this observation. It is conceivable that this decrease in NRF2 activity could be due to some type of feedback down-regulation of the antioxidant pathway. This could also explain the reduced luciferase expression at high concentrations of KP alone. One possible mechanism by which this may occur is the negative regulation of mTORC1 or p21 as both have been shown to have negative feedback on NRF2, and both can be activated by AKT, a common activator not only of mTORC1 and AKT but also NRF2, therefore it is possible overactivation of NRF2 is negatively regulated by a feedback loop (Kapuy, Papp, Vellai, Bánhegyi, & Korcsmáros, 2018; Matsuoka & Yashiro, 2014; Paladino, Conte, Caggiano, Pierantoni, & Faraonio, 2018; Romorini et al., 2016). Regardless of the explanation, further investigation is warranted, as it could reveal important connections between NRF2 and cell survival. Alternatively, extremely high levels of induction of the antioxidant system could trigger a cellular death response; these possibilities will be discussed in chapter 3.

Another interesting effect observed was the apparent variability in activation of the ARE at the 15 μ M KP concentration. The data presented in Fig 1.5 along with multiple other trials (Fig. 1.10, 1.15, 1.17, 1.19) indicate a decrease in luciferase activity moving from 5 μ M to 15 μ M KP. However, on other occasions, the 15 μ M sample showed slightly elevated induction relative to the 5 μ M concentration (Fig. 1.4, 1.13, 1.16, 1.18, 1.21).

As it relates to the objective of this study overall, the data in Fig. 1.5, especially the combinations of 4 μ M SFN with 5 μ M KP, demonstrates the ability of the combination treatment to reach a much higher threshold of activation than either compound individually and supports the model presented in schematic 4.

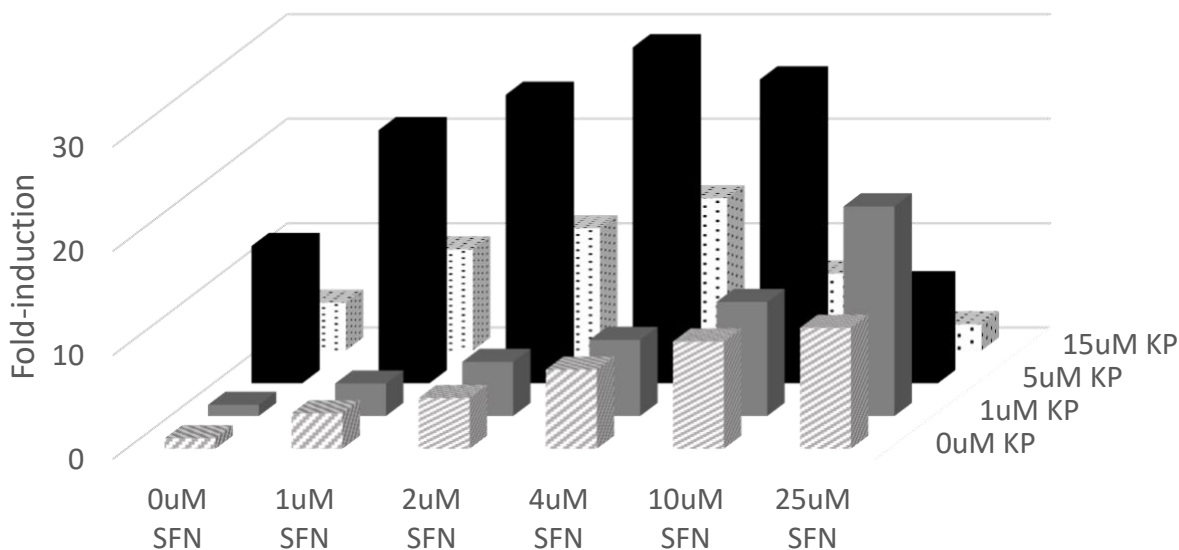


Figure 1.5 Luminescence dose-response of HepG2/NRF2 cells to SFN & KP at 20hrs. Y-axis shows the level of luminescence produced. The X-axis shows the effect of increasing SFN concentrations. Z-axis shows the effect of increasing KP. The standard deviation for each data point was less than 10% +/- of the plotted values. All data points were statistically significant with a p-value <0.01.

NQO1 Induction via SFN and KP

Due to the results of enhanced ARE activation observed with SFN and KP combined treatments, further evaluation of the activation of NRF2 by looking at key genes transcribed by NRF2 activity was carried out. As discussed previously, NQO1 is a traditional target of NRF2 activity, therefore Fig. 1.6 shows RTqPCR results of NQO1 normalized to GAPDH. For this experiment, there were six treatment groups for HepG2 cells selected based on the data seen in Fig. 1.5, and

the experiments were carried out in T-25 culture plates. The results shown in Fig 1.6 correlates with Fig 1.5 by indicating SFN has the ability not only to increase ARE activation but also the induction of NQO1 in a dose-dependent manner at 4 μ M and 25 μ M SFN, without KP. Likewise, KP alone had the ability to induce NQO1 almost two-fold in comparison to SFN alone. The combined effect at 25 μ M SFN and 5 μ M KP produced an enhanced expression that exceeded either compound alone. This was interesting because ARE activation at this concentration in the luciferase reporter system had the opposite effect and was decreased. It is possible that this discrepancy is due to the use of HepG2 cells instead of HepG2/NRF2 cells. The impact of the reporter construct on this attenuation may warrant further investigation. Another interesting feature of this data is seen in the 4 μ M SFN and 5 μ M KP treatment. In the HepG2/NRF2 treated cells the ARE assay indicated enhanced activation while here it appears that there is a decreased expression of NQO1 relative to KP alone, although a slight increase over the control is still observed. It should be also noted that this data is based on single treatments in T-25 plates, so they lack the statistical data necessary to validate the precise levels of induction. Despite the caveats of NQO1 induction correlations with ARE activation clearly indicates the enhanced activation of the NRF2 pathway through combination treatment is possible as represented by the generally increased expression of NQO1 (Fig. 1.6). This data further supports the proposed model that a multi-targeted approach can result in enhanced activity of the antioxidant pathway.

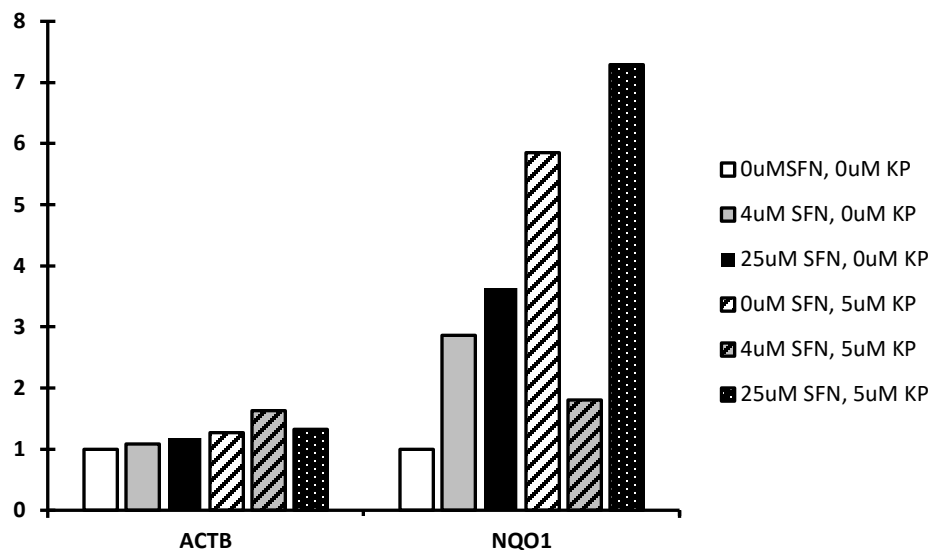


Figure 1.6 RTqPCR fold-induction of HepG2 cell treatment with SFN and KP and analysis of NQO1 induction. These results of fold induction were all normalized to the expression of GAPDH for each treatment group. These columns were generated based on an n of 1 for each treatment and therefore are not statistically significant.

Enhanced ARE activation with other ARE inducers

To further investigate the enhanced ARE activation seen with the combined treatment of SFN and KP, the effects of KP with other ARE inducers were evaluated to see if the ability to enhance activation of the ARE activity was more universal. Prior studies in this lab suggested the balm of Gilead essential oil (BOG) was an ARE activator. The data presented in Fig. 1.7 demonstrates the dose-response behavior for increasing concentrations of the BOG oil in water as represented by the total percent of the oil in the solution. For example, 0.05% would represent 1µl of oil in 2L of DI water. This data indicated that BOG does have the ability to generate a modest induction of ARE by itself leading to a maximum threshold of almost 4-fold induction at 0.2% BOG. Concentrations above this produced a dramatic reduction in luciferase activity, indicating a shutdown of NRF2 activation. Gas chromatography/mass spectrometry (GC/MS) analysis of the oil indicated that the compound sabinene was a primary constituent of this oil, so studies to

examine the ability of this compound to induce ARE activation in the reporter cell line were carried out. In addition, enhanced activation via combined treatment with KP was also explored.

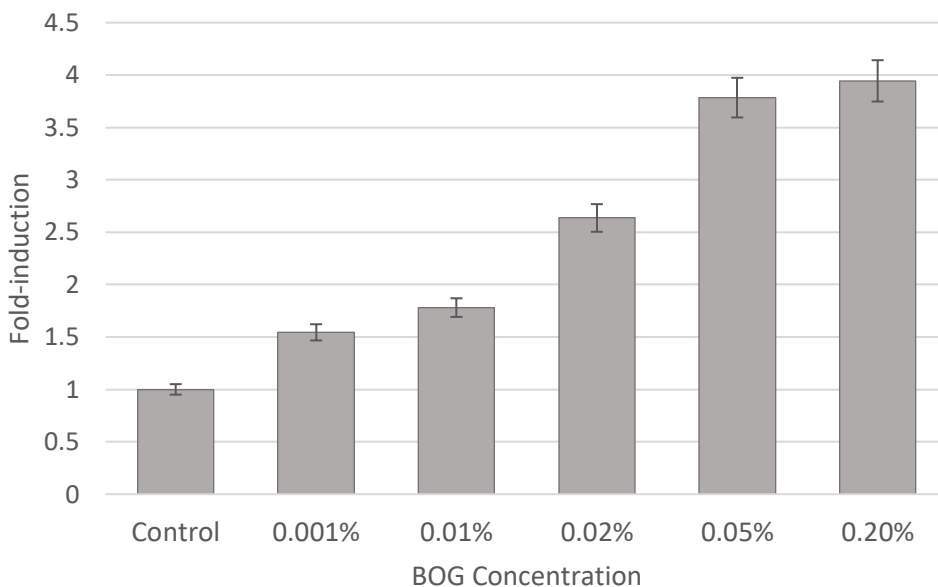


Figure 1.7 Luciferase activity in HepG2/NRF2 cells in response to the increasing balm of Gilead oil. Values plotted on the Y-axis corresponds to the fold increase in luminescence compared to the untreated samples. The data points represented in this figure are the average of four individual samples. P-value <0.05.

Sab (see Fig. 1.8 for molecular structure) did appear to have a slight induction of ARE individually, though only about 2-fold (Fig. 1.9) (p-value <0.03). It was not as potent as BOG, which could be due to other compounds in BOG oil that were also responsible for its antioxidant properties. Figure 1.9 shows the dose-response behavior of Sab along the front row, demonstrating the increase in luciferase activity based on Sab alone. Individually, KP had a typical dose-response behavior up to 5 μ M as shown in the first column (p-value <0.001). The induction by Sab reached a maximum of 2-fold around 3.10x10⁻⁶ μ M. However, the combined effect of Sab and KP resulted in much higher induction at saturation; just as with the SFN and KP combination data. Specifically, treatments consisting of 5 μ M KP and 3.10x10⁻⁸ μ M Sab to 3.10x10⁻⁷ μ M Sab showed enhanced activation of NRF2 (p-value <0.04). The peak of this

enhanced activation reached a maximum at $1.24 \times 10^{-7} \mu\text{M}$ Sab and $5 \mu\text{M}$ KP. This combination treatment resulted in an eight-fold increase in contrast to $1.24 \times 10^{-7} \mu\text{M}$ Sab alone and a two-fold increase compared to $5 \mu\text{M}$ KP alone. At higher concentrations of Sab such as $1.24 \times 10^{-6} \mu\text{M}$ and $3.10 \times 10^{-6} \mu\text{M}$ in combination with KP, the NRF2 induction decreased to a level similar to the KP control. The results of both of Fig. 1.5 and Fig. 1.10 indicate that this enhanced activation of ARE is not unique to SFN/KP but may be a more universal feature of KP. Additionally, it is interesting that in both Fig. 1.5 and Fig. 1.10 at high levels of SFN and Sab respectively, there was a decrease in the ARE induction – this will be addressed further in chapter 3.

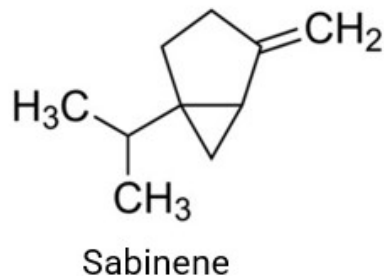


Figure 1.8 Molecular structure of Sab.

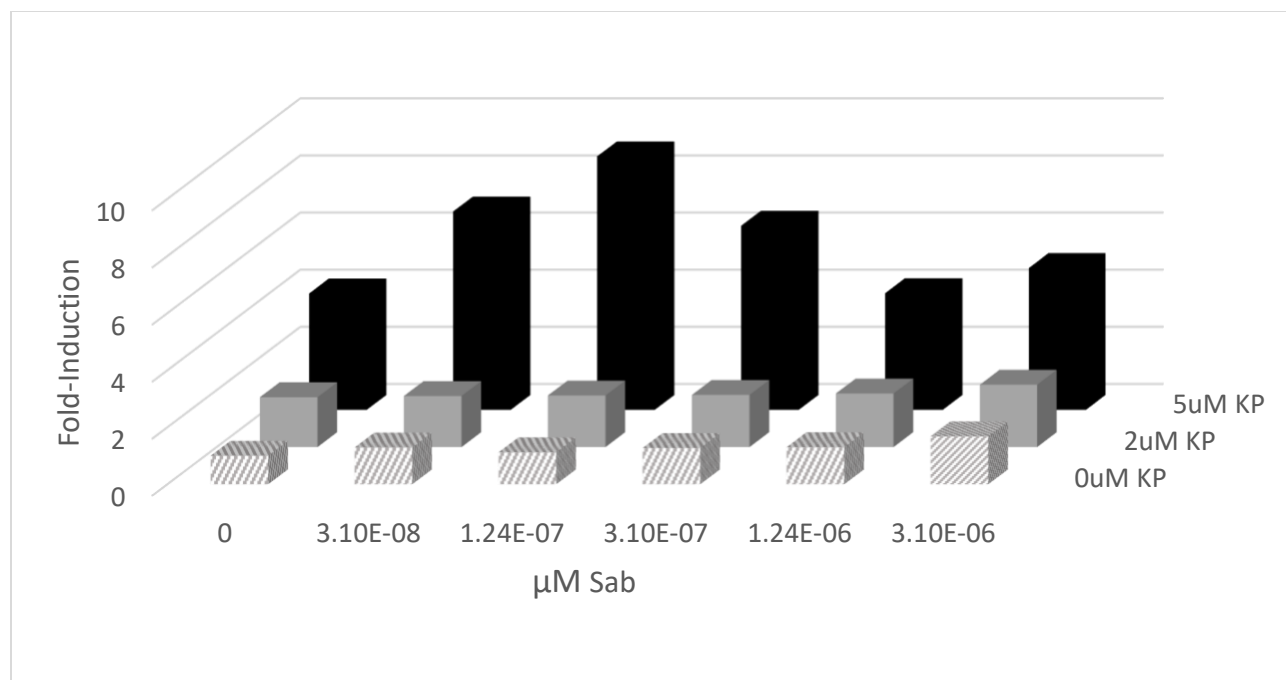


Figure 1.9 Luminescence assay demonstrates the pattern of NRF2 induction with varying concentrations of Sab and KP. Values plotted on the Y-axis corresponds to the fold increase in luminescence compared to the untreated samples. The X-axis shows the effect of increasing Sab concentrations. Z-axis shows the effect of increasing KP. This was performed in a 96-well plate, with each treatment group being represented as the average of four samples. The standard deviation is based on four individual samples and is within 10% of the plotted values. This data was statistically significant and had a p-value <0.05.

To continue evaluating whether the enhanced activation of ARE, additional pure compounds were tested with KP. To further evaluate the enhanced luciferase activity, the compound tetrafluorohydroquinone (TFHQ), an electrophile, was used to evaluate its induction of ARE, given the known fact that electrophiles can activate NRF2 via their interaction with Keap1 (Baird & Yamamoto, 2020; Jaramillo & Zhang, 2013; Juge, Mithen, & Traka, 2007; Li et al., 2019; Tastan et al., 2017). Fig. 1.11A depicts the dose-response for TFHQ. In this experiment, ARE induction reached maximum activation around 50μM TFHQ and then attenuated as concentrations exceeded this treatment. This is the first report of this compound

inducing ARE activation, so determining dose-response data was carried out as an initial objective.

Once an effective dose-response for TFHQ was established it was then used in combination with KP to observe the effects on ARE activity. The molecular structure of TFHQ can be seen in Fig. 1.10. The effects of TFHQ alone, in Fig. 1.11B, shows that 50 μ M TFHQ can induce ARE 3-fold in comparison with the no-treatment control group (p-value <0.01). However, when 20 μ M TFHQ was combined with 5 μ M KP there was a 23-fold induction in comparison with no treatment (p-value 0.112) and a 2-fold induction compared to the 5 μ M KP without TFHQ. This again suggests that the enhanced activation of ARE could be the result of a coordinated approach to targeting specific mechanisms of the NRF2 pathway, namely Keap1 (early response) and GSK-3 β (delayed response). Once again, 50 μ M TFHQ and 5 μ M resulted in a decreased induction of ARE compared with KP alone. This is consistent with other combinations used previously. Additionally, it is interesting that there was only a marginal enhancement of ARE activation with TFHQ for the 15 μ M KP data (back row). However, given the observation that 15 μ M KP has been shown to attenuate ARE-dependent expression in many experiments, this does not impact the overall interpretation of the data.



Tetrafluorohydroquinone

Figure 1.10 Molecular structure of TFHQ.

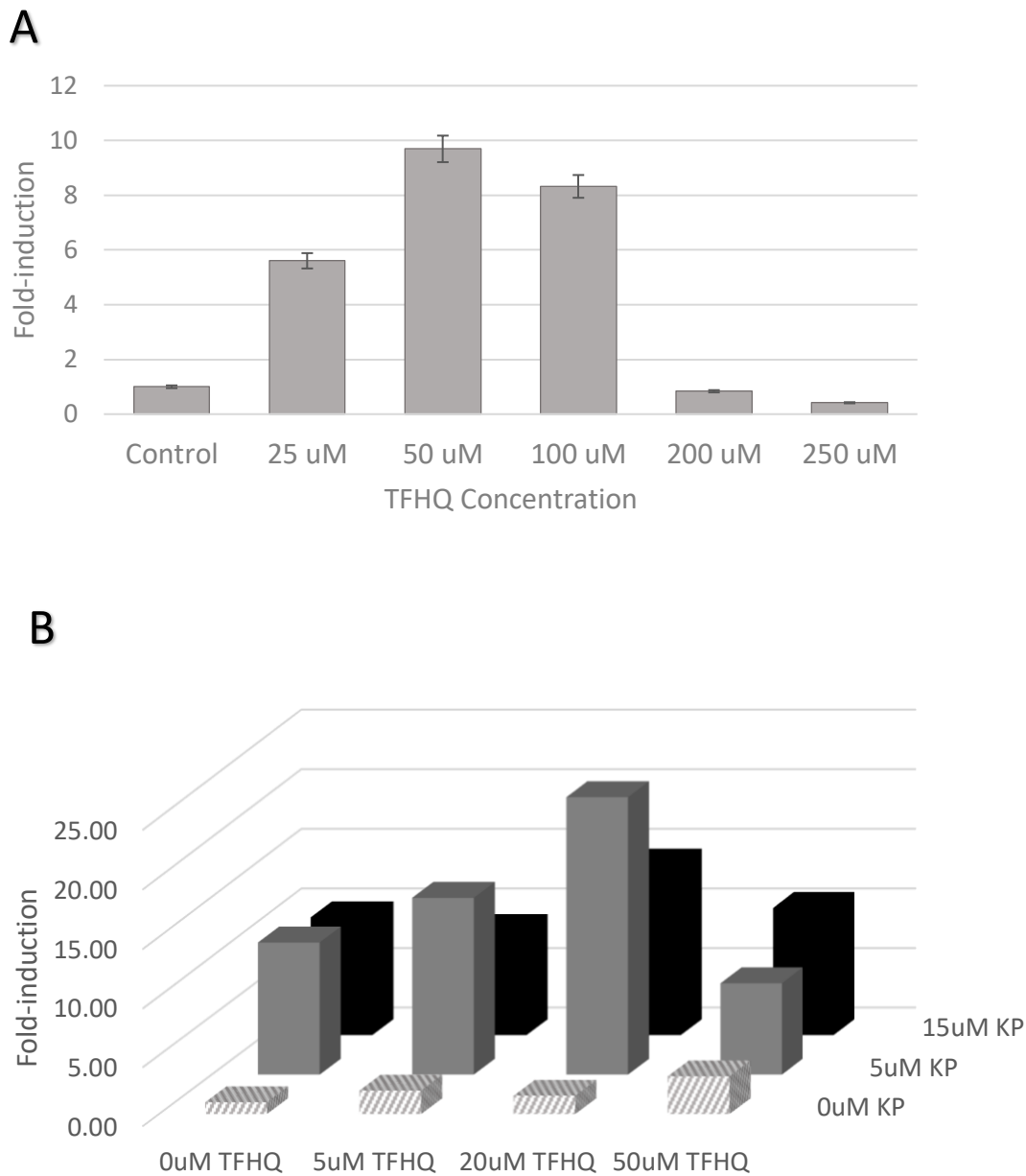


Figure 1.11 ARE activation via TFHQ individually and in combination with KP. A) Luminescence Dose-response of HepG2/NRF2 cells to TFHQ represented as fold-induction on the Y-axis and increasing concentration of TFHQ on the X-axis. This data set was based on n=4 and had a p-value of <0.02. B) Luminescence assay demonstrates the pattern of NRF2 induction with varying concentrations of TFHQ and KP. Values plotted on the Y-axis corresponds to the fold increase in luminescence compared to the untreated samples. The X-axis shows the effect of increasing TFHQ concentrations. Z-axis shows the effect of increasing KP. This was performed in a 96-well plate, with each treatment group being represented as the average of four samples. The standard deviation is based on four individual samples and was not within 10% of the plotted values.

Clearly, KP promotes enhanced activation with a number of other co-activators, which presumably have their mode of action at the NRF2/Keap1 complex. To evaluate whether the enhanced activation of ARE was dependent on KP as one of the activators, the combined effects of two classical activators (not KP) were investigated. To do so, three treatment groups were established using SFN and TFHQ. The first group only contained SFN, the second only TFHQ, and the third contained both SFN and TFHQ. Fig. 1.12 demonstrates dose-dependent induction of the ARE using both pure compounds. SFN reached maximum activation of 10-fold at 4 μ M (p-value <0.001), while TFHQ reached maximum activation of 7-fold induction at 50 μ M (p-value <0.001). When combined, no enhanced activation was observed. For example, the maximum activation for the combined treatment reached a 10-fold induction with both 4 μ M SFN and 20 μ M TFHQ (Fig. 1.12 rightmost black-dotted column) (p-value equal to 0.004). Interestingly, it appears that the combined effect of these two ARE inducers led to a slightly reduced induction of the antioxidant pathway relative to SFN alone. The fact that neither compound led to an enhanced effect that was greater than either compound individually does suggest that KP is significant in the enhanced induction of the antioxidant pathway described in this research. The same effect is not replicated using other “traditional” ARE activators.

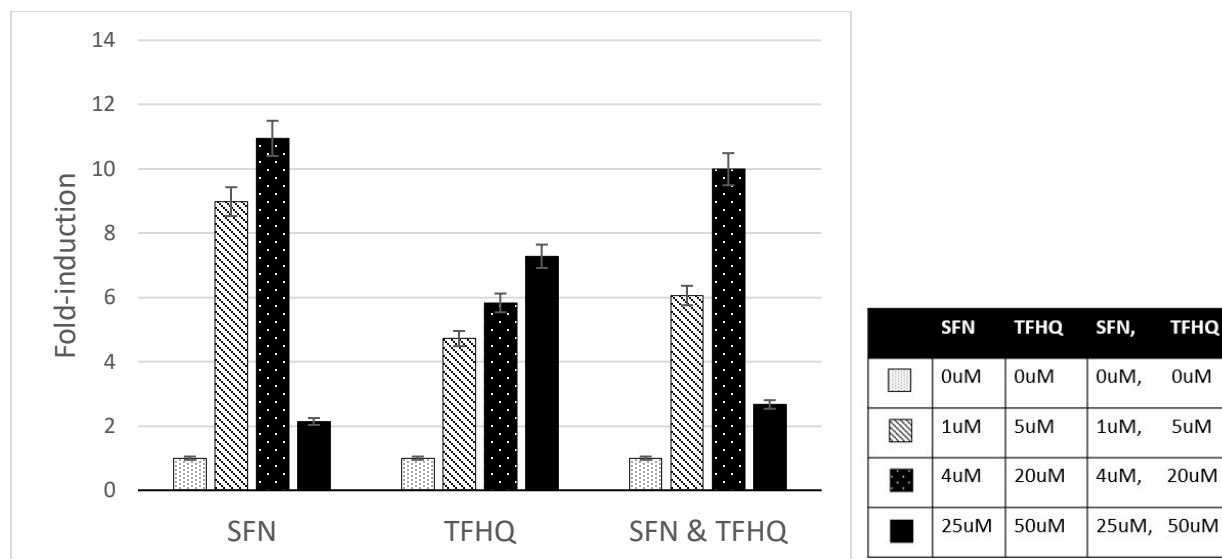


Figure 1.12 Luminescence assay of NRF2 induction based on the treatment of SFN, TFHQ, and both compounds combined. In each cluster (left, middle, right) the gray-dotted column is the control and represents no treatment. In the left-most cluster of data, these treatments contain only SFN. The gray-diagonally-striped column contains 1 μ M SFN. The black-dotted column consists of 4 μ M SFN alone. The solid black column consists of 25 μ M SFN alone. In the middle data cluster, only TFHQ was used for treatment. The gray-diagonally-striped column contains 5 μ M TFHQ. The black-dotted column consists of 20 μ M TFHQ. The solid black column consists of 50 μ M TFHQ. The right-most data cluster consists of both SFN and TFHQ. The gray-diagonally-striped column consists of 1 μ M SFN and 5 μ M TFHQ. The black-dotted column consists of 4 μ M SFN and 20 μ M TFHQ. The solid black column consists of 25 μ M SFN and 50 μ M TFHQ. Each of these columns is representative of the average of four individual samples and has a p-value of <0.01.

Altogether, the combined data seen in Fig. 1.5, 1.9, and 1.11B shows that individually KP, SFN, Sab, and TFHQ all have a positive effect on the ARE activation in this reporter system. Moreover, the combined effect of KP with other inducers of NRF2 resulted in enhanced activation of the ARE that was significantly greater than the individual effect of any of these inducers. Furthermore, Fig. 1.12 suggests that the mechanism by which enhancement of the ARE is activated is important – given, that in the absence of KP, enhanced activation did not occur. This data is consistent with the hypothesis that enhanced activation of the ARE is achievable through a targeted approach as represented in schematic 4.

Non-enhancing Pure Compounds & KP

Although it does appear that there are a variety of compounds that can synergize with KP to lead to enhanced ARE induction, several compounds examined lacked ARE activation properties. As part of the effort to explore potential antioxidant compounds that could lead to enhanced activity with KP, trans-2-decenal (T2D), cinnamaldehyde (CIN), and curcumin (CURC) were also evaluated, based on their expected ability to activate NRF2 (Baird & Yamamoto, 2020; Boo, 2020; Hseu et al., 2018; Tastan et al., 2017; Tayyem et al., 2006; Uchi, Hiroshi, MD, PhD et al., 2016; Yin et al., 2016). These structures can be seen in Fig. 1.13.

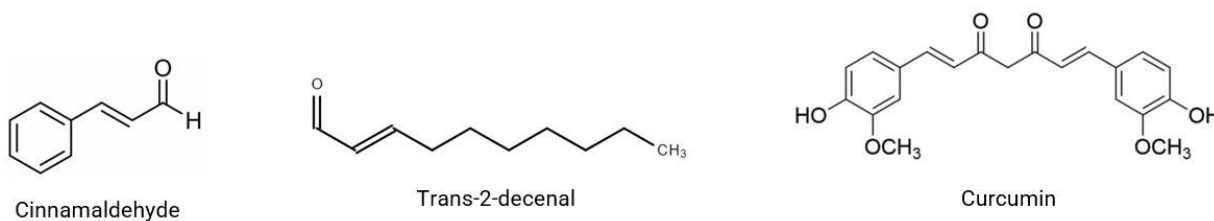


Figure 1.13 The molecular structures of CIN, T2D, and CURC.

Fig. 1.14 shows the effects of T2D and KP. The first row indicated that T2D did not have a significant inductive effect on NRF2 by itself. Although 15 μ M appears to have a slight induction of the ARE, generating an almost 2-fold activation, there did not seem to be as strong an effect as seen with other compounds. As this is an aldehyde, the expectation was that its electrophilic properties would activate the ARE. However, aldehydes are also air sensitive and upon storage can become oxidized. It is possible that while in storage this compound became oxidized and was no longer viable at the time of treatment, however, this was not confirmed beforehand. The KP control (first column), did have a standard dose-dependent increase in ARE

activation that correlates with data previously shown. The combined effect of T2D and KP did not appear to produce the enhanced activation of ARE, however, this is likely due to the ineffectiveness of T2D as an activator. Likewise, T2D did not lead to an attenuation of ARE.

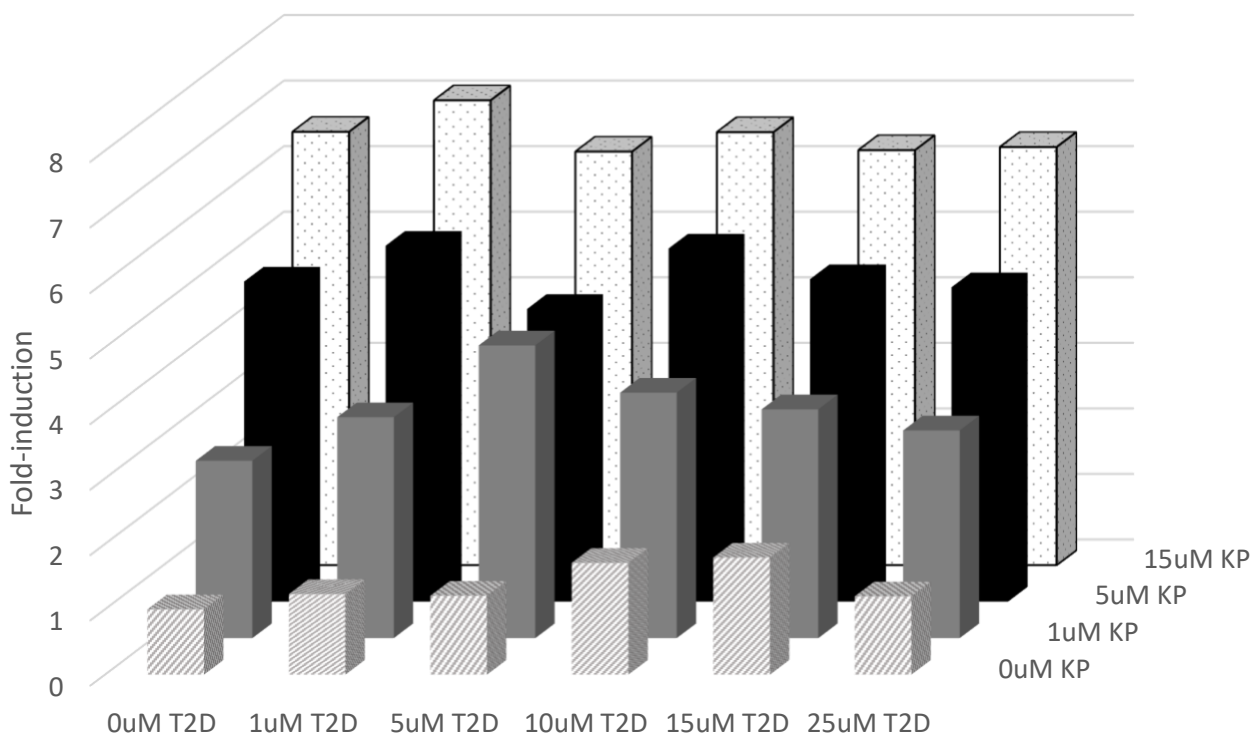


Figure 1.14 Luminescence assay demonstrates the pattern of NRF2 induction with varying concentrations of T2D and KP. Values plotted on the Y-axis corresponds to the fold increase in luminescence compared to the untreated samples. The X-axis shows the effect of increasing T2D concentrations. Z-axis shows the effect of increasing KP. This was performed in a 96-well plate, with each treatment group being represented as the average of four samples. The standard deviation is based on four individual samples and is within 10% of the plotted values.

The next compound evaluated was CIN. The first row in Fig. 1.15 shows that even at 50 μ M CIN did not seem to have a significant increase in activation compared to the control (only a 1.23-fold induction with 50 μ M CIN). The KP control (first column), demonstrated that KP did induce luciferase expression. Similarly, to what was seen with T2D and KP in Fig. 1.14, Fig.

1.15 also indicated that there was not a significantly enhanced effect in the combined treatment of CIN and KP that was greater than KP alone. A minor effect was observed in the 1 μ M KP treatment, however, the maximum induction did not exceed that observed with higher KP concentrations. This is likely attributed to a lack of NRF2 activation by the CIN individually.

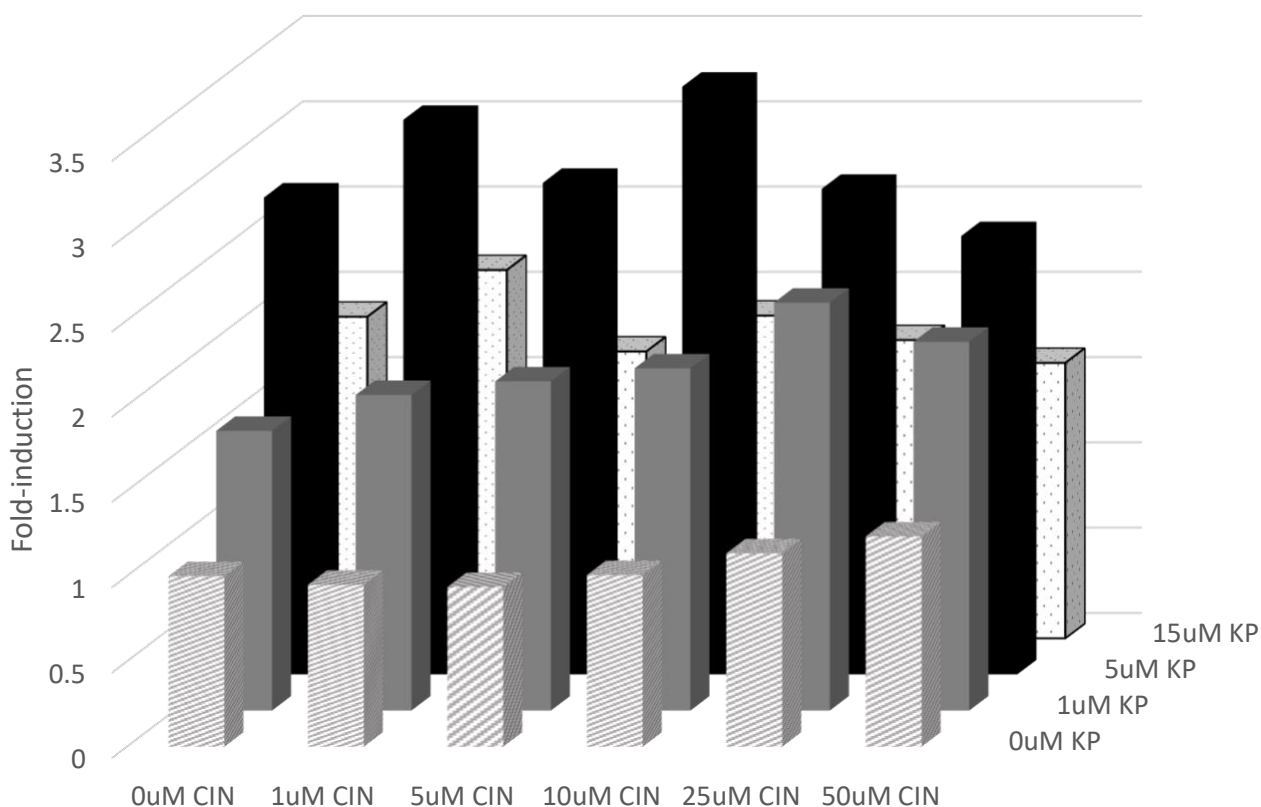


Figure 1.15 Luminescence assay demonstrates the pattern of NRF2 induction with varying concentrations of CIN and KP. Values plotted on the Y-axis corresponds to the fold increase in luminescence compared to the untreated samples. The X-axis shows the effect of increasing CIN concentrations. Z-axis shows the effect of increasing KP. This was performed in a 96-well plate, with each treatment group being represented as the average of four samples. The standard deviation is based on four individual samples and is within 10% of the plotted values.

The last pure compound that was investigated was CURC. The data shown in Fig. 1.16, indicated that CURC treatment alone did have a slight induction of ARE. The first row shows that at 25 μ M CURC had a 2-fold induction of ARE. The first column again showed the expected induction pattern via KP. However, the most intriguing aspect of Fig. 1.16 is that CURC seemed to have a slightly different pattern of effects when combined with varying concentrations of KP. At 1 μ M KP, it appears that 25 μ M of CURC did lead to enhanced activation of ARE, generating a 4-fold induction which is ~3x greater than 1 μ M KP alone. When combined with 5 μ M KP, however, CURC did not lead to an enhanced activation that exceeded the threshold generated by KP alone. Then lastly the back row indicated that at 15 μ M KP, there was attenuated ARE induction. The mechanism by which this might have occurred is unknown. The data presented in Fig. 1.16 does demonstrate some qualitative similarities with SFN and TFHQ that enhanced activation does occur with 25 μ M CURC and 1 μ M KP and attenuation occurred at higher KP doses. It is likely that other, currently unidentified, confounding variables are responsible for the lack of enhancement at 5 μ M KP.

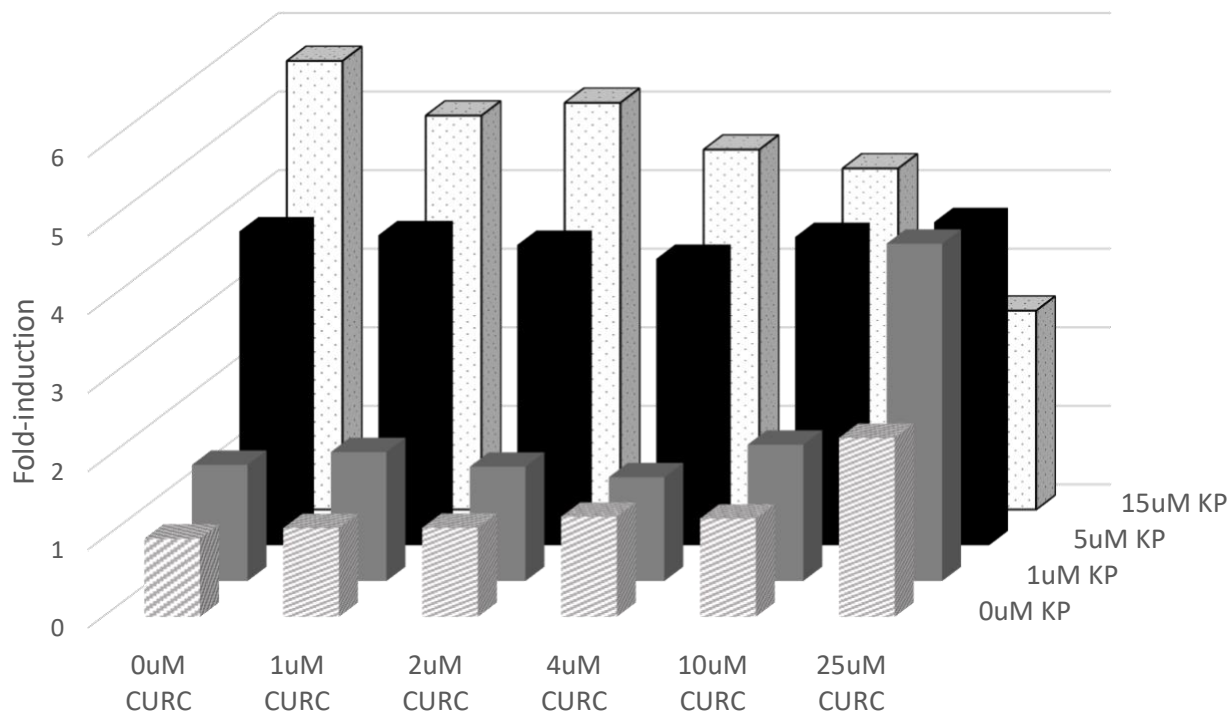


Figure 1.16 Luminescence assay demonstrates the pattern of NRF2 induction with varying concentrations of CURC and KP. Values plotted on the Y-axis corresponds to the fold increase in luminescence compared to the untreated samples. The X-axis shows the effect of increasing CURC concentrations. Z-axis shows the effect of increasing KP. This was performed in a 96-well plate, with each treatment group being represented as the average of four samples. The standard deviation is based on four individual samples and is within 10% of the plotted values.

Overall, the general lack of enhanced ARE activation by these three compounds is likely due to the non-inducing behavior modeled in Fig 1.14, 1.15, 1.16 by T2D, CIN, and CURC, respectively. This data is also consistent with our hypothesis that enhanced ARE activity would be observed with the combination treatment of compounds able to activate the early response of the NRF2 pathway in coordination with a compound regulating the delayed response, such as KP (as modeled in schematic 4).

Crude Extract Induction of NRF2

Having established an enhanced ARE induction effect of KP on several pure activator compounds, experiments were then carried out using crude extract material with known ARE induction effects. The extracts chosen were BROCC (known to contain SFN), CIL (known to contain T2D), CAS (known to contain cinnamaldehyde), and TURPD (known to contain CURC) (Baird & Yamamoto, 2020; Boo, 2020; Foudah et al., 2021; Nandini et al., 2020; Tastan et al., 2017; Tayyem et al., 2006).

The results in Fig. 1.17 demonstrate the effect of KP on reporter activation by BROCC extract on HepG2/NRF2 cells. Luminescence data from this figure indicate ARE activation by both BROCC and KP individually. Alone BROCC had a modest dose-dependent induction of ARE activation, resulting in slightly higher than a 2-fold induction at 0.01% BROCC (p-value <.02). Again, the KP control continued to demonstrate dose-dependent induction of ARE with maximum induction of almost 5-fold. Of significance, is the observation that the combined effect of BROCC and KP in each row indicated enhanced activation. Synergistic induction of ARE with a maximum effect was observed at 0.01% BROCC and 1 μ M KP. This treatment resulted in a 6-fold induction of ARE which is a 4-fold increase (p-value equal to 0.002) in comparison to 1 μ M KP alone. Similarly, at 5 μ M KP substantially enhanced induction of ARE was achieved in the combined treatment. This time maximum induction occurred at a slightly lower concentration of BROCC, 0.005% BROCC, and 5 μ M KP. Both the 0.005% BROCC and 0.01% BROCC with 5 μ M KP had similar levels of activation generating a 7-fold induction (p-value equal to 0.01). This is fairly comparable to the maximum induction seen at 1 μ M KP and is only ~2.1x greater than 5 μ M KP without BROCC. In the last row (15 μ M KP), another interesting set of data appeared. Again, it appeared that the BROCC and KP generated an enhanced activation of ARE and even climaxed at

a lower concentration of BROCC, reaching a 6-fold induction at 0.0025% BROCC and 7-fold induction at 0.005% BROCC, both in combination with 15 μ M KP.

At the highest concentration of BROCC (0.02%), there was a drop in ARE activation for each of the KP combinations. This parallels some of the results found in previous data such as SFN (Fig. 1.4) and TFHQ (Fig. 1.11). Again, these drops in NRF2 activity are interesting aspects of the experiment that will be discussed in a later chapter.

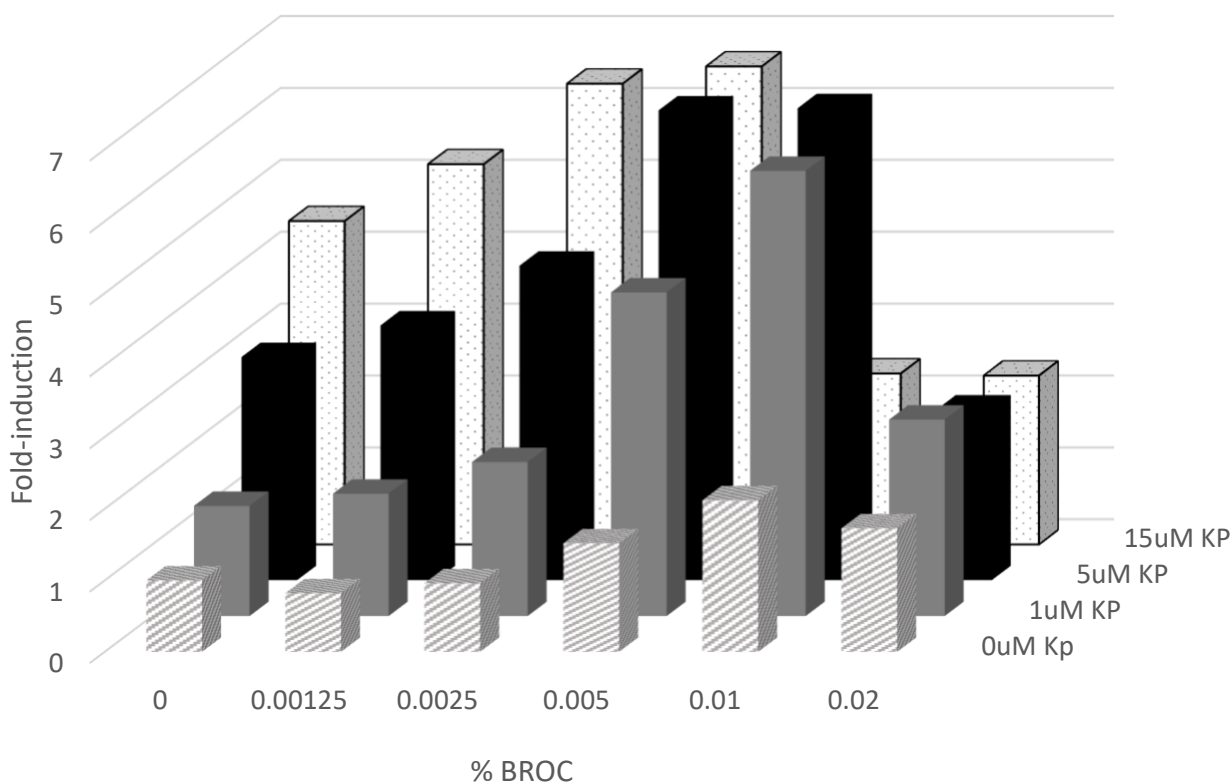


Figure 1.17 Luminescence assay demonstrates the pattern of NRF2 induction with varying concentrations of BROCC and KP. Values plotted on the Y-axis corresponds to the relative fold increase in luminescence compared to the untreated samples. The X-axis shows the effect of increasing BROCC concentrations. Z-axis shows the effect of increasing KP. This was performed in a 96-well plate, with each treatment group being represented as the average of four samples. The standard deviation is based on four individual samples and is within 10% of the plotted values. The p-value was <0.02.

Figure 1.18 presents data showing the effect of CIL and KP on HepG2/NRF2 cell induction of ARE. The first row indicated that CIL had a modest dose-dependent induction of ARE. Alone, CIL was able to cause a 2-fold induction of NRF2 at 0.02% in comparison with the control (p-value <0.04). Based on our data it does appear that CIL in combination with KP enhances the induction of luciferase expression. The greatest enhanced activation occurred at 0.02% CIL and 15 μ M KP generating a 12-fold induction (p-value <0.001) in comparison with the zero-treatment group and a 2-fold induction in comparison with 0% CIL and 15 μ M KP (p-value <0.02). Interestingly, it appears that at these concentrations of CIL, a maximum saturation was not achieved, as attenuation was not observed. It is likely this is the result of the concentration range that was used. Further testing would need to be done to evaluate the maximum threshold for CIL and to determine whether attenuation in the combined treatments would occur as with the other treatments.

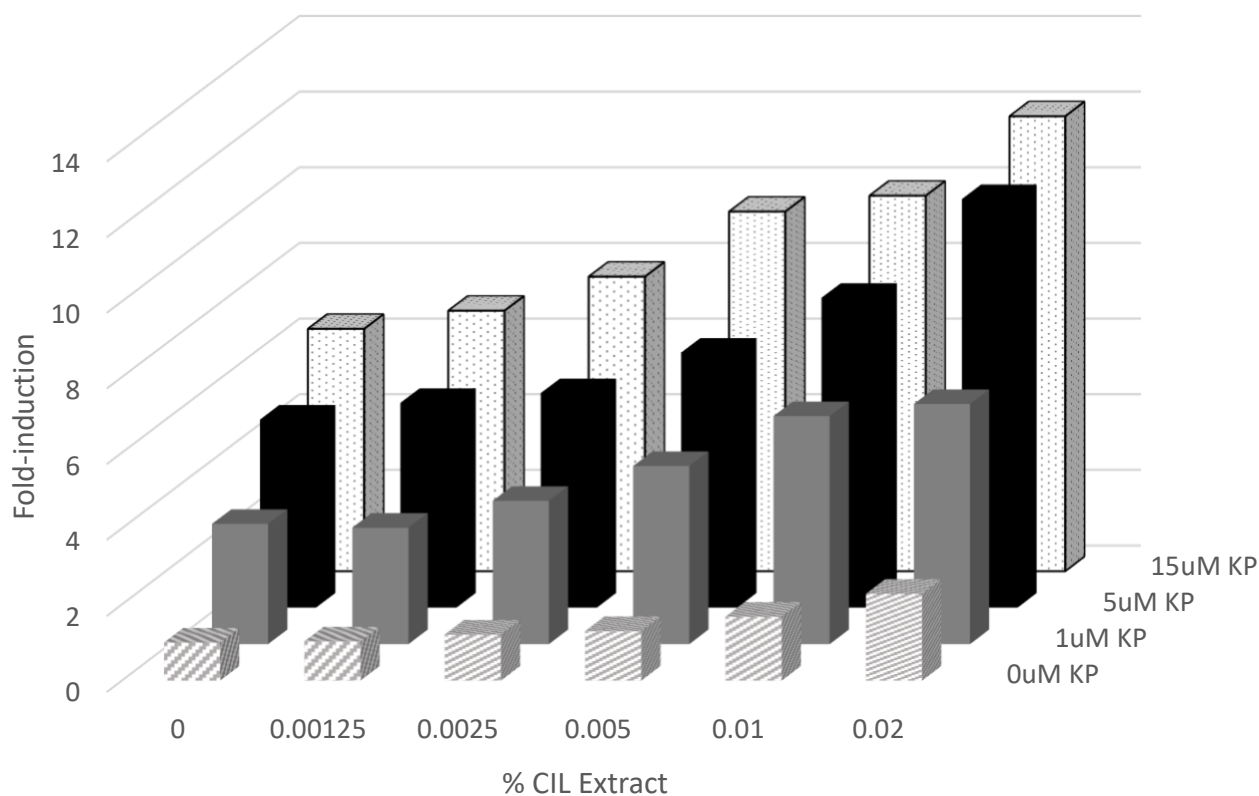


Figure 1.18 Luminescence assay demonstrates the pattern of NRF2 induction with varying concentrations of CIL and KP. Values plotted on the Y-axis corresponds to the relative fold increase in luminescence compared to the untreated samples. The X-axis shows the effect of increasing CIL concentrations. Z-axis shows the effect of increasing KP. This was performed in a 96-well plate, with each treatment group being represented as the average of four samples. The standard deviation is based on four individual samples and is within 10% of the plotted values. The p-value was <0.04.

The last natural product that was investigated was CAS due to its known antioxidant effects and it being a primary source of CIN. Fig. 1.19A shows the initial concentrations of CAS extract used in the treatment of HepG2/NRF2 cells. The only treatment groups in this experiment that produced any NRF2 activity were the control (first column), and the treatment groups containing 0.015mg/ml CAS. The total luminescence at concentrations exceeding this threshold

had a 10-fold decrease in NRF2 activity. It is likely that this decrease is due to cytotoxic concentrations of CAS however further testing would be needed to confirm.

Fig. 1.19B shows a lower range of treatment concentrations of CAS. The first row indicates that CAS alone had a slightly inductive effect on NRF2, specifically at 0.015mg/ml, while KP alone followed the expected trend. When combined with 0.015mg/ml CAS, both 1 μ M and 5 μ M KP resulted in enhanced activation of NRF2 resulting in a 7-fold increase in ARE activity. Although, only the combination of 0.015mg/ml CAS and 5 μ M KP was statistically significant (p-value <0.05). This data shows that the maximum threshold for CAS activation occurred at 0.015mg/ml CAS and 1 μ M KP. A similar effect also occurred with 0.015mg/ml CAS, 5 μ M KP. In comparison with 0mg/ml CAS and 1 μ M KP, 0.015mg/ml CAS with 1 μ M KP generated a 3-fold higher induction of NRF2. Likewise, 0.015mg/ml CAS with 5 μ M KP generated a 2-fold higher induction in comparison to the 0mg/ml CAS and 5 μ M KP, although this comparison was not statistically significant (p-value 0.206). Once again, the NRF2 activity was attenuated in reactions containing 15 μ M KP in the presence of CAS.

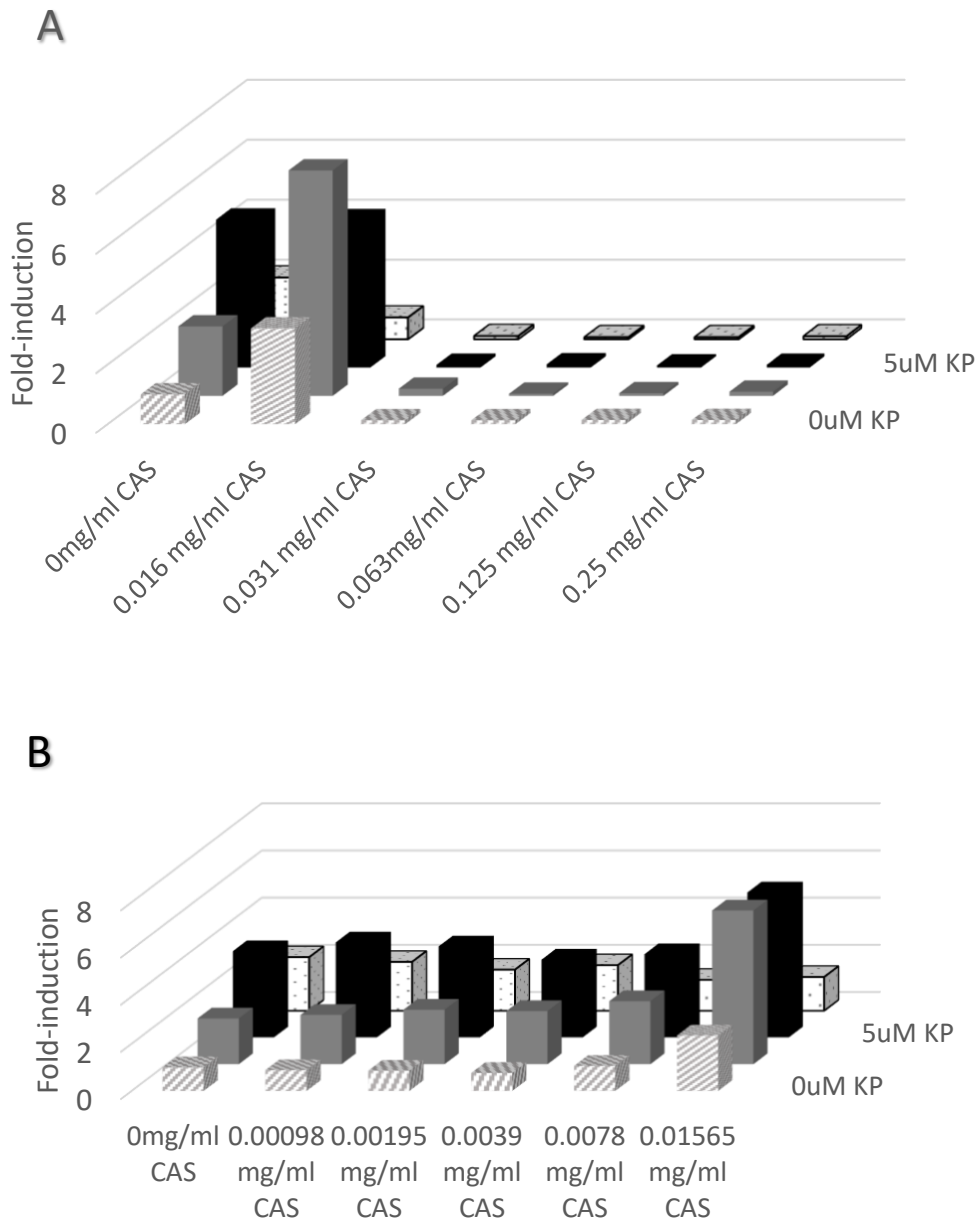


Figure 1.19 Luminescence assay demonstrates the pattern of NRF2 induction with varying concentrations of CAS and KP. Values plotted on the Y-axis corresponds to the fold increase in luminescence compared to the untreated samples. The X-axis shows the effect of increasing CAS concentrations. Z-axis shows the effect of increasing KP. This was performed in a 96-well plate, with each treatment group being represented as the average of four samples. The standard deviation is based on a minimum of three individual samples. A two-tailed T-test indicated the data in Fig. 19B only had a statistically significant comparison between the 0mg/ml CAS, 0μM KP and 0.015mg/ml CAS, 5μM KP (p-value <0.05) and 0mg/ml CAS, 0μM KP compared to 5μM KP alone (p-value <0.001).

Altogether, the data represented by the combination of crude extracts such as BROCC, CIL, and CAS, with KP (Fig. 1.17, 1.18, 1.19) demonstrates an enhanced ARE activation that is greater than achievable by any of the ARE inducers used alone. The enhanced effect is likely due to the antioxidant properties of these compounds that lead to the induction of the early response in the NRF2 pathway as this is supported by the literature (Foudah et al., 2021; Nandini et al., 2020; Uchi, Hiroshi, MD, PhD et al., 2016; Yang et al., 2015). These, combined with KP, resulted in enhanced activity of luciferase consistent with our hypothesis.

NRF2 Induction via Combinations of Natural Products without KP

Although it is clear that KP can work in coordination with various natural products containing antioxidant properties to enhance the induction of the antioxidant system, we wanted to confirm that this effect was due to the specific combination with a GSK- β inhibitor. Therefore, we tested combinations of two of the natural products shown to induce ARE activity in the absence of KP. Results shown previously for the pure compounds SFN and TFHQ indicated no enhanced activation, however, in the crude material, the possibility of the presence of non-Keap1-dependent activation could not be ruled out. Based on the results from Fig. 1.17 and 1.18, BROCC and CIL were chosen to evaluate this effect.

Fig. 1.20 confirms that BROCC and CIL alone have a positive effect on ARE activity. BROCC clearly had a more potent induction of ARE, leading to a greater than 4-fold increase (p-value equals 0.002), which could be due to the SFN it contains, or other antioxidant compounds found in this crude extract. Although CIL was not as potent, it still resulted in a relative increase relative to the control, although this data was not statistically significant (p-value equals 0.066). The combination of BROCC & CIL appeared to have a very modest additive effect on the antioxidant activation (p-value <0.001), however, in comparison with the enhanced activation

observed in the KP treatments, this was minimal (Fig. 1.17, 1.18). This is likely due to the absence of a GSK-3 β inhibitor, such as KP, in the crude extract, although the small effect observed could indicate the presence of a minor component capable of blocking GSK-3 β to a small degree. Without a significant inhibitor of the delayed response, these crude extract combinations failed to produce enhanced luciferase activity, which is consistent with the hypothesis represented in schematic 4 – that enhanced activity would result from a targeted approach of both the early and the delayed response in the NRF2 pathway.

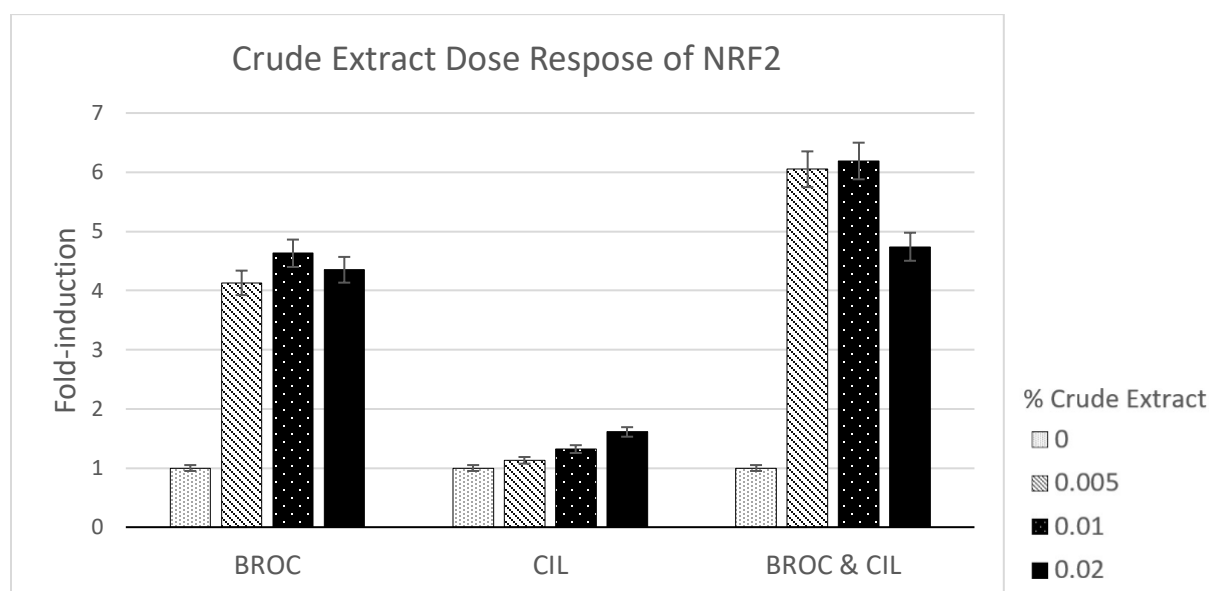


Figure 1.20 Luminescence assay demonstrates NRF2 induction based on the treatment of crude extracts. The leftmost cluster contains BROC alone. The middle cluster contains CIL alone. The right-most cluster contains a combination of BROC and CIL. Each of the columns in this figure represents the average of four individual samples within 10% of the standard deviation.

Altogether, this data supports the hypothesis that enhanced activation of the ARE occurs in the presence of two inducers that simultaneously target both the early and the delayed response of the NRF2 pathway. Based on the literature, it is likely that BROC and CIL do not lead to enhanced activation, because they both contain a high amount of electrophiles, which

would interact with Keap1 in the early response mechanism of the NRF2 pathway, but not the delayed response (Foudah et al., 2021; Nandini et al., 2020; Yang et al., 2015).

NRF2 Attenuating Natural Products

Curcumin is known to have antioxidant effects through its electrophilic interaction with Keap1 (Baird & Yamamoto, 2020; Boo, 2020; Tastan et al., 2017). Curcumin is a compound found within the natural product turmeric powder (Tayyem et al., 2006). The data in Fig 1.16 indicated that 25 μ M CURC and 1 μ M KP lead to enhanced activation of ARE, so it is reasonable to assume that TURPD would have a similar effect. Interestingly, Fig. 1.21 did not indicate significant enhancement in KP activation of the antioxidant pathway. On the contrary, TURPD appeared to have an attenuating effect on the induction of NRF2, particularly at 15 μ M and 5 μ M KP. While KP still acts as an activator, in the presence of TURPD, this effect appeared to be reversed in a dose-dependent manner. A possible explanation for this is that since TURPD is a crude material, there could be another compound within this complex mixture that is having a negative effect on ARE activity, or possibly cell survival. Previous studies have shown that turmeric does have the ability to enhance apoptosis via increased expression of Bax, and caspase-3 (Benzie, Wachtel-Galor, & Packer, 2011).

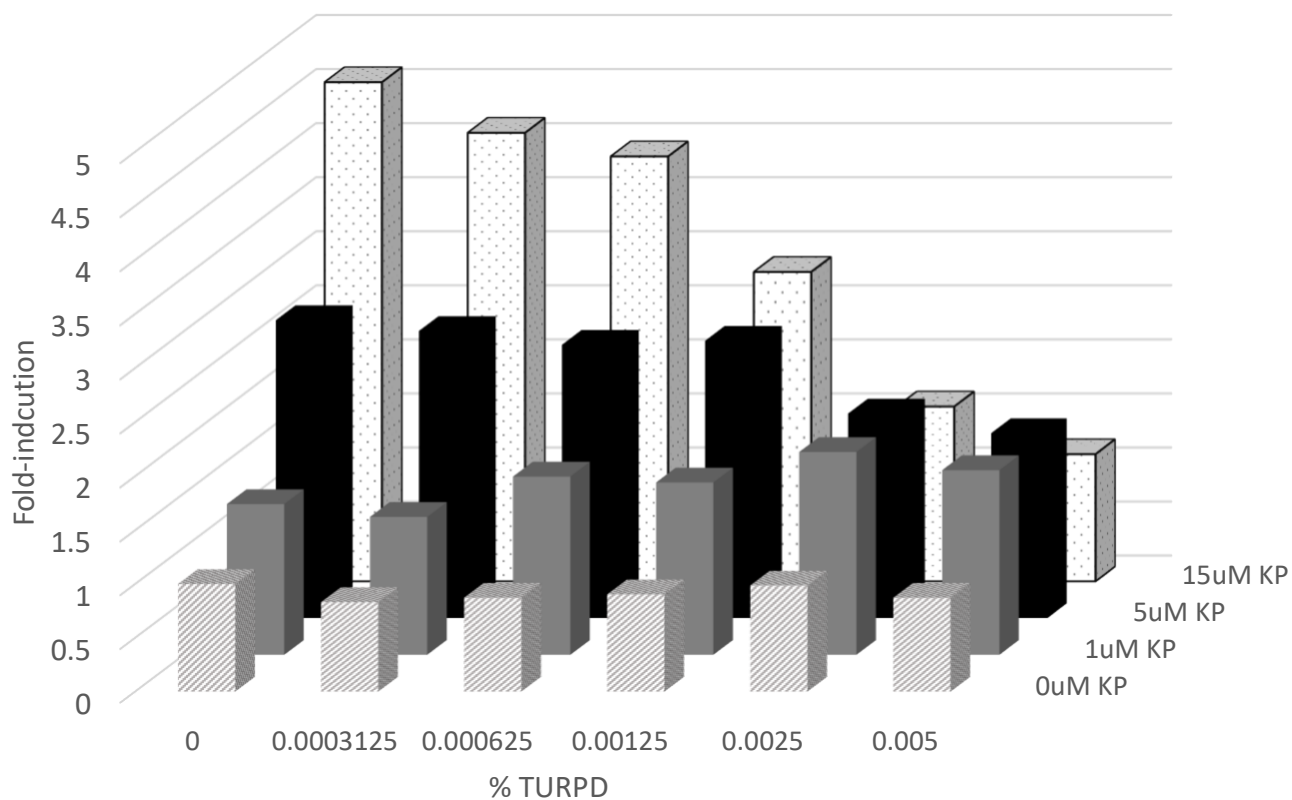


Figure 1.21 Luminescence assay demonstrates the pattern of NRF2 induction with varying concentrations of TURPD and KP. Values plotted on the Y-axis corresponds to the fold increase in luminescence compared to the untreated samples. The X-axis shows the effect of increasing TURPD concentrations. Z-axis shows the effect of increasing KP. This was performed in a 96-well plate, with each treatment group being represented as the average of four samples. The standard deviation is based on four individual samples and was not within 10% of the plotted values.

Conclusion

Many pure compounds and natural products such as SFN, BROc, and CIL have been shown to have antioxidant effects (Boo, 2020; Fahey et al., ; Gamet-Payraastre et al., 2000; Tastan et al., 2017; Tayyem et al., 2006). In this study, we evaluated the ability to generate a dose-response of the antioxidant system through the treatment of both pure compounds as well as natural products. Our data indicates three novel aspects. *The first novel result from this study was the ability of Sab to induce NRF2 activity.* We originally tested Sab, because it was a component of the balm of Gilead oil, which previous data demonstrated had the ability to induce ARE activation in our model.

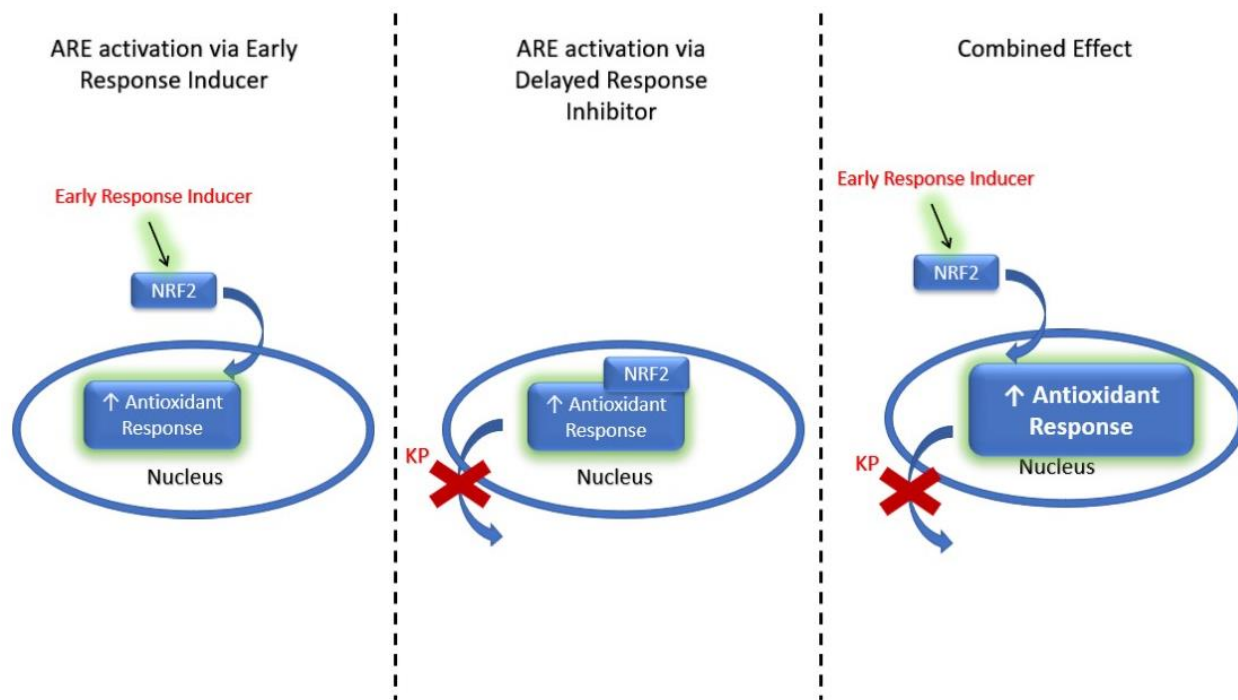
The second novel discovery was the ability of TFHQ to induce NRF2. Although it has been shown that electrophiles can interact with Keap1 to induce the antioxidant system, TFHQ had not previously been identified as an activator of this system. Our data does not confirm the interaction of TFHQ with Keap1, but this would be the most likely mechanism by which it activates NRF2.

However, the most interesting aspect of our data lies in the enhanced activation that was demonstrated across multiple treatment combinations. Sab, TFHQ, SFN, BROc, and CAS all demonstrated the ability to lead to enhanced activation of NRF2 when treated in conjunction with KP (as seen in schematic 5). This is significant because it indicates that these trends are not isolated phenomena. Based on what we know of the NRF2 pathway, it is likely that the impact of these treatments is a result of the “dual targeting” approach. By treating HepG2/NRF2 cells with compounds that likely interact with both the early and the late responses in the pathway a

tremendous increase in NRF2 activity was achieved. The strongest enhanced activation of the ARE was the combination of 4 μ M SFN and 5 μ M KP, which lead to 32-fold induction (Fig. 1.4).

When HepG2/NRF2 cells are treated with SFN and TFHQ, there was no enhanced activity of NRF2 based on the combined treatment. Again, the mechanism of TFHQ has not been confirmed and would require further study, but it is likely that enhanced activity of NRF2 was not achieved because these compounds operate through a similar mechanism.

In conclusion, our data demonstrate a dose-dependent response of NRF2 activation through the treatment of multiple compounds. This data suggests that the NRF2 system can be greatly enhanced by targeting regulators that increase the nuclear translocation of NRF2 and decrease the nuclear export of NRF2; as modeled in schematic 5.



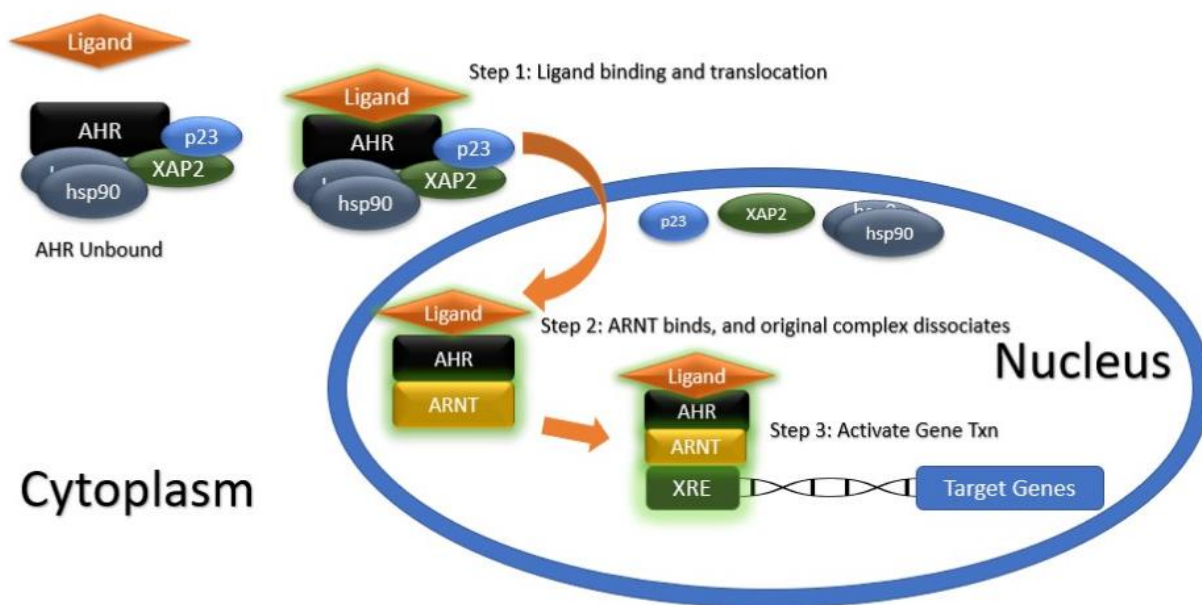
Schematic 5. Proposed mechanism by which coordinated treatment leads to enhanced ARE activation in the HepG2/NRF2 reporter system. The left and middle columns illustrate the solo induction of a particular compound on the activation of the antioxidant system. The right column depicts the enhanced induction of the antioxidant system when targeted with a combination treatment that utilizes different mechanisms.

Chapter 2 – Activation of Aromatic Hydrocarbon Receptor by Kenpaullone

Introduction

In light of the enhanced ARE activation seen through multiple treatments in Chapter 1, the next step was to evaluate the potential cross-talk between the antioxidant pathway and other cytoprotective pathways in the body. NRF2 is the major regulator of the antioxidant pathway but has also been shown to have connections to xenobiotic metabolism (Hayes, Dinkova-Kostova, & McMahon, 2009; Kalthoff, Ehmer, Freiberg, Manns, & Strassburg, 2010; Shin et al., 2007). Both NRF2 and the aryl hydrocarbon receptor (AHR) are transcription factors that regulate the production of cytoprotective genes (Shin et al., 2007). Many of the ligands for AHR are carcinogens and the AHR plays a major role in mitigating the toxic effects of these substances (Shin et al., 2007). Ironically, the toxicity of certain chemicals is enhanced by the pathway designed to eliminate them. For example, the CYP enzymes are a class of mono-oxygenases that catalyze the oxidative metabolism of aromatic hydrocarbons leading to the production of reactive electrophilic products that damage the cell and also may cause DNA damage resulting in carcinogenesis. One major difference is how the two pathways are activated: NRF2 is regulated via sequestration by Keap1, whereas AHR is activated by appropriate ligand binding. The ligand for AHR could be endogenous or exogenous and include compounds such as dioxins, flavonoids, and tryptophan photoproducts (Furue, Takahara, Nakahara, & Uchi, 2014). There are two major categories of environmental compounds that activate AHR signaling: halogenated aromatic hydrocarbons (HAH), such as 2,3,7,8-tetrachlorodibenzop-dioxin (TCDD), and polycyclic aromatic hydrocarbons (PAH), such as benzo(a)pyrene (Furue et al., 2014; Hayes et al., 2009; Itkin et al., 2020; Zhang, N., 2011). Most AHR ligands are very hydrophobic and can enter the cell via diffusion and bind with AHR (Furue et al., 2014; Itkin et al., 2020). When inactive, AHR exists as a multiprotein complex containing two heat shock proteins 90s (hsp90), one

immunophilin-like X-associated protein 2 (XAP2), and one co-chaperone protein p23 (Fig. 5) (Furue et al., 2014; Itkin et al., 2020; Zhang, 2011). Upon ligand binding, this entire complex will translocate to the nucleus (Furue et al., 2014; Hayes et al., 2009; Itkin et al., 2020; Shin et al., 2007; Zhang, 2011). Once in the nucleus, the aryl hydrocarbon receptor nuclear translocator (ARNT) will bind to the complex, and both hsp90s, the XAP2, and p23 will dissociate, leaving ARNT, AHR and the ligand to be recruited to the xenobiotic response element (XRE), also referred to as the dioxin response element. The XRE will then promote the transcription of a battery of xenobiotic metabolism genes (Furue et al., 2014; Hayes et al., 2009; Itkin et al., 2020; Shin et al., 2007). It is well established that the consensus sequence found in the promoter of AHR genes is 5'-(T/G)NGCGTG(A/C)(G/C)A-3' (A Lusska, E Shen, & J P Whitlock, 1993; Yao & Denison, 1992). Target genes of AHR include Cytochrome P450 family 1 subfamily A polypeptide 1 (CYP1A1), CYP1A2, CYP1B1, aldehyde dehydrogenase 3a1 (Aldh3a1), Gsta1 (Gst alpha 1), NAD(P)H: quinone oxidoreductase 1 (NQO1), and UDP-glucuronosyltransferase 1a6 (Ugt1a6) (Hayes et al., 2009; Itkin et al., 2020).



Schematic 6. Model showing the general mechanism associated with AHR activation by aromatic hydrocarbons. Aromatic hydrocarbons function as ligands for the AHR, which then translocates into the nucleus and dissociates from the other components of the heterodimer. ARNT, binds to the AHR and facilitates nuclear translocation and interaction with the XRE.

It has been discovered that TCDD, PAH, and other bifunctional inducers have the ability to activate both the ARE and the XRE, resulting in target gene expression for both pathways, indicating that the induction of these pathways is not completely independent from one another. Although the details regarding the mechanistic activation of both the ARE and the XRE have not been fully elucidated, it has been proposed that TCDD could cause increased ARE-dependent gene expression by stimulating a protein-protein interaction between the AHR and NRF2, which could increase the stability of the heterodimer complex recruited to ARE promoter sequences (Hayes et al., 2009).

Additionally, it has been demonstrated that NRF2 plays a role in regulating the production of AHR. More specifically, through NRF2 interaction with the ARE, there is an increased transcription of AHR, and increased interaction downstream between the AHR and XRE (Shin et al., 2007). In contrast, NRF2 can be controlled via NRF2 autoregulation as well as

via AHR. AHR interaction at the XRE will also result in increased expression of NRF2 (Furue et al., 2014; Li et al., 2019).

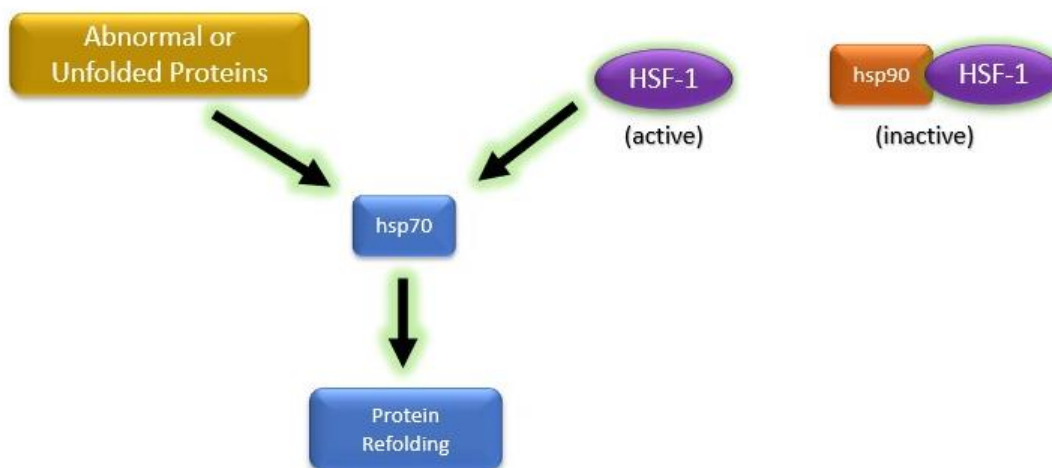
It should also be noted that as certain AHR ligands, such as dioxins, are metabolized by CYP1A1, there is increased oxidative stress introduced in the cell (Furue et al., 2014). The large increase in ROS will then be mitigated by the NRF2 antioxidant pathway (Oh & Jun, 2017).

Although all the relationships between NRF2 and AHR have yet to be fully understood, there has been significant evidence pointing to the connection between these two cytoprotective pathways. In light of the connections between NRF2 and AHR, this study investigated the possible activation of AHR by the NRF2 activator KP and evaluated the potential for enhanced activation of this pathway using methodologies described in the previous chapter.

Not only is NRF2 connected to AHR activation but also to heat shock proteins (HSP) – another cytoprotective mechanism. These proteins are important for the folding of nascent proteins, and the refolding of proteins that may have been damaged due to oxidative stress (Hardesty & Kramer, 2001; Jones, Moussaud, & McLean, 2014). Furthermore, HSPs prevent abnormal folding, the generation of redundant structures, and harmful nonnative proteins. Finally, these chaperone proteins are able to target irreversibly denatured proteins for degradation. When the cell experiences harmful conditions there is an upregulation in HSPs to help mediate the effects and initiate cytoprotective processes (Jones et al., 2014; Sherman & Goldberg, 2001).

Hsp 70 kDa (hsp70) and hsp90 are some of the most important chaperone proteins related to the stress response. Yet, hsp90 is not only involved in managing protein misfolding but also in functioning as a negative regulator of heat shock factor 1 (HSF-1), which is a transcription factor involved in regulating the expression of heat shock proteins (Sherman & Goldberg, 2001; Zhang,

Y. et al., 2011). Under basal conditions, hsp90 is bound to HSF-1, keeping it inactive (Fig. 4) (Westerheide & Morimoto, 2005; Zhang et al., 2011). When stimulated, HSF-1 and hsp90 will dissociate. Hsp90 will begin regulating protein folding and HSF-1 will cause induction of hsp70 and hsp90 via binding to the heat shock elements (HSEs) and increasing transcription (Jones et al., 2014; Lazaro et al., 2017; Zhang et al., 2011). It is also unclear if HSF-1 can directly increase hsp70 activity (Jones et al., 2014). Stimulation of HSF-1 can also occur via the presence of ROS causing the binding of NRF2 to the ARE, located in the promoter region of HSF-1 and also via an NRF2-independent mechanism (Zhang et al., 2011). Additionally, there has been a number of studies indicating that there are a large number of substances that can induce both NRF2 and hsp70 via HSF-1-dependent mechanisms (Satoh et al., 2015; Zhang et al., 2011).



Schematic 7. Regulation of hsp70 and its ability to modulate protein folding.

Regardless of how these heat shock proteins are activated, it is very evident that in many cases of cell stress or harmful conditions both the cytoprotective pathways of NRF2 and hsp70 are upregulated (Jones et al., 2014; Lazaro et al., 2017; Rinaldi Tosi, Bocanegra, Manucha, Gil Lorenzo, & Vallés, 2011; Zhang et al., 2011). Due to the connections between NRF2, AHR and

HSPs we hypothesized that activation of the antioxidant system could lead to activation of these pathways as well.

Materials and Methods

CYP1A1 Luminescence Protocol

The HepG2 cell line (HB-8065™) was obtained from ATCC. These cells were cultured at 37°C under 5% CO₂ in a complemented (10% FBS, pen-strep 1X) corning EMEM media. Cells were grown in a clear T-25 to about 70% confluency and then transferred to a white bottom 96-well plate. Cells were then administered the appropriate treatment in groups of four. Cells were then allowed to incubate for 20h at 37°C under 5% CO₂. The treatment solution was then aspirated and washed with 50µl of 1X PBS. The media was then aspirated and replaced with 50µl of a 100µM solution of Luciferin-CEE (Promega, USA) in 100% EMEM. Luciferin-CEE is a selective substrate for CYP1A1 that is metabolized to produce luciferin in proportion to the amount of enzymatic activity. HepG2 cells were then incubated for 3h at 37°C under 5% CO₂. Once incubation was complete, 25µl of the media was transferred to a white bottom 96-well plate along with 25µl of Luciferin Detection Reagent, containing the enzyme luciferase. The plate was then incubated at RT for 20min. To assess CYP1A1 activity, a TECAN infinite M200 Pro plate-reader was then used to measure luminescence for each sample. The standard deviation was also calculated for all replicate samples to fall within 10% of the average value.

RT qPCR Protocol

HepG2/NRF2 cells are grown to 70% confluency at 37°C under 5% CO₂ in a T-25. Once confluency was reached, complemented EMEM was replaced and treated in a clear T-25 with the appropriate SFN/KP concentration. A simple dose-response treatment was administered for each compound as well as combination treatment groups. The cells were then allowed to incubate under these conditions for 20h. Upon completion, RNA isolation was performed using 1ml of

TRIzol reagent (per T-25) and transferred to a 1.5ml microfuge tube following the Invitrogen protocol. RNA concentration was then determined using a Thermo Scientific NanoDrop 2000 spectrophotometer. To prepare each sample, 2µg of RNA, 16µl of nuclease-free water, and 4µl of RT reverse transcriptase Supermix (Invitrogen, Carlsbad, CA) were combined in a PCR tube. The thermal cycler was set for 5min priming at 25°C, 20min reverse transcription at 46°C, and 1min RT inactivation at 95°C. To prepare each sample, 2µl of cDNA, 6µl RNase free water, 10µl SYBR Green, and 2µl 10X Primer master mix were combined in a PCR tube. Each sample was then placed into the thermal cycler and subjected to 40 cycles of PCR. The thermal cycler was set to begin with 3min at 95°C and then cycled through intervals of 10sec at 95°C, 10sec at 60°C, 10sec at 72°C, ending with 5sec at 65°C and 95°C. Primers used can be seen in Table 2. These were designed using the DNA sequence based on exons shared by all isoforms (if possible) of the gene. Primer3 (<https://bioinfo.ut.ee/primer3-0.4.0/>) was then used to generate primers that had a product size ranging between 80-140bps. The T_m was set to 60°C, a GC clamp was added, and the GC content range was set to 40-60%.

RT-PCR Protocol

HepG2/NRF2 cells are grown to 70% confluency at 37°C under 5% CO₂ in a T-25. Once confluency was reached, complemented EMEM was replaced and treated in a clear T-25 with the appropriate SFN/KP concentration. A dose-response treatment using the concentrations indicated in the results was performed for each compound as well as combination treatment groups. The cells were then allowed to incubate under these conditions for 20h. Upon completion, RNA isolation was collected using 1ml of TRIzol reagent (per T-25) and transferred to a 1.5ml microfuge tube following the Invitrogen manufacturers protocol. RNA concentration was then

determined using a Thermo Scientific NanoDrop 2000 To prepare each sample, 2µg of RNA, 16µl of nuclease-free water, and 4µl of RT reverse transcriptase Supermix (Invitrogen, Carlsbad, CA) were combined in a PCR tube. The thermal cycler was set for 5min priming at 25°C, 20min reverse transcription at 46°C, and 1min RT inactivation at 95°C. To prepare each sample, 2µg of template DNA was added along with 1µl of Primer (forward), 1µl of Primer (reverse), 21µl nuclease-free water, and 25µl of Taq 2X Master Mix and were combined in a PCR tube. Each sample was then placed into the thermal cycler and subjected to 35 cycles of PCR. The thermal cycler was set to begin with 3min at 95°C and then cycled through intervals of 20sec at 95°C, 30sec at 60°C, 30sec at 72°C, ending with 5min at 72°C. Primers used were as seen in Table 2. These were designed using the DNA sequence based on exons shared by all isoforms (if possible) of the gene. Primer3 (<https://bioinfo.ut.ee/primer3-0.4.0/>) was then used to generate primers that had a product size ranging between 80-140bps. The T_m was set to 60°C, a GC clamp was added, and the GC content range was set to 40-60%.

Agarose Gel Electrophoresis

Amplified PCR products were analyzed by 1.5% agarose gel electrophoresis. The agarose gel consisted of 1X TAE (Genesee Scientific APEX 50X TAE Buffer. Cat #: 20-193) and 1.5% agarose (Genesee Scientific APEX Agarose LE, Quick Dissolve. Cat #: 20-102QD) along with 12µl of 10mg/ml ethidium bromide (EtBr) to give a final concentration of 0.006%. 1Kb+ ladder (Invitrogen) 5µl was loaded along with 10µl of each sample and electrophoresed for 40mins at 150V. Results were visualized using a BioRad ChemiDoc MP Imaging System.

Results and Discussion

Investigation into the potential activation of cytoprotective pathways

As shown previously in Fig. 1.5, it was evident that there was an enhanced activation of the NRF2 pathway as seen in the increased induction of NQO1. Additionally, the luminescence data indicated enhanced activation of the ARE. The data reported in the literature led us to investigate the potential activation of the HSPs and AHR, given that the reported ability of several different compounds induce to NRF2 as well as hsp70, and AHR, quantitative PCR experiments were carried out (Sato et al., 2015; Zhang et al., 2011).

However, the results shown in Fig 2.1 did not indicate activation of hsp70 with either SFN or KP alone or when combined. This failed to support our hypothesis that the induction of NRF2 might lead to increased activation of the heat shock proteins. Despite indications of HSP70 activation through qPCR, it is worth noting that gel analysis was not performed with this primer set and therefore in the absence of a positive control cannot be fully substantiated.

In contrast, the AHR pathway was also evaluated, given the reported connections between the antioxidant gene induction and AHR-dependent pathways, an evaluation of the effects of SFN and KP on the AHR was also evaluated. To probe AHR-dependent induction, RTqPCR experiments were carried out with each pure compound along with the combination of the two. CYP1A1, a classical marker of AHR activity, was used to assess AHR induction (Hayes et al., 2009; Itkin et al., 2020). Figure 2.1 evaluates the induction of CYP1A1 under the same treatment conditions used for ARE activation. The data indicated that SFN alone did not cause any significant induction of CYP1A1. These results are consistent with the literature, given that previous studies have indicated that SFN has the ability to reduce CYP1A1 expression in rat

liver cells, as well as acting as a competitive inhibitor of CYP isoforms (Maheo et al., 1997; Yang et al., 2015; Yin et al., 2016; Zhou et al., 2007). Due to the fact that SFN can negatively regulate CYP1A1 at a transcriptional level, it makes sense that SFN alone does not lead to CYP1A1 induction.

However, 5 μ M KP alone was able to induce CYP1A1. This is a novel finding as KP is a known GSK3 β inhibitor but has not been previously shown to induce CYP1A1 activation of the AHR. The combinations of 5 μ M KP with 4 μ M and 25 μ M SFN respectively continued to show CYP1A1 expression; however, no enhanced activation was observed. Given that SFN negatively impacts CYP1A1 expression these results are consistent with the literature.

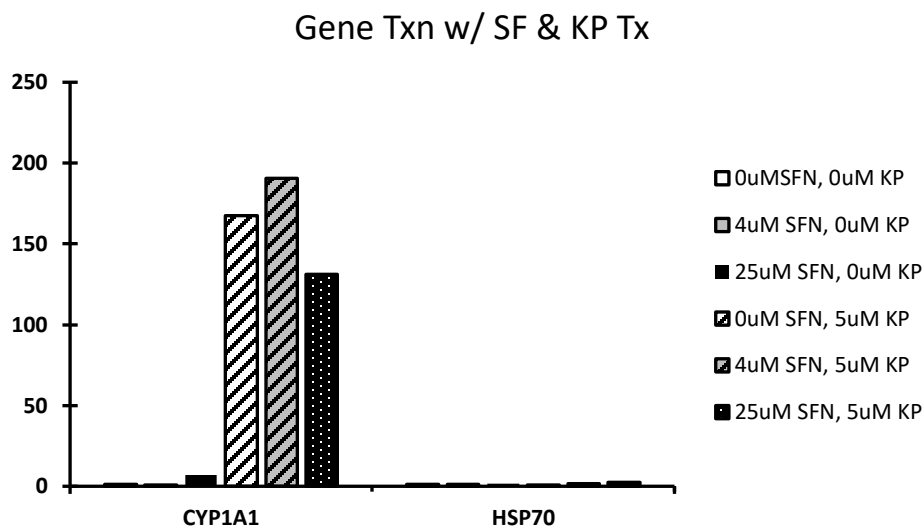


Figure 2.1 RTqPCR fold-induction of HepG2 cell treatment with SFN and KP and analysis of CYP1A1 induction. Normalized to GAPDH and ACTB. These columns were generated based on an n of 1 for each treatment and therefore are not statistically significant.

To confirm the ability of KP to induce CYP1A1 expression, RT PCR was performed, and the products were analyzed by electrophoresis on a 1.5% agarose gel to visualize the data. The data shown in Fig. 2.3 indicates that in the 0 μ M SFN, 0 μ M KP control no induction of CYP1A1 was induced, as expected. However, 5 μ M KP alone was able to cause induction of CYP1A1 167-fold using GAPDH and ACTB as internal controls.

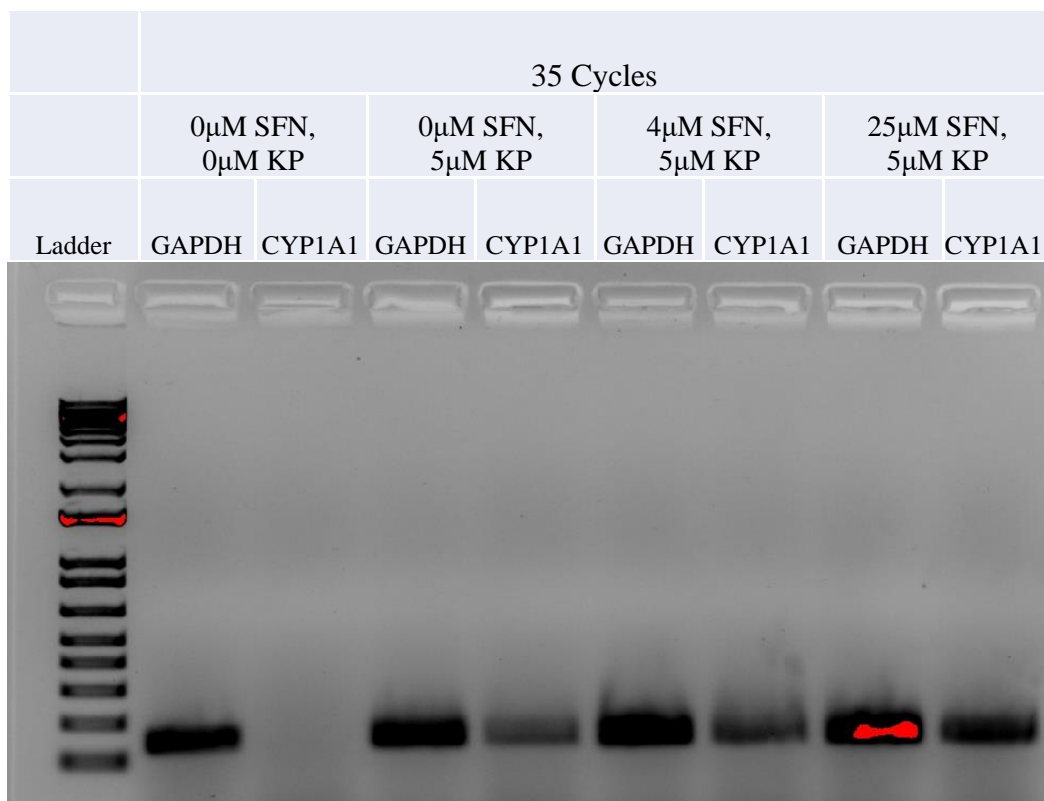
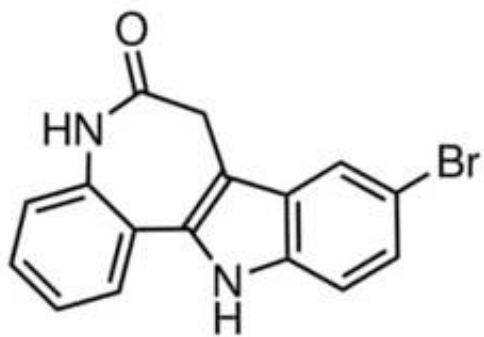


Figure 2.2 1.5% Agarose gel electrophoresis of mRNA RT-PCR analysis of GAPDH (control) and CYP1A1 with various treatment concentrations of SFN and KP. These columns were generated based on an n of 1 for each treatment and therefore are not statistically significant.

The combined data from Fig. 2.1, 2.2, strongly suggests the *novel finding that KP is able to induce the AHR system, leading to increased expression of CYP1A1*. Although the initial hypothesis was that AHR could be activated via increased activation of NRF2, the data does not support this. As shown previously, combined KP and SFN treatments resulted in enhanced activation of the ARE via the NRF2 pathway. However, KP treatment alone appears to activate the AHR without the influence of SFN. This is easily rationalized as a direct binding and activation of KP to the AHR. Since KP is aromatic (Fig. 2.3), this explanation for activation is the simplest and most reasonable.



Kenpaullone

Figure 2.3 Chemical structure of kenpaullone.

Determination of KP dose-response for AHR induction

Given the novel finding that KP has the ability to induce CYP1A1, characterization of this effect was established with a dose-response for CYP1A1 activity. To do so a luminescence assay was used to measure the fold-induction of CYP1A1 after treatment with KP. The data presented in Figure 2.4 suggests that the maximum induction of CYP1A1 occurred at 5 μ M KP resulting in an 8-fold increase compared to the control (p-value <0.001).

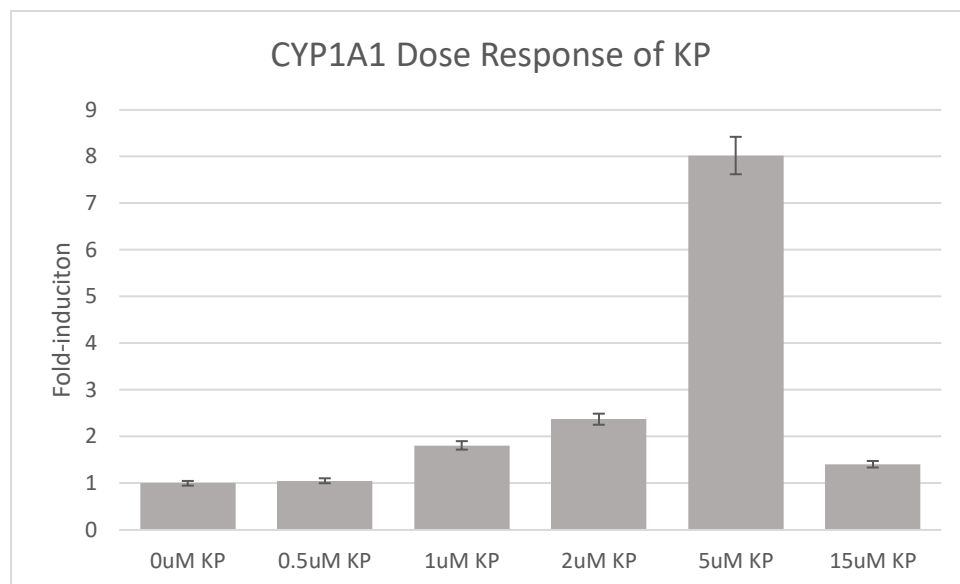


Figure 2.4 Luminescence assay indicating fold-induction of CYP1A1 activity in HepG2 cells treated with KP. Each of these data points were based on four individual samples although not all of the data was not within 10% of the standard deviation.

As an additional control, a known inducer of CYP1A1, β NF, was used to validate the results with KP in this assay. The structure of β NF can be seen in Fig. 2.5. The results shown in Fig. 2.6 indicate that saturation reached a maximum between 10-25 μ M, which is consistent with the literature (Nannelli et al., 2009).

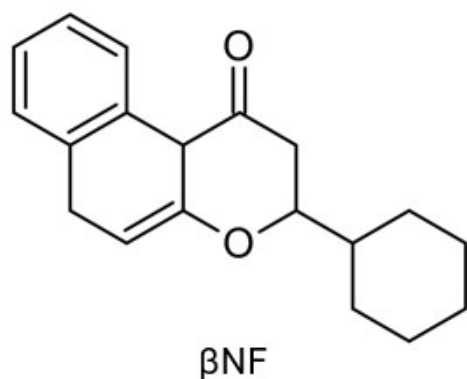


Figure 2.5 Molecular structure of β NF.

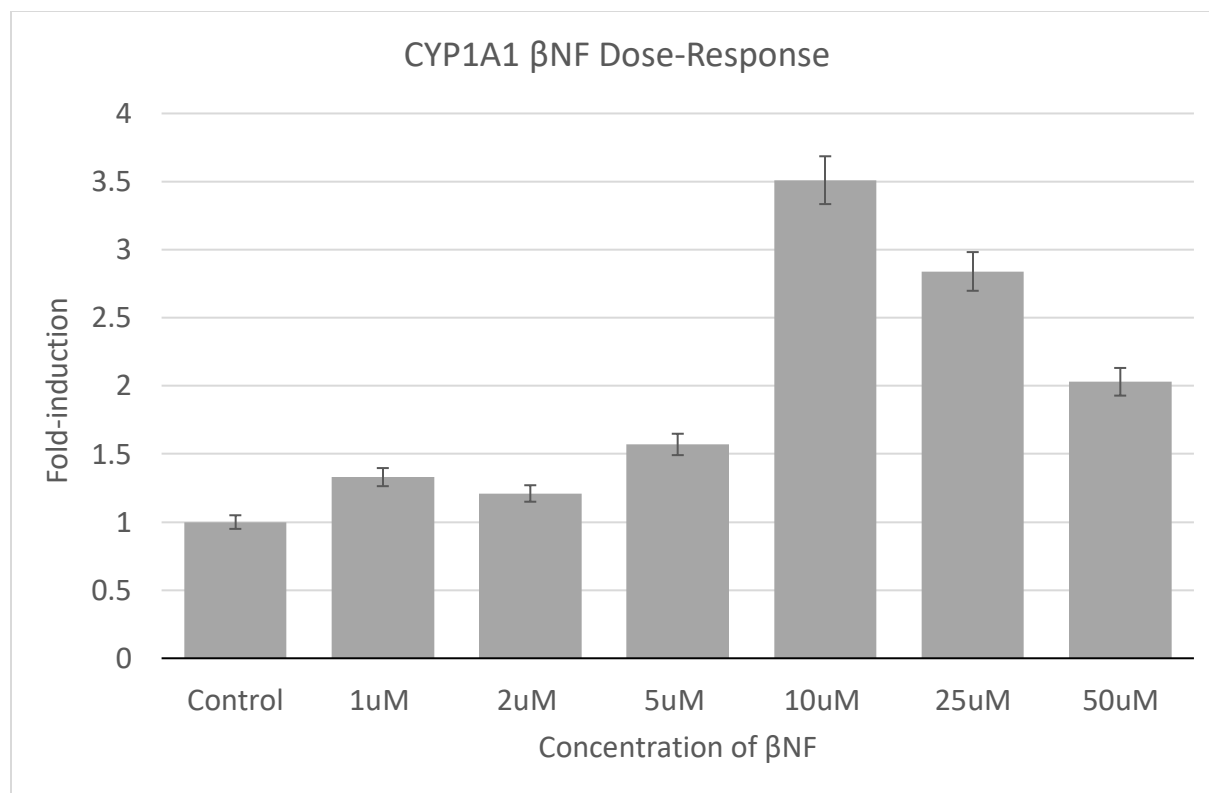


Figure 2.6 Luminescence assay indicating fold-induction of CYP1A1 activity in HepG2 cells treated with β NF. Each of these data points represents the average of at least two individual samples, although the standard deviation of this data was not within 10%.

Although it is likely that KP acts directly by binding to the AHR, a mechanism similar to that observed in ARE activation could not be ruled out. For example, if KP affected a similar delayed response in the AHR pathway, increased activation would also be an expected outcome. To probe this, a known AHR activator, β NF was used in conjunction with KP. The expected result under these conditions would be an enhanced activity of the AHR, similar to what was seen in the dual-target treatment of the ARE. If KP is acting as an inhibitor of the delayed response, there should be an increased fold-induction that is significantly greater than whether KP or β NF individually. However, this is not what was observed in Fig. 2.7. The results of Fig 2.7 demonstrate the expected dose response for β NF (first row), which corresponds to the results of Fig. 2.6. The first column contains the KP dose-response and displayed the same fold-induction seen in Fig. 2.4. The combination of KP and β NF did not appear to lead to enhanced

activation; in fact, it caused the opposite effect – attenuation. This suggests that KP is not acting to inhibit the delayed response but acting as an AHR ligand that is being competitively inhibited. Although 5 μ M KP with 1 μ M β NF did lead to a 6-fold induction, 5 μ M KP alone caused an 8-fold induction and therefore an enhancement of CYP1A1 activity is not observed. Interestingly, increasing concentrations of β NF seemed to attenuate the CYP1A1 induction of KP. It is possible that because β NF is a potent AHR ligand, KP induction of CYP1A1 would become competitively inhibited from activating the AHR via its aromatic structure. When comparing KP and β NF it appears that β NF antagonizes the activity of KP. Another significant result is that KP had the ability to cause a 9-fold induction at 5 μ M, compared to β NF, which generated a 3.5-fold induction at 10 μ M. Therefore, KP seems to be a more effective activation of the AHR than β NF; inducing a greater expression of CYP1A1 at a smaller concentration. Based on the data in this experiment that KP could be a very important compound as it has the ability to behave as a bifunctional activator of AHR and the ARE providing cytoprotective effects for the cell.

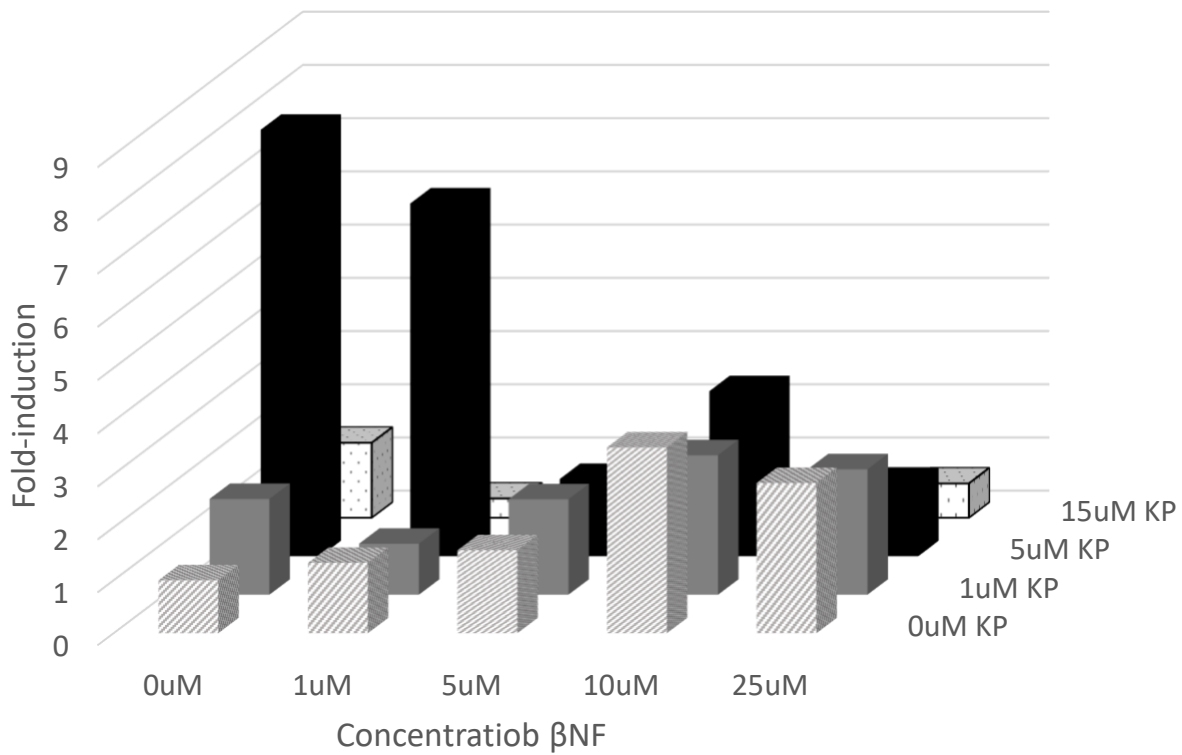


Figure 2.7 Luminescence assay indicating fold-induction of CYP1A1 activity in HepG2 cells treated with β NF and KP. Each of these data points represents the average of at least two individual samples, although the standard deviation of this data was not within 10%.

Conclusion

In conclusion, we found KP to be a novel inducer of CYP1A1 activity. The effective dose response seems to reach a maximum threshold at 5 μ M KP. However, in combination with antioxidant compounds and inducers of the AHR, it does not appear to cause any enhanced activation of CYP1A1. The data presented in Fig. 2.6 indicates that CYP1A1 activity is likely increased due to KP acting as an AHR ligand and not via its inhibition of GSK-3 β in the delayed response of the antioxidant pathway.

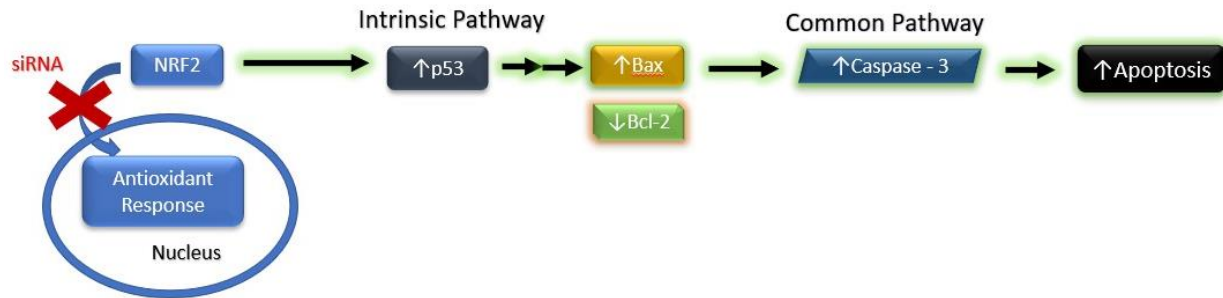
Chapter 3 – Potential Cross-talk between NRF2 and other Cytoprotective Pathways

Introduction

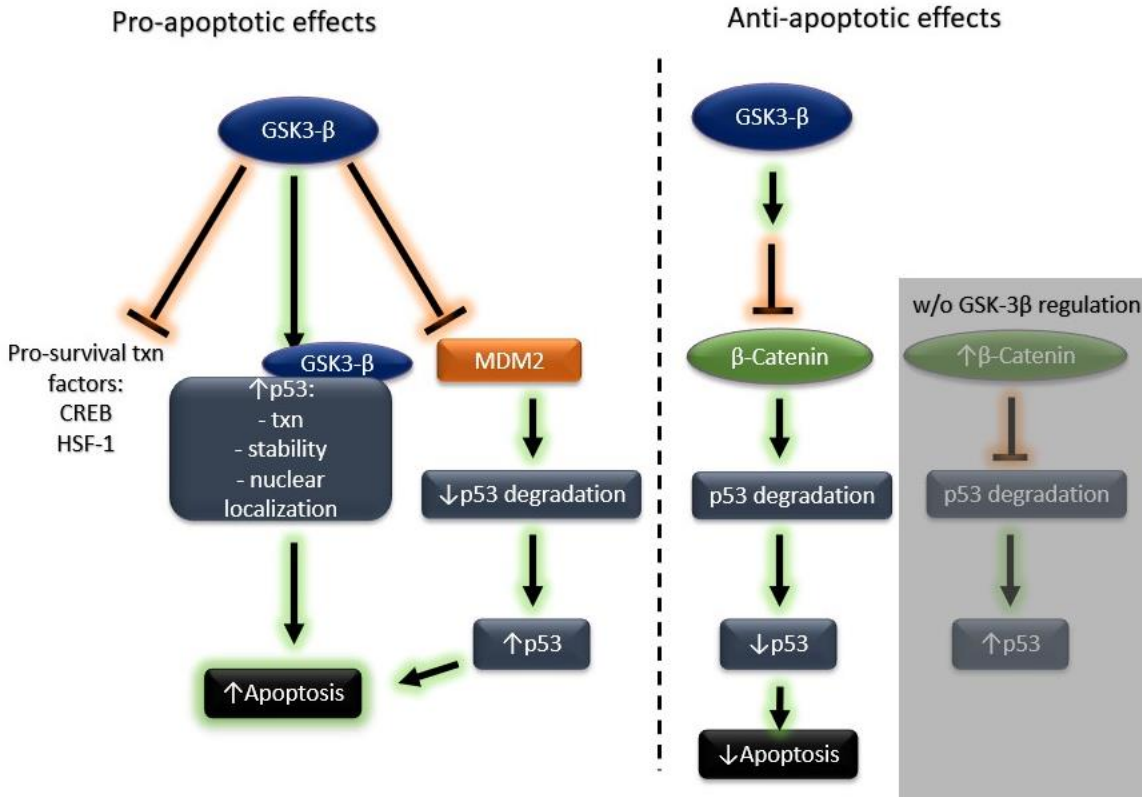
In the previous chapters the activation of NRF2 and AHR, along with HSP70, by compounds and extracts associated with antioxidant action were evaluated. In this chapter, an attempt to rationalize the attenuated ARE activation at high concentrations that were observed in multiple experiments. There has been much data that suggests an overactivation of cytoprotective pathways could lead to the induction of apoptosis. Therefore, it was hypothesized that the attenuation of ARE activation observed in the combined treatment experiments was the result of programmed cell death due to the over-stimulation of the NRF2 pathway.

It is understood that under normal conditions, NRF2 has cytoprotective functions and typically prevents apoptosis and promotes cell survival. This has been evidenced by siRNA knockdown of NRF2 resulting in increased proapoptotic Bax, decreased anti-apoptotic B-cell lymphoma-2 (Bcl-2), and increased caspase-3 cleavage and apoptosis (as seen in Schematic 8) (Lee, Lee, & Lee, 2015). However, GSK-3 β has been shown to not only regulate NRF2 but also to play a role in both cell survival pathways as well as apoptosis. GSK-3 β is suggested to have anti-apoptotic roles under normal conditions via murine double minute 2 homolog (MDM2)-dependent breakdown of p53 (Jacobs et al., 2012). GSK-3 β also has pro-apoptotic roles within the cell. One of the conditions that leads to GSK-3 β facilitation of apoptosis is oxidative stress. GSK-3 β leads to apoptosis by inhibiting cell survival transcription factors including HSF1 and stimulating pro-apoptotic transcription factors including p53 (as seen in Schematic 9) (Grimes & Jope, 2001; Jacobs et al., 2012; Watcharasit et al., 2002). Not only does GSK-3 β promote p53 transcription it also regulates the intracellular localization of p53 (Jacobs et al., 2012). Furthermore, GSK-3 β has been shown to associate directly with p53 and phosphorylate the Ser-

315, and Ser376 positions on p53 and increase the stability of p53 (Jacobs et al., 2012; Pluquet, Qu, Baltzis, & Koromilas, 2005; Qu et al., 2004). Overall, one might rationalize that oxidative stress will induce cytoprotective pathways initially, but at some point, it will switch to triggering apoptosis when the cell is beyond repair.



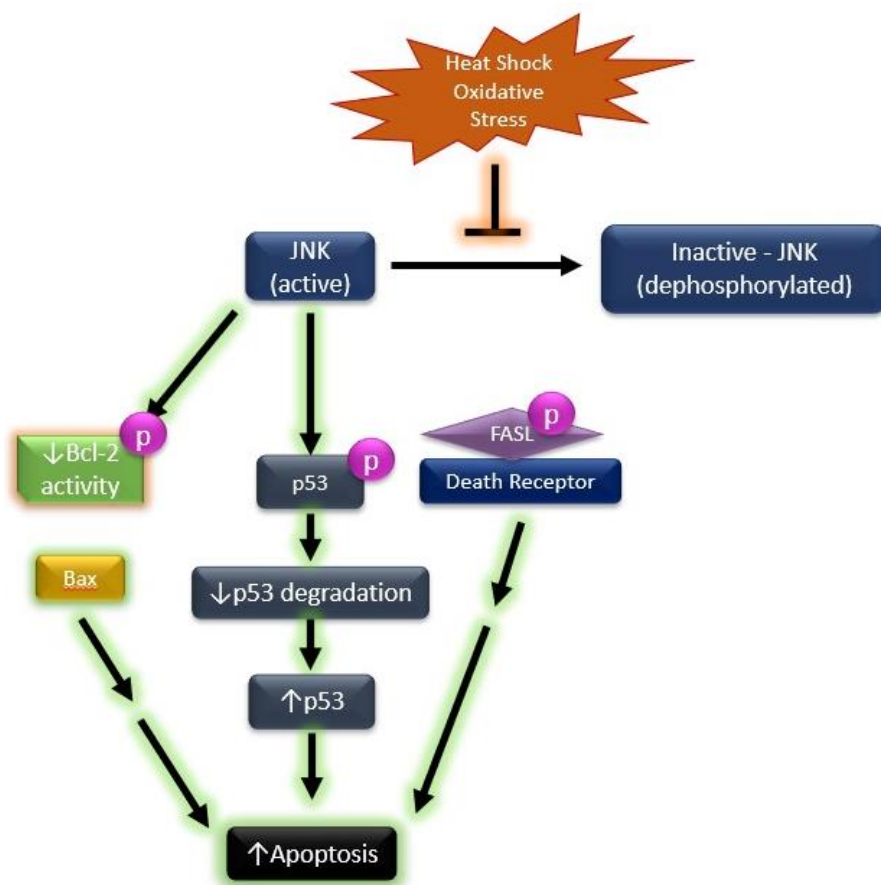
Schematic 8. Effect of siRNA knockdown of NRF2. Results in decreased antioxidant pathway activation. This leads to increased p53, pro-apoptotic Bax, enhanced cleavage of Caspase-3, and decreased anti-apoptotic Bcl-2.



Schematic 9. GSK-3 β Regulation of Apoptosis. The left portion of the schematic depicts mechanisms by which GSK-3 β functions as pro-apoptotic. The cellular conditions ultimately dictate what function active GSK-3 β demonstrates. Under DNA damage, GSK-3 β can inhibit the increase of pro-survival transcription (txn) factors such as cAMP response element binding protein (CREB) and heat shock factor 1 (HSF-1). Active GSK-3 β can also inhibit MDM2, which is responsible for tagging p53 for degradation. The inhibition of MDM2 allows for p53 to accumulate in the cell and induce apoptosis via the intrinsic pathway. Further GSK-3 β can directly increase the transcription of p53, the nuclear localization, and the stability of p53. GSK-3 β when active can bind to the C-terminal region of p53, as well as directly phosphorylate Ser-33, Ser-315, and Ser-376. Increased nuclear localization of p53 could be facilitated by the direct binding of GSK-3 β as well as the increased transcription of specific genes that regulate intracellular localization. The anti-apoptotic effects of GSK-3 β can be facilitated by the downstream negative regulation of β -Catenin, suppressing the inhibitory effect of β -Catenin on p53 degradation, therefore allowing p53 to be degraded.

It has been shown that an overexpression of hsp70 and hsp90 results in the inhibition of apoptosis and hinders caspase activation (Garrido, C. et al., 1999; Garrido, Carmen et al., 2006; Lanneau et al., 2008; Mosser et al., 2000). It also appears that HSPs can prevent both the intrinsic and extrinsic pathways of apoptosis at the pre-mitochondrial level, along with the

mitochondrial and post-mitochondrial levels (Lanneau et al., 2008). However, when HSPs are unable to effectively reduce the accumulation of abnormal proteins to a level that is suitable for cell survival, the accumulation of these abnormal proteins will instead induce programmed cell death (Gabai, Meriin, Yaglom, Volloch, & Sherman, 1998; Sherman & Goldberg, 2001). The mechanism by which this occurs has been well established (and can be seen in Schematic 10). It has been shown that oxidative stress and heat shock function to inhibit the dephosphorylation of c-Jun N-terminal kinase (JNK) (Meriin et al., 1999; Sherman & Goldberg, 2001). Decreased dephosphorylation of JNK results in increased activity of JNK. JNK, when active, has multiple mechanisms by which it can then induce apoptosis. One mechanism is via phosphorylation of the proapoptotic protein p53, therefore reducing its degradation and increasing p53 accumulation (Fuchs, Adler, Pincus, & Ronai, 1998; Sherman & Goldberg, 2001). The second mechanism by which JNK can induce apoptosis is independent of p53. This method involves the phosphorylation of the antiapoptotic proteins B-cell lymphoma 2 (Bcl-2) and B-cell lymphoma-extra large (Bcl-xL) therefore decreasing their activity and allowing apoptosis to progress (Sherman & Goldberg, 2001; Srivastava, Mi, Hardwick, & Longo, 1999). The third way in which JNK is involved in activating apoptosis is by activating the Fas ligand (FASL), which in turn binds to the receptor on the cell and initiates a cascade of events leading to apoptosis (Faris et al., 1998; Faris, Latinis, Kempiak, Koretzky, & Nel, 1998; Sherman & Goldberg, 2001). Therefore, it is clear that there is a relationship between the failure of cytoprotective pathways and the induction of apoptosis.



Schematic 10. Three mechanisms by which JNK can induce apoptosis. Heat shock and Oxidative stress inhibit the inactivation of JNK, allowing it to stimulate apoptosis in three ways. First, by phosphorylating Bcl-2, resulting in decreased anti-apoptotic activity; this allows Bax to progress the intrinsic apoptotic pathway. Second by phosphorylating p53 to prevent its degradation and allow for accumulation and progression of the intrinsic apoptotic pathway. Third, by tagging the FASL to bind to the death receptor and initiate apoptosis via the extrinsic pathway.

As discussed in chapter 2, there are connections between the NRF2 pathway and AHR. However, the AHR has also been identified to have correlations with apoptosis. One study in particular showed that the inhibition of AHR increased apoptotic events (Pollet et al., 2018). Another study investigated the anti-apoptotic role of AHR. It was shown that TCDD interaction with AHR resulted in suppressed induction of apoptosis (Bekki et al., 2015). The mechanisms underlying the anti-apoptotic role of AHR have been studied in more detail but are beyond the scope of this research. Yet it should be noted that AHR disrupts both the intrinsic and extrinsic

signaling of apoptosis (Bekki et al., 2015; Chopra & Schrenk, 2011; Pru et al., 2009).

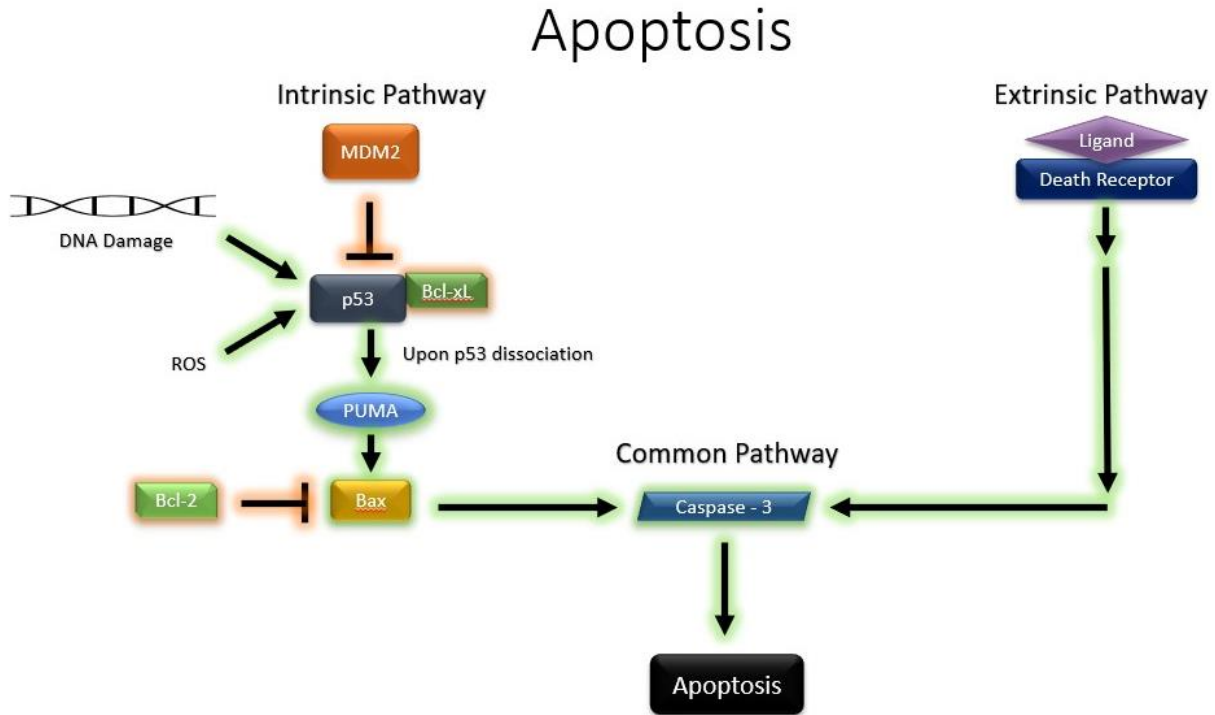
Furthermore, it has been shown that TCDD increased the expression of cyclooxygenase-2 (COX-2) via the activation of AHR (Bekki et al., 2015; Tsujii & DuBois, 1995). COX-2 is a critical enzyme in the inflammation pathway and plays a role in preventing apoptosis (Bekki et al., 2015). Additionally, this is interesting because COX-2 expression is also known to be induced via NRF2-dependent mechanisms (Jessen et al., 2020).

Programmed cell death, otherwise known as apoptosis, is a controlled mechanism for the cell to commit suicide when the cell has been damaged and is beyond repair. Apoptosis can be initiated via two distinct pathways: the extrinsic pathway and the intrinsic pathway. The extrinsic pathway is regulated via ligand binding to the death receptor (Schematic 11) (Kalimuthu & Se-Kwon, 2013; Merlin, Rupasinghe, Dellaire, & Murphy, 2021). One of the ligands responsible for receptor-mediated apoptosis is FASL (Merlin et al., 2021; Sherman & Goldberg, 2001). Upon extrinsic activation, the recruitment and activation of initiator caspases 8 and 10 will begin a series of events that eventually lead to the main executioner caspase 3 (Kalimuthu & Se-Kwon, 2013; Merlin et al., 2021). Caspase enzymes are named for the cysteine proteases in the active site that have the ability to cleave the aspartate residues of proteins (Rai, Tripathi, Sharma, & Shukla, 2005). Increased caspase activity is responsible for the amplification of the apoptotic pathway and irreversible cell death. Caspase 3 is important because it represents the beginning of the execution pathway, which is the final cascade of events that follows both extrinsic and intrinsic mechanisms of apoptotic initiation (Kumar Palai & Ranjan Mishra, 2015). Once caspase 3 is activated the cell will undergo DNA fragmentation, nuclear fragmentation, membrane blebbing as well as other changes, all resulting from programmed cell death (Kalimuthu & Se-Kwon, 2013; Levine, 1997).

The intrinsic pathway, also known as the mitochondrial pathway, is mainly regulated by the transcription factor p53. Under normal conditions, p53 is found at very low levels within the cell and is known as the cellular gatekeeper for growth and division (Kalimuthu & Se-Kwon, 2013; Levine, 1997). Cell cycle progression and DNA repair are regulated by p53 under basal conditions. Yet under stressful conditions and DNA damage, p53 is responsible for initiating the intrinsic apoptotic pathway (Kalimuthu & Se-Kwon, 2013; Merlin et al., 2021). Within the intrinsic pathway, there are a number of proteins within the Bcl-2 family. The most important pro-apoptotic proteins include Bcl-2-associated X protein (Bax) and p53 upregulated modulator of apoptosis (PUMA). Important anti-apoptotic proteins include Bcl-2 and Bcl-xL (Hardwick & Soane, 2013; Merlin et al., 2021; Tsujimoto, 1998). Bcl-2 inhibits apoptosis by regulating the release of cytochrome c from the mitochondria, while Bcl-xL inhibits apoptosis by associating with p53 and preventing apoptotic activity (Dlugosz et al., 2006; Zilfou, Spector, & Lowe, 2005).

MDM2 acts as a negative regulator of p53 via ubiquitination and degradation, however under conditions of cell stress, such as ROS and DNA damage, p53 will become activated and accumulate within the cell (Kalimuthu & Se-Kwon, 2013; Merlin et al., 2021). One of the mechanisms by which p53 accumulates is via the inhibition of the negative regulator MDM2 by GSK-3 β (Jacobs et al., 2012). Increased activity of p53 within the cell will result in the induction of PUMA transcription (Zilfou et al., 2005). Once induced, PUMA then has multiple effects. First, it has the ability to bind to Bcl-xL and allow for p53 to dissociate. Second, PUMA will bind to other anti-apoptotic proteins, ultimately leading to the activation of Bax and the release of cytochrome c from the mitochondria (Kalimuthu & Se-Kwon, 2013; Yu & Zhang, 2008). The activation of p53 will also result in the upregulation of Bax and downregulation of Bcl-2

(Kalimuthu & Se-Kwon, 2013). These events then lead to the activation of caspase 3 and the initiation of the execution pathway for programmed cell death (Merlin et al., 2021).



Schematic 11. The extrinsic and intrinsic model for caspase-3 activation and ultimately apoptosis. The extrinsic pathway is activated via ligand binding to the death receptor and a cascade of subsequent signals that lead to caspase-3 activation. The intrinsic pathway is stimulated by oxidative stress and DNA damage; both of which lead to the activation of p53 and the subsequent proteins involved in activating caspase-3. Upon reaching caspase-3 the remaining steps in the apoptotic pathway are the same for both intrinsic and extrinsic, hence the name “common pathway”. Ultimately programmed cell death is the final result.

Overall, programmed cell death can be modulated through multiple cytoprotective pathways. Oxidative stress can initiate apoptosis via the JNK pathway, GSK-3 β , under the correct conditions, can induce apoptosis, and NRF2 can lead to apoptosis by increasing p53. In light of the connections between cytoprotective pathways and programmed cell death, it was logical to investigate the potential induction of apoptosis. Data previously presented in chapter 1

suggested that at high concentrations of a dual-targeted treatment of HepG2/NRF2 cells that a maximum threshold was reached, and beyond that threshold it appeared to result in an over-stimulation of the ARE reporter – this over-stimulation seemed to lead to attenuation of luciferase activity. Given the data presented in the literature, it is reasonable to hypothesize that apoptosis is induced as the result of an “over-stimulation” of the cytoprotective pathways and that the attenuation of ARE activation at high concentrations could be due to the induction of programmed cell death. This chapter will discuss the results of this investigation.

Materials and Methods

NRF2 ARE Luminescence Protocol

The HepG2/NRF2 cell line is a HepG2 ARE reporter cell line (NRF2 Antioxidant Pathway) and was obtained from BPS Bioscience (Catalog #60513). This cell line contains a firefly luciferase gene under the control of an antioxidant response element (ARE). HepG2/NRF2 cells were cultured at 37°C under 5% CO₂ in a complemented (10% FBS, pen-strep 1X, 0.01% geneticin) corning EMEM media. Cells were grown in a clear T-25 to about 70% confluency and then transferred to an SPL Life Sciences Co., Ltd. DNase/RNase/DNA free (ISO 13485) white bottom 96-well plate. Cells were then administered the appropriate treatment in groups of four following incubation of 20h at 37°C under 5% CO₂. Growth media was aspirated and replaced with 25µl of EMEM with no supplementation. To assess NRF2 activity, 25µl of a luciferase glo assay substrate (Promega, USA) was added to each well. The 96-well plate was then placed on a shaker at 300-500rpm for at least 10min. A TECAN infinite M200 Pro plate-reader was then used to measure luminescence for each well. Quadruplicated values were then averaged and then used to determine fold induction in comparison with the control. The standard deviation was also calculated for all replicate samples to fall within 10% of the average value.

RT qPCR Protocol

HepG2/NRF2 cells are grown to 70% confluency at 37°C under 5% CO₂ in a T-25. Once confluency was reached, complemented EMEM was replaced and treated in a clear T-25 with the appropriate treatment concentration for KP, SFN, BRUS, or appropriate combinations. A simple dose-response treatment was administered for each compound as well as combination treatment groups. The cells were then allowed to incubate under these conditions for 20h. Upon

completion, RNA isolation was performed using 1ml of TRIzol reagent (per T-25) and transferred to a 1.5ml microfuge tube following the Invitrogen protocol. RNA concentration was then determined using a Thermo Scientific NanoDrop 2000 spectrophotometer. To prepare each sample, 2µg of RNA, 16µl of nuclease-free water, and 4µl of RT reverse transcriptase Supermix (Invitrogen, Carlsbad, CA) were combined in a PCR tube. The thermal cycler was set for 5min priming at 25°C, 20min reverse transcription at 46°C, and 1min RT inactivation at 95°C. Next, 2µl of cDNA, 6µl RNase free water, 10µl SYBR Green, and 2µl 10X Primer master mix were combined in a PCR tube. Each sample was then placed into the thermal cycler and subjected to 40 cycles of PCR. The thermal cycler was set to begin with 3min at 95°C and then cycled through intervals of 10sec at 95°C, 10sec at 60°C, 10sec at 72°C, ending with 5sec at 65°C and 95°C. Primers used were as seen in Table 2. These were designed using the DNA sequence based on exons shared by all isoforms (if possible) of the gene. Primer3 (<https://bioinfo.ut.ee/primer3-0.4.0/>) was then used to generate primers that had a product size ranging between 80-140bps. The T_m was set to 60°C, a GC clamp was added, and the GC content range was set to 40-60%.

Apoptosis Caspase Protocol

Caspase-Glo 3/7 assay was obtained (Promega, USA) and used to assess caspase-3 activity. HepG2 cells were treated with various compound combinations in groups of three. Cells were then incubated for 20h at 37°C under 5% CO₂ 96-well plate. Upon the completed treatment time, the supernatant was aspirated and replaced with 25ul of 100% EMEM. To assess caspase activity 25µl of the substrate was added. A TECAN infinite M200 Pro plate-reader was then used to measure luminescence for each well. The entire protocol was followed according to manufacturer specifications.

LDH Assay Protocol

Cell toxicity produced by various treatment groups was measured by lactate dehydrogenase (LDH) leakage into the culture medium. After treatment of HepG2/NRF2 cells, the culture medium was extracted and centrifuged at 3,000 rpm for 5 min in order to take a cell-free supernatant. The LDH activity in the medium was measured using an LDH assay kit (Cayman Chemical Co., Item no 601170). The test is based on the conversion of lactate into pyruvate in the presence of LDH with a parallel reduction of nicotinamide adenine dinucleotide. Creation of NADH and H⁺ from the reaction are used by diaphorase to catalyze the reduction of tetrazolium salt to a highly-colored formazan which absorbs between 490-520nm; the quantity of formazan is proportional to the amount of LDH released into the culture medium. 10µl of Assay Buffer was added to each 96-well and incubated for 1h at 37°C. Aliquots of 75µl supernatant media were transferred to a new transparent 96-well plate. To each well 75ul of LDH Reaction Solution was also added. The reaction mixture was then incubated at 37°C for 30min. Absorbance was set to 490nm and was recorded using a microplate spectrophotometer system TECAN infinite M200 Pro.

Results and Discussion

Investigation into the potential induction of apoptosis

Due to the many correlations between cytoprotective pathways and apoptosis, the following objective was to evaluate the possible activation of apoptosis in scenarios where pathways such as the antioxidant system might be overactivated. For example, induction of the NRF2 pathway using SFN and KP as demonstrated in chapter 1 resulted in initial activation at lower doses, but higher combined dosing caused attenuation of the effect. The results in Fig 3.1 depicts the enhanced induction seen in 4 μ M SFN with 5 μ M KP and the attenuation thereafter at 25 μ M SFN and 5 μ M KP. Therefore, RTqPCR was used for the analysis of NQO1, an ARE-dependent enzyme, and PUMA1, a protein that is upregulated in response to the activation of p53-mediated apoptosis. These were both normalized to GAPDH (see Fig. 3.2). For this experiment, there were six treatment groups for HepG2 cells based on composite data acquired from SFN and KP treatments in chapter 1.

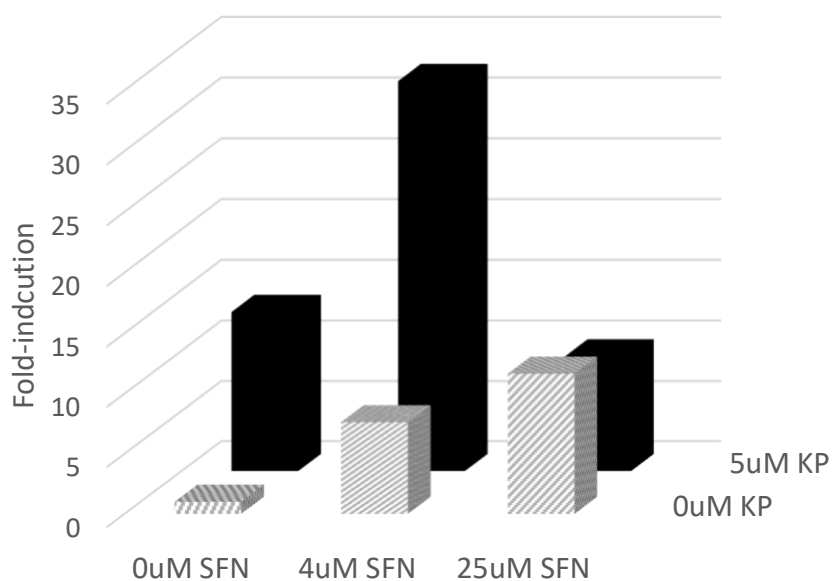


Figure 3.1 Luminescence dose-response of HepG2/NRF2 cells to SFN & KP at 20hrs. Y-axis shows the level of luminescence produced. The X-axis shows the effect of increasing SFN concentrations. Z-axis shows the effect of increasing KP. The standard deviation for each data point was less than 10% +/- of the plotted values. All data points were statistically significant with a p-value <0.01.

The results shown in Fig 3.2 support ARE data found in 3.1 which indicated SFN has the ability not only to increase ARE activation but also the induction of NQO1 in a dose-dependent manner at 4 μ M and 25 μ M SFN, without KP. Likewise, KP alone had the ability to induce NQO1 almost two-fold in comparison to SFN alone. However, in the induction of NQO1, the combined effect at 25 μ M SFN and 5 μ M KP produced an enhanced induction that exceeded either compound alone. This was interesting, because ARE activation of the luciferase reporter at this concentration had the opposite effect, and was decreased, even though there was an activation at lower concentrations. It is possible that this discrepancy is due to the treatment of HepG2 cells

instead of HepG2/NRF2 cells. The other interesting feature of this data lies in the 4 μ M SFN and 5 μ M KP treatment. In the HepG2/NRF2 treated cells, the ARE assay indicated enhanced activation, while here it appeared that there is a decreased production of NQO1; although this could be explained by the sample size of one. Each qPCR treatment group is represented by RNA isolation from 1 T-25. Although each T-25 was seeded homogenously, it is possible that the lack of statistical data for this point is the reason a decrease in NQO1 induction is observed. Regardless, the treatments appeared to induce NQO1 expression relative to controls, at least suggesting a proof of concept.

The effects of the combined treatment of SFN and KP on PUMA expression was also evaluated. Of the four isoforms of PUMA found in humans, the PCR primer was designed to bind to three of the four variants. Interestingly, Fig. 3.2 seemed to indicate that there was some induction of apoptosis at 4 μ M SFN alone and minimal induction in all other treatment groups. In fact, at high SFN and all combined treatments PUMA was actually down-regulated considerably. This failed to directly support our hypothesis as it was originally presented that PUMA1 would be highest at 25 μ M SFN and 5 μ M KP given the attenuation observed in the ARE activation. However, the data does not contradict our hypothesis either. We predicted that an over-activation of the antioxidant system would result in a negative-feedback that attenuates the cytoprotective pathway and activates the apoptotic system. The qPCR data shown in Fig. 3.2 did not show the same over-activation seen in the luminescence data, based on the NQO1 expression profile, therefore increased induction of PUMA would not be expected as the qPCR data did not suggest that a high enough threshold was reached to trigger apoptosis and shut down the antioxidant system. However, because the luminescence data was done in a HepG2/NRF2 cell line and the

RNA isolation and PCR was performed using HepG2 cells, a follow-up experiment was done in the HepG2/NRF2 cell line, in order to identify potential cell line differences in behavior.

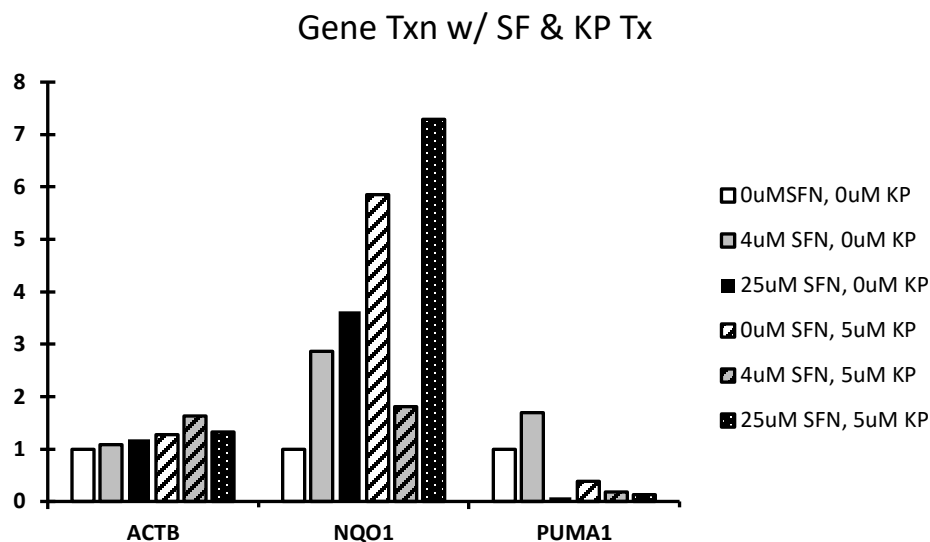


Figure 3.2 RTqPCR fold-induction of HepG2 cell treatment with SFN and KP and analysis of NQO1 and PUMA1 induction. Normalized to GAPDH. These columns were generated based on an n of 1 for each treatment and therefore are not statistically significant.

The experiment was repeated with the HepG2/NRF2 cell line under the same conditions.

Fig. 3.3 indicates that there was less NQO1 activation in the HepG2/NRF2 cell line than the HepG2 cell line resulting in a maximum of a 3-fold induction instead of a 7-fold induction. Despite the quantitative difference between the two cell lines, the qualitative results between both experiments were consistent. Again, attenuation of expression for NQO1 was not observed under the combined high-dose conditions. As with the HepG2 cells, the data shown in Fig. 3.3 did not indicate an increase in PUMA1 compared to the control in the HepG2/NRF2 cell line. In fact, reduced expression of PUMA1 was observed.

Overall, neither cell line resulted in the expected result of apoptosis activation under conditions that had previously been shown to over-activate the antioxidant pathway in the ARE reporter system. Yet, because the NQO1 data did not reach a threshold level, this data does not

contradict the hypothesis, as both cell lines (Fig 3.2, 3.3) demonstrated induction of NQO1 with no attenuation. This indicates the cytoprotective mechanism being initiated in both cell lines and under such conditions, apoptosis would not be expected. Supporting this idea is the apparent inverse relationship between NQO1 and PUMA induction, the 7-fold increase in NQO1 in HepG2 cells almost completely eliminates PUMA expression, while the more modest induction in HepG2/NRF2 cells has a minimal effect on PUMA.

Although a loose correlation between NQO1 and PUMA expression was observed, there are many questions that remain unanswered. Most importantly, the NQO1 data using RTqPCR did not reproduce the observed attenuation seen in the luciferase reporter system, thus the apoptotic markers would also not be expected, even if the two were related.

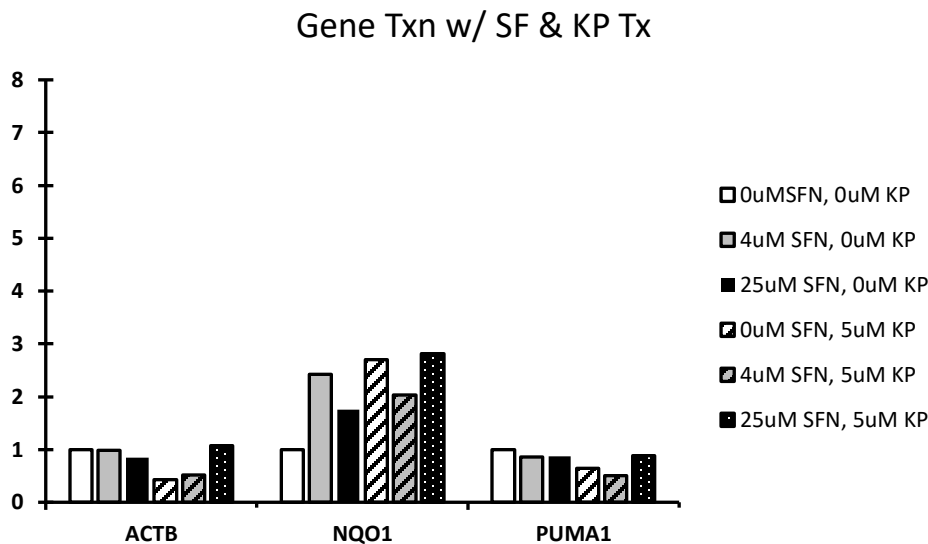


Figure 3.3 RTqPCR fold-induction of HepG2/NRF2 cell treatment with SFN and KP and analysis of NQO1 and PUMA1 induction. Normalized to GAPDH. These columns were generated based on an n of 1 for each treatment and therefore are not statistically significant.

Due to the unexpected results, attempts to validate our data regarding PUMA1 were carried out. To do this, RTPCR was performed and the results were analyzed using a 1.5% agarose gel to ensure proper primer functioning in the assays. The results in Fig. 3.4 indicate that

GAPDH control, as well as NQO1, did result in the expected pattern of induction. Due to the absence of a band for PUMA1, the data from the RTqPCR were not validated for this gene.

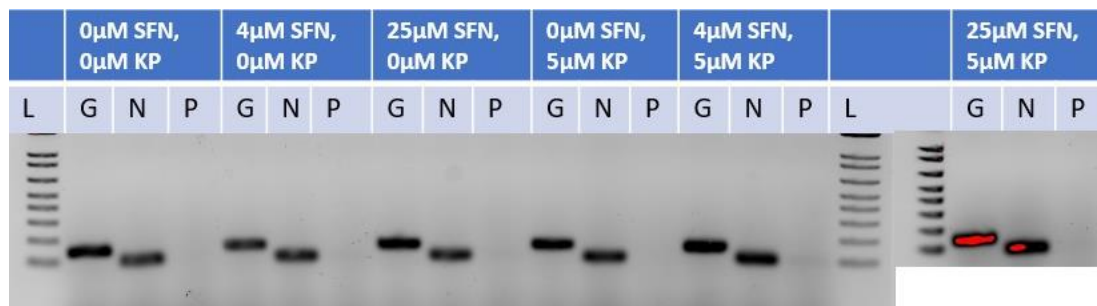


Figure 3.4 RT-PCR of HepG2/NRF2 cell treatment with SFN and KP and analysis of GAPDH, NQO1, and PUMA1 induction. Abbreviations used are as follows, G: GAPDH; N: NQO1; P: PUMA1. These bands were generated based on an n of 1 for each treatment and therefore are not statistically significant.

However, a subsequent experiment using the combination of Sab and KP was also performed using RT-PCR and gel analysis. The data in Fig. 3.5 suggests that our PUMA1 primer did work properly and expression was highest under control conditions, as indicated in the RTqPCR experiments. It appears that both 0.005% and 0.05% Sab did increase NQO1 induction, as did 5μM KP. This data confirms what was observed in the ARE luminescence data, regarding the activation of ARE by Sab and KP. The PUMA data, once again, suggests these treatments reduce PUMA expression rather than induce expression. It appears there is some PUMA activity with 0.005% Sab and 15μM KP. However, the highest concentration of 0.05% Sab and 15μM KP, which was originally predicted to have the greatest induction of apoptosis, based on luciferase data, instead had decreased PUMA1. Taken together, this data does not contradict the stated hypothesis, given that no attenuation was achieved. Presumably, because an over-activation threshold was not reached, in which case apoptosis would not be expected. However, the data does support a model where NRF2 activation causes a reduction of p53 activity.

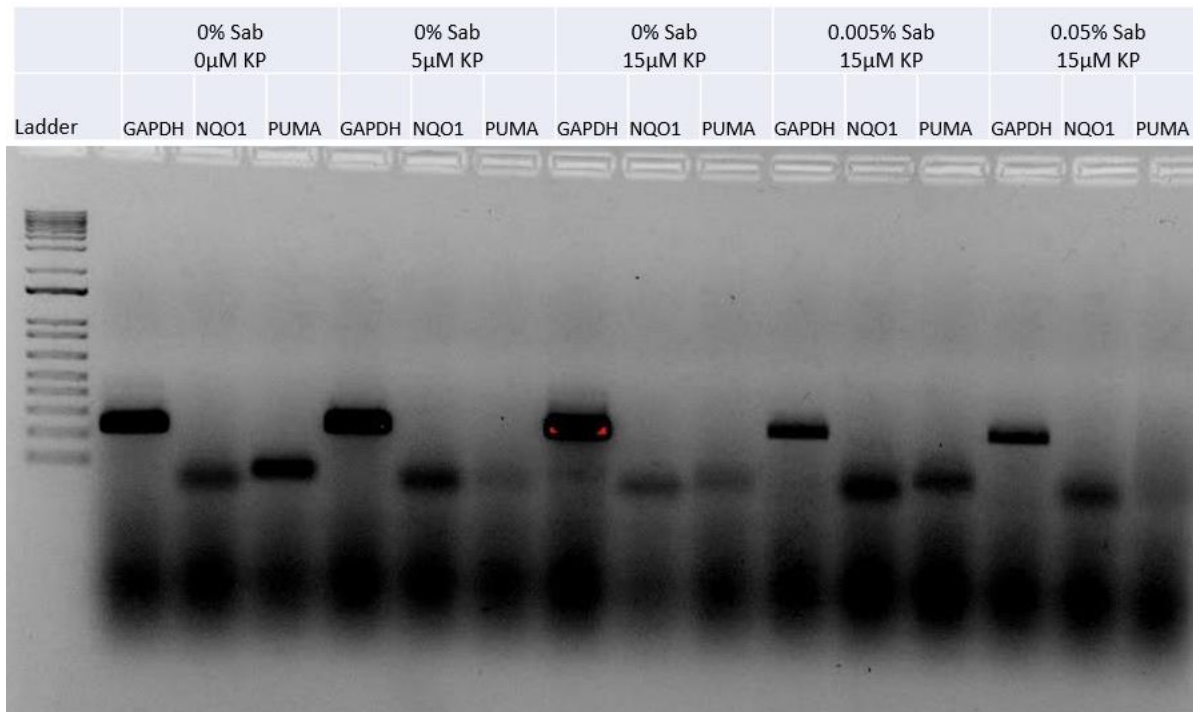


Figure 3.5 RT-PCR of HepG2/NRF2 cell treatment with Sab and KP and analysis of GAPDH, NQO1, and PUMA1 induction. These bands were generated based on an n of 1 for each treatment and therefore are not statistically significant.

It is possible that the lack of observed attenuation in the qPCR could be due to the format in which these experiments were carried out. For example, qPCR experiments were performed in a T-25, as opposed to the 96-well plate platform used for luminescence. As an alternative attempt to monitor apoptosis in HepG2/NRF2 cells in the 96-well format, the SFN and KP combination was again used to evaluate caspase-3 induction via a luminescence assay, as caspase-3 is a downstream marker of apoptosis. Fig. 3.6 indicates that in the presence of just 15 μ M KP, there was a 3-fold induction of caspase-3, however, in the presence of SFN, that induction was attenuated. This suggests that SFN has a protective effect against programmed cell death. The fact that KP could induce apoptosis alone, at the highest concentration is consistent with the variable results observed in the ARE reporter system where at times 15 μ M KP did cause attenuation. Further, the fact that SFN appeared to protect against apoptosis would suggest that KP alone was the cause, possibly through off-target effects rather than overactivation of the ARE

as KP has been shown to have a small effect on the induction of apoptosis (Kitabayashi et al., 2019). To further probe the source of the attenuation effect observed with SFN and KP, an additional experiment using a positive control was carried out involving the compound BRUS which is a suspected proapoptotic compound (Ye et al., 2018).

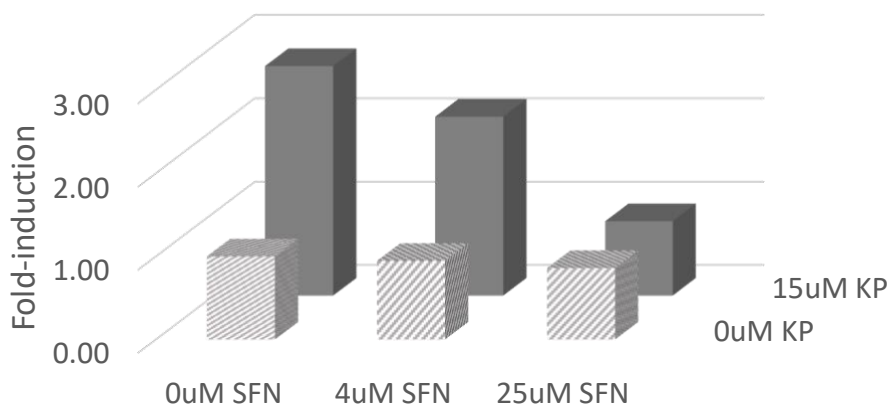


Figure 3.6 Caspase Luminescence assay demonstrates the pattern of ARE induction with varying concentrations of SFN and KP. A) Y-axis shows the level of luminescence produced. The X-axis shows the effect of increasing SFN concentrations. Z-axis shows the effect of increasing KP. Each of the data points represents the average of three individual samples and is within 10% of the standard deviation.

Brusatol Induction of Apoptosis

Brusatol (BRUS) was used as a positive control, as it is a known inducer of apoptosis (Ye et al., 2018). Initially, BRUS was used in the luciferase reporter system to assess its effects on the ARE reporter, with results shown in Fig. 3.7. This data indicates that alone, BRUS does not appear to cause a significant decrease in ARE activation in HepG2/NRF2 cells on its own. There was a modest reduction of 2-fold at 5 μ M BRUS. This may suggest that the activation of apoptosis attenuates the ARE activation. While it is a known inducer of apoptosis, BRUS has also been

shown to have the ability to inhibit NRF2. Therefore, it could cause attenuation of the ARE activation due to its interaction with the antioxidant pathway (Cai, Liu, Han, & Yang, 2019; Ye et al., 2018). However, despite the expected increase in ARE activation in response to the dose-dependent administration of KP, BRUS showed a dose-dependent attenuation of the ARE activation. This is represented in the back row of data in Fig. 3.7, where KP at 15 μ M produced a 4-fold induction of luciferase. Increasing BRUS from 0.2 μ M to 5 μ M resulted in a steady reduction of the ARE reporter activity producing an approximately 10-fold reduction in signal compared to control in the high dose combined treatment, and a more than 40-fold reduction compared to KP alone. The near complete inactivation of the ARE at 5 μ M BRUS and 15 μ M KP is similar to the type of decreased luminescence response seen in the maximum concentrations of overactivated AREs as seen in the earlier experiments using SFN and KP, Sab and KP, TFHQ and KP, along with BROCC and KP, CAS and KP.

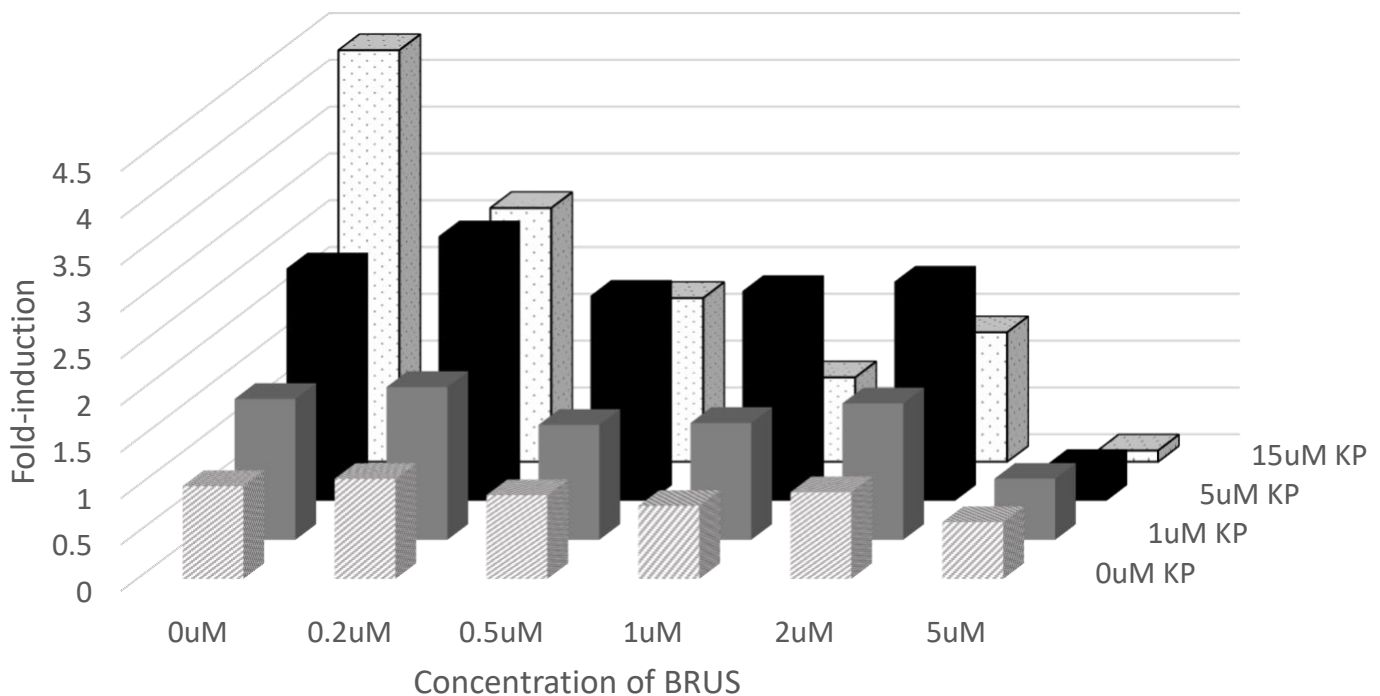


Figure 3.7 Luminescence assay demonstrates the pattern of NRF2 induction with varying concentrations of BRUS and KP. Y-axis shows the level of luminescence produced. The X-axis shows the effect of increasing BRUS concentrations. Z-axis shows the effect of increasing KP. Each of the data points represents the average of three individual samples and is not within 10% of the standard deviation.

Having established that BRUS decreased activation of the ARE in HepG2/NRF2 cells, subsequent studies using the primers made to evaluate apoptosis RTqPCR experiments were carried out to confirm if the apoptosis marker PUMA responded to BRUS treatment alone or in combination. This would help answer the question of whether or not BRUS is acting as an inducer of apoptosis or an inhibitor of NRF2 in these conditions. Fig. 3.8 indicates the results of BRUS and KP treatment groups in HepG2/NRF2 cells using RTqPCR. In this treatment setup, it appeared that BRUS does attenuate the induction of NQO1, but only in combination with KP, which is consistent with the ARE reporter data. Without KP there was a slight induction of

NQO1 up to 2-fold in the presence of 5 μ M BRUS, the mechanism by which this could occur is unknown.

Interestingly, when testing for PUMA1, there was only a 3-fold induction in the presence of 5 μ M BRUS and 15 μ M KP. To further investigate, another primer, for the fourth isoform of PUMA in human cells was designed and named PUMA2. Data with this primer indicated up to 13-fold activation of PUMA with BRUS and KP combinations. The qualitative results given in Fig. 3.8 indicated that BRUS and KP do in fact trigger apoptosis based on reduced NQO1 and increased PUMA.

This does not eliminate the possibility that BRUS utilizes another mechanism to inhibit ARE activation as BRUS has also been reported to be a specific inhibitor of NRF2 directly (Cai et al., 2019; Yu, Shang, Huang, Yao, & Song, 2020). It does, however, confirm that apoptosis is being activated. Perhaps at the highest concentrations is not just apoptosis activated, but the antioxidant system is deactivated as well. This would support the hypothesis that at higher concentrations or overactivations of cytoprotective pathways through some form of cross-talk could be shut down to allow for programmed cell death to take place.

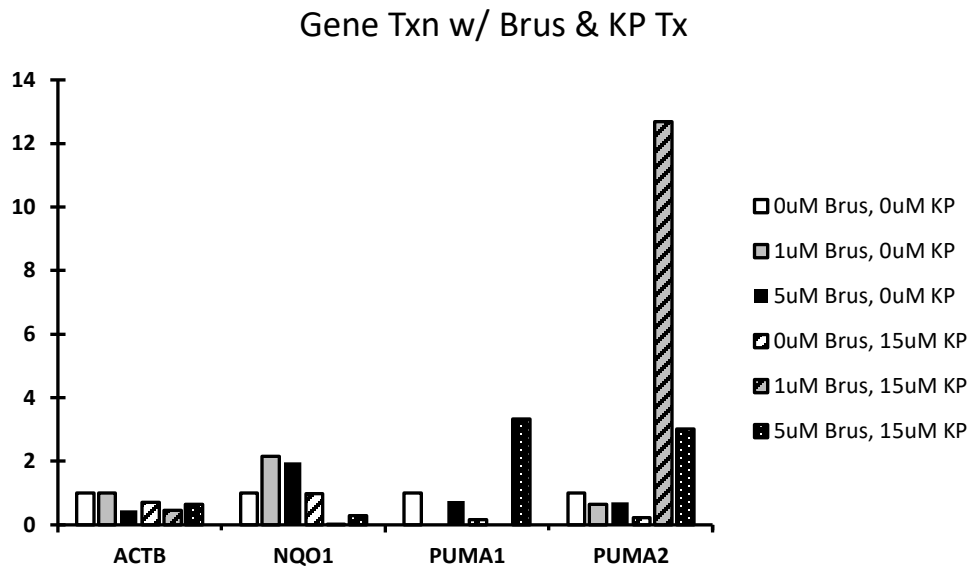


Figure 3.8 RTqPCR fold-induction of HepG2/NRF2 cell treatment with BRUS and KP and analysis of ACTB, NQO1, PUMA1, and PUMA2 induction. Normalized to GAPDH. These columns were generated based on an n of 1 for each treatment and therefore are not statistically significant.

In addition to performing RTqPCR, the evaluation of apoptotic activity was assessed using a caspase-3 luminescence assay. Fig. 3.9 shows that KP did have a modest induction of caspase-3 which is consistent with the data presented in Fig. 3.8. Further, it showed BRUS alone did not induce caspase activity. It was originally thought that caspase-3 induction would have increased in a dose-dependent manner with increasing concentrations of BRUS, and yet it had a modest reduction in caspase-3 activity. However, it did generate increased caspase-3 activity in the presence of KP. These results are also consistent with the data presented in Fig. 3.8.

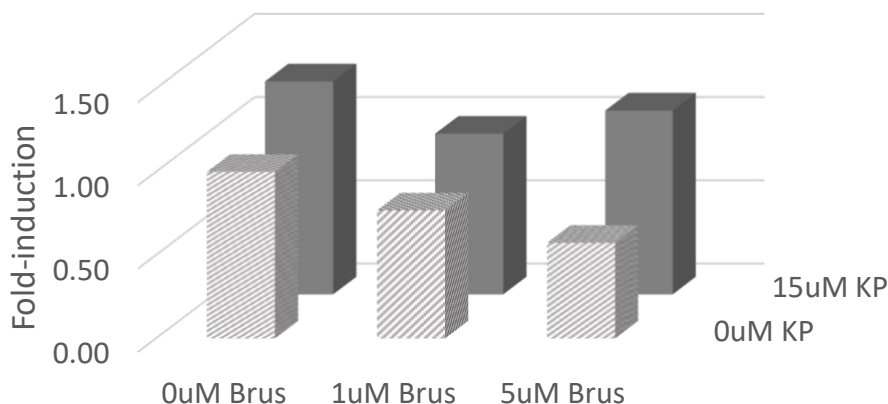


Figure 3.9 Caspase Luminescence assay demonstrates the pattern of ARE induction with varying concentrations of BRUS and KP. Y-axis shows the level of luminescence produced. The X-axis shows the effect of increasing BRUS concentrations. Z-axis shows the effect of increasing KP. Each of the data points represents the average of three individual samples and is not within 10% of the standard deviation.

Overall, it appears that BRUS by itself does not increase markers for apoptosis. However, at 15 μ M KP apoptosis is slightly stimulated and this effect can be enhanced by BRUS. In other words, BRUS appears to sensitize the cells to KP-induced apoptosis. The data also suggests that attenuated ARE activity observed with SFN and KP treatments, as well as other antioxidant combinations, may not be apoptosis-related.

Investigation into the potential induction of necrosis

An alternative explanation for the attenuation seen in ARE activity is that at high concentration combinations the cell experiences non-programmed cell death. Therefore, it was relevant to investigate the possibility of necrotic activity. To evaluate necrosis an LDH luminescence assay was used. Fig 3.10A indicates that in the presence of SFN and KP there is no more necrosis than compared to the control. Triton X was the positive control indicating increased LDH and necrosis. Fig. 3.10B evaluated the prevalence of necrosis with BRUS and KP. This data suggests

there was about a 20-25% increase in necrosis with the highest combination of 5 μ M BRUS and 15 μ M KP compared to the control. However, this data did not produce a strong necrotic response, which suggests that of the two mechanisms for cell death, apoptosis is more likely to be occurring than necrosis.

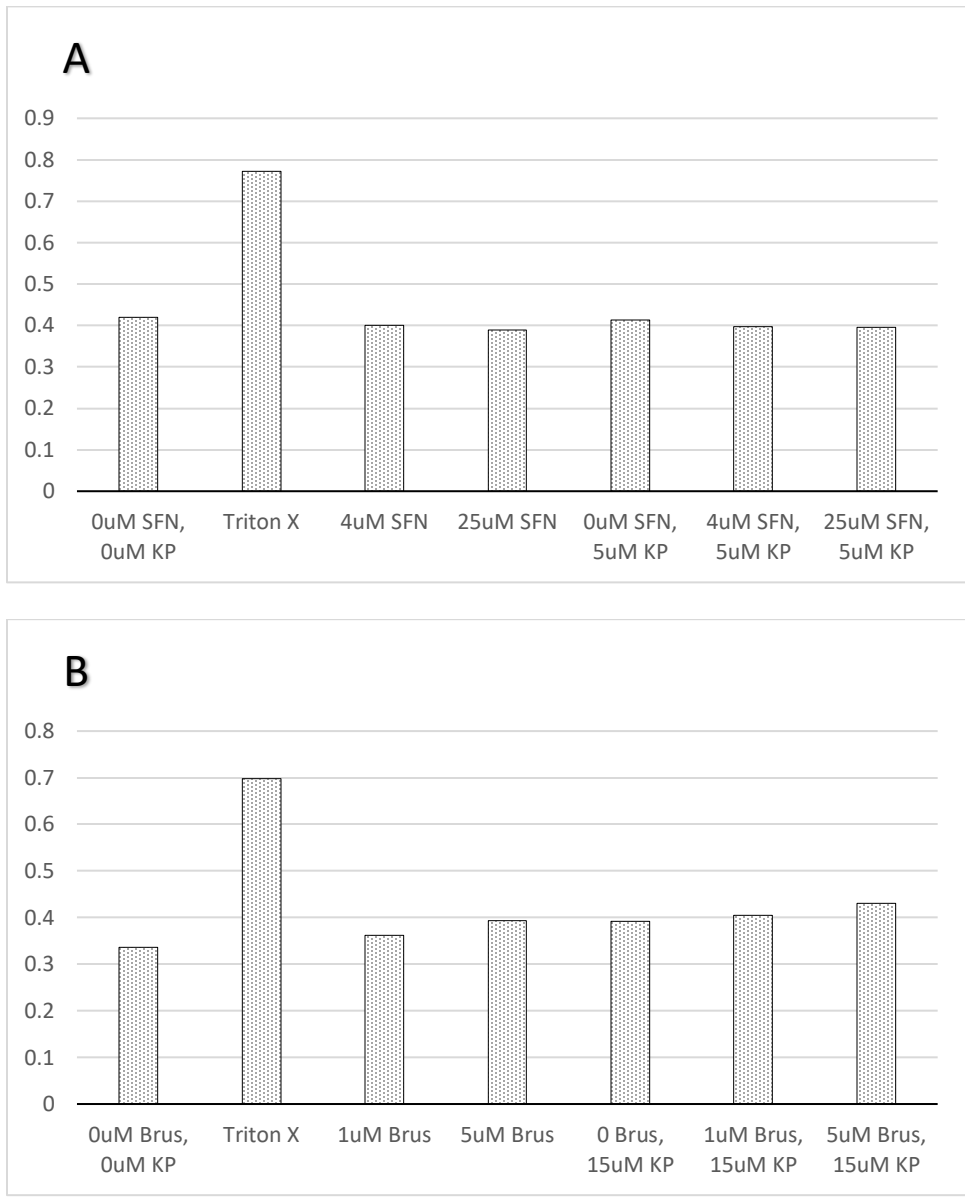


Figure 3.10 LDH assay assessing necrosis prevalence A) with various treatment combinations of SFN and KP. B) with BRUS and KP. For both graphs Triton X is the positive control, 0 μ M SFN and 0 μ M KP is the negative control. Each of the data points represents the average of three individual samples and is within 10% of the standard deviation.

Conclusion

In summary, the results of this chapter indicate that the combination treatments of SFN and KP, as well as Sab and KP, induced an increase of NQO1, suggesting that the antioxidant system is being enhanced in the coordinated treatments. This data supports the hypothesis of enhanced activity of the antioxidant system through a coordinated approach. However, the qPCR, RT-PCR, and caspase-3 results from ARE activating combinations (Fig 3.2, 3.3, 3.4, 3.5,3.6) did not indicate attenuation at high concentrations, as seen in the ARE reporter system. Additionally, it was originally thought that the antioxidant-inducing combinations would lead to apoptosis when the cytoprotective system of the cell reaches threshold and becomes over-activated. However, this effect was not seen. This is likely because in the qPCR and RT-PCR experiments over activation and attenuation of the antioxidant system were never achieved. Therefore, the hypothesis that over-activation of the NRF2 pathway could induce apoptosis is still possible.

While BRUS has the ability to function as an inducer of apoptosis, it also has the ability to inhibit NRF2 activity (Cai et al., 2019; Ye et al., 2018). Based on this dual function, the attenuation in the ARE reporter system with the treatment of BRUS and KP could be the result of either mechanism. After further evaluation of whether or not apoptosis was being induced by BRUS, it appears that BRUS has a modest effect on PUMA induction but not on caspase-3 in the HepG2/NRF2 cell line. Further, it appears that in the presence of KP, BRUS enhances the induction of PUMA and caspase-3. The mechanism by which this occurs is not fully understood. Lastly, the combination of ARE inducers did not lead to necrosis. Therefore, it is more probable that under over-activation of the antioxidant system apoptosis would be induced, as this explanation is consistent with the literature (Kapuy et al., 2018; Matsuoka & Yashiro, 2014; Paladino et al., 2018; Romorini et al., 2016).

References

- A Lusska, E Shen, & J P Whitlock, J. (1993). Protein-DNA interactions at a dioxin-responsive enhancer. analysis of six bona fide DNA-binding sites for the liganded ah receptor. *The Journal of Biological Chemistry*, 268(9), 6575-6580. doi:10.1016/S0021-9258(18)53289-0
- Andelová, H., Rudolf, E., & Cervinka, M. (2007). In vitro antiproliferative effects of sulforaphane on human colon cancer cell line SW620. *Acta Medica (Hradec Kralove)*, 50(3), 171-176. Retrieved from <https://pubmed.ncbi.nlm.nih.gov/18254269/>
- BAIN, J., McLAUHLAN, H., ELLIOTT, M., & COHEN, P. (2003). The specificities of protein kinase inhibitors: An update. *Biochemical Journal*, 371(1), 199-204. doi:10.1042/bj20021535
- Baird, L., & Yamamoto, M. (2020). The molecular mechanisms regulating the KEAP1-NRF2 pathway. *Molecular and Cellular Biology*, 40(13), 99.
- Bekki, K., Vogel, H., Li, W., Ito, T., Sweeney, C., Haarmann-Stemmann, T., . . . Vogel, C. F. A. (2015). The aryl hydrocarbon receptor (AhR) mediates resistance to apoptosis induced in breast cancer cells. *Pesticide Biochemistry and Physiology*, 120, 5-13. doi:10.1016
- Benzie, I. F. F., Wachtel-Galor, S., & Packer, L. (2011). *Herbal medicine*. Baton Rouge: CRC Press. doi:10.1201/b10787 Retrieved from <https://www.taylorfrancis.com/books/9781439807163>
- Boo, Y. C. (2020). Natural Nrf2 modulators for skin protection. *Antioxidants*, 9(9), 9. doi:10.3390/antiox9090812

- Brieger, K., Schiavone, S., Miller, F. J., & Krause, K. -. (2012). Reactive oxygen species: From health to disease. *Swiss Medical Weekly*, *142*, w13659. doi:10.4414/smw.2012.13659
- Briolotti, P., Chaloin, L., Balaguer, P., Da Silva, F., Tománková, V., Pascussi, J., . . . Gerbal-Chaloin, S. (2015). Analysis of glycogen synthase kinase inhibitors that regulate cytochrome P450 expression in primary human hepatocytes by activation of β -catenin, aryl hydrocarbon receptor and pregnane X receptor signaling. *Toxicological Sciences: An Official Journal of the Society of Toxicology*, *148*(1), 261-275. doi:10.1093/toxsci/kfv177
- Cadenas, E., & Davies, K. J. (2000). Mitochondrial free radical generation, oxidative stress, and aging. *Free Radical Biology & Medicine*, *29*(3-4), 222-230. doi:10.1016/s0891-5849(00)00317-8
- Cai, S. J., Liu, Y., Han, S., & Yang, C. (2019). Brusatol, an NRF2 inhibitor for future cancer therapeutic. *Cell & Bioscience*, *9*(1), 45. doi:10.1186/s13578-019-0309-8
- Chen, X., Liu, Y., Zhu, J., Lei, S., Dong, Y., Li, L., . . . Zhao, Y. (2016). GSK-3 β downregulates Nrf2 in cultured cortical neurons and in a rat model of cerebral ischemia-reperfusion. *Scientific Reports*, *6*(1), 20196. doi:10.1038/srep20196
- Chopra, M., & Schrenk, D. (2011). Dioxin toxicity, aryl hydrocarbon receptor signaling, and apoptosis—Persistent pollutants affect programmed cell death. *Critical Reviews in Toxicology*, *41*(4), 292-320. doi:10.3109/10408444.2010.524635
- Clarke, J. D., Hsu, A., Williams, D. E., Dashwood, R. H., Stevens, J. F., Yamamoto, M., & Ho, E. (2011). Metabolism and tissue distribution of sulforaphane in Nrf2 knockout and wild-type mice. *Pharmaceutical Research*, *28*(12), 3171-3179. doi:10.1007/s11095-011-0500-z

- Cornejo, P., Vargas, R., & Videla, L. A. (2013). Nrf2-regulated phase-II detoxification enzymes and phase-III transporters are induced by thyroid hormone in rat liver. *BioFactors (Oxford, England)*, 39(5), 514-521. doi:10.1002/biof.1094
- Das, K., & Roychoudhury, A. (2014). Reactive oxygen species (ROS) and response of antioxidants as ROS-scavengers during environmental stress in plants. *Frontiers in Environmental Science*, 0 doi:10.3389/fenvs.2014.00053
- Demuro, S., Di Martino, R. M. C., Ortega, J. A., & Cavalli, A. (2021). GSK-3 β , FYN, and DYRK1A: Master regulators in neurodegenerative pathways. *International Journal of Molecular Sciences*, 22(16) doi:10.3390/ijms22169098
- Dhakshinamoorthy, S., & Jaiswal, A. K. (2001). Functional characterization and role of INrf2 in antioxidant response element-mediated expression and antioxidant induction of NAD(P)H:Quinone oxidoreductase1 gene. *Oncogene*, 20(29), 3906-3917. doi:10.1038/sj.onc.1204506
- Dhalla, N. S., Temsah, R. M., & Netticadan, T. (2000). Role of oxidative stress in cardiovascular diseases. *Journal of Hypertension*, 18(6), 655-673. doi:10.1097/00004872-200018060-00002
- Dlugosz, P. J., Billen, L. P., Annis, M. G., Zhu, W., Zhang, Z., Lin, J., . . . Andrews, D. W. (2006). Bcl-2 changes conformation to inhibit bax oligomerization. *The EMBO Journal*, 25(11), 2287-2296. doi:10.1038/sj.emboj.7601126
- Du, Y., Wu, J., & Luo, L. (2018). Secreted heat shock protein 90 α attenuated the effect of anticancer drugs in small-cell lung cancer cells through AKT/GSK3 β / β -catenin

- signaling. *Cancer Control: Journal of the Moffitt Cancer Center*, 25(1), 1073274818804489. doi:10.1177/1073274818804489
- Ebert, B., Kisiela, M., Malátková, P., El-Hawari, Y., & Maser, E. (2010). Regulation of human carbonyl reductase 3 (CBR3; SDR21C2) expression by Nrf2 in cultured cancer cells. *Biochemistry*, 49(39), 8499-8511. doi:10.1021/bi100814d
- Erickson, A. M., Nevarea, Z., Gipp, J. J., & Mulcahy, R. T. (2002). Identification of a variant antioxidant response element in the promoter of the human glutamate-cysteine ligase modifier subunit gene. revision of the ARE consensus sequence. *The Journal of Biological Chemistry*, 277(34), 30730-30737. Retrieved from <https://www.ncbi.nlm.nih.gov/pubmed/12070177>
- Faris, M., Kokot, N., Latinis, K., Kasibhatla, S., Green, D. R., Koretzky, G. A., & Nel, A. (1998). The c-jun N-terminal kinase cascade plays a role in stress-induced apoptosis in jurkat cells by up-regulating fas ligand expression. *Journal of Immunology (Baltimore, Md.: 1950)*, 160(1), 134-144. Retrieved from <https://pubmed.ncbi.nlm.nih.gov/9551965/>
- Faris, M., Latinis, K. M., Kempniak, S. J., Koretzky, G. A., & Nel, A. (1998). Stress-induced fas ligand expression in T cells is mediated through a MEK kinase 1-regulated response element in the fas ligand promoter. *Molecular and Cellular Biology*, 18(9), 5414-5424. doi:10.1128/MCB.18.9.5414
- Foudah, A. I., Alqarni, M. H., Alam, A., Ayman Salkini, M., Ibnouf Ahmed, E. O., & Yusufoglu, H. S. (2021). Evaluation of the composition and in vitro antimicrobial, antioxidant, and anti-inflammatory activities of cilantro (*coriandrum sativum* L. leaves)

- cultivated in saudi arabia (al-kharj). *Saudi Journal of Biological Sciences*, 28(6), 3461-3468. Retrieved from <https://www.ncbi.nlm.nih.gov/pmc/articles/PMC8176008/>
- Fuchs, S. Y., Adler, V., Pincus, M. R., & Ronai, Z. (1998). MEKK1/JNK signaling stabilizes and activates p53. *Proceedings of the National Academy of Sciences of the United States of America*, 95(18), 10541-10546. Retrieved from <https://www.jstor.org/stable/45926>
- Furue, M., Takahara, M., Nakahara, T., & Uchi, H. (2014). Role of AhR/ARNT system in skin homeostasis. *Archives of Dermatological Research*, 306(9), 769-779. doi:10.1007/s00403-014-1481-7
- Gameiro, I., Michalska, P., Tenti, G., Cores, Á, Buendia, I., Rojo, A. I., . . . León, R. (2017). Discovery of the first dual GSK3 β inhibitor/Nrf2 inducer. A new multitarget therapeutic strategy for alzheimer's disease. *Scientific Reports*, 7(1), 45701. doi:10.1038/srep45701
- Gamet-Payraastre, L., Li, P., Lumeau, S., Cassar, G., Dupont, M. A., Chevolleau, S., . . . Tercé, F. (2000). Sulforaphane, a naturally occurring isothiocyanate, induces cell cycle arrest and apoptosis in HT29 human colon cancer cells. *Cancer Research*, 60(5), 1426-1433. Retrieved from <https://pubmed.ncbi.nlm.nih.gov/10728709/>
- Garrido, C., Bruey, J. M., Fromentin, A., Hammann, A., Arrigo, A. P., & Solary, E. (1999). HSP27 inhibits cytochrome c-dependent activation of procaspase-9. *FASEB Journal: Official Publication of the Federation of American Societies for Experimental Biology*, 13(14), 2061-2070. doi:10.1096/fasebj.13.14.2061
- Garrido, C., Brunet, M., Didelot, C., Zermati, Y., Schmitt, E., & Kroemer, G. (2006). Heat shock proteins 27 and 70: Anti-apoptotic proteins with tumorigenic properties. *Cell Cycle (Georgetown, Tex.)*, 5(22), 2592-2601. doi:10.4161/cc.5.22.3448

- Giulio, R. T. D., & Clark, B. W. (2015). The elizabeth river story: A case study in evolutionary toxicology. *Journal of Toxicology and Environmental Health, Part B*, 18(6), 259-298. doi:10.1080/15320383.2015.1074841
- Griendling, K. K., Camargo, L. L., Rios, F., Alves-Lopes, R., Montezano, A. C., & Touyz, R. M. (2021). Oxidative stress and hypertension. *Circulation Research*, 128(7), 993-1020. doi:10.1161/CIRCRESAHA.121.318063
- Grimes, C. A., & Jope, R. S. (2001). The multifaceted roles of glycogen synthase kinase 3beta in cellular signaling. *Progress in Neurobiology*, 65(4), 391-426. doi:10.1016/s0301-0082(01)00011-9
- Guieu, B., Jourdan, J., Dreneau, A., Willand, N., Rochais, C., & Dallemagne, P. (2021). Desirable drug-drug interactions or when a matter of concern becomes a renewed therapeutic strategy. *Drug Discovery Today*, 26(2), 315-328. doi:10.1016/j.drudis.2020.11.026
- Gureev, A. P., Popov, V. N., & Starkov, A. A. (2020). Crosstalk between the mTOR and Nrf2/ARE signaling pathways as a target in the improvement of long-term potentiation. *Experimental Neurology*, 328, 113285. doi:10.1016/j.expneurol.2020.113285
- Gwon, Y., Oh, J., & Kim, J. Sulforaphane induces colorectal cancer cell proliferation through Nrf2 activation in a p53-dependent manner. Retrieved from <https://appliedbiolchem.springeropen.com/articles/10.1186/s13765-020-00578-y>
- Hardesty, B., & Kramer, G. (2001). Folding of a nascent peptide on the ribosome. *Progress in Nucleic Acid Research and Molecular Biology*, 66, 41-66. Retrieved from <https://www.ncbi.nlm.nih.gov/pubmed/11051761>

- Hardwick, J. M., & Soane, L. (2013). Multiple functions of BCL-2 family proteins. *Cold Spring Harbor Perspectives in Biology*, 5(2), a008722. doi:10.1101/cshperspect.a008722
- Hayes, J. D., & Dinkova-Kostova, A. T. (2014). The Nrf2 regulatory network provides an interface between redox and intermediary metabolism. *Trends in Biochemical Sciences*, 39(4), 199-218. doi:10.1016/j.tibs.2014.02.002
- Hayes, J. D., Dinkova-Kostova, A. T., & McMahon, M. (2009). Cross-talk between transcription factors AhR and Nrf2: Lessons for cancer chemoprevention from dioxin. *Toxicological Sciences*, 111(2), 199-201. doi:10.1093/toxsci/kfp168
- Heron, M. (2021). Deaths: Leading causes for 2019. *National Vital Statistics Reports*, 70(9)
Retrieved from <https://www.cdc.gov/nchs/data/nvsr/nvsr70/nvsr70-09-508.pdf>
- Hseu, Y., Korivi, M., Lin, F., Li, M., Lin, R., Wu, J., & Yang, H. (2018). Trans-cinnamic acid attenuates UVA-induced photoaging through inhibition of AP-1 activation and induction of Nrf2-mediated antioxidant genes in human skin fibroblasts. *Journal of Dermatological Science*, 90(2), 123-134. doi:10.1016/j.jdermsci.2018.01.004
- Huang, X., Chen, H., Yu, H., Yan, Y., Liao, Z., & Huang, Q. (2014). Nrf2-dependent upregulation of antioxidative enzymes: A novel pathway for hypoxic preconditioning-mediated delayed cardioprotection. *Molecular and Cellular Biochemistry*, 385(1-2), 33-41. doi:10.1007/s11010-013-1812-6
- Hybertson, B. M., Gao, B., Bose, S. K., & McCord, J. M. (2011). Oxidative stress in health and disease: The therapeutic potential of Nrf2 activation. *Molecular Aspects of Medicine*, 32(4-6), 234-246. doi:10.1016/j.mam.2011.10.006

- Itkin, B., Breen, A., Turyanska, L., Sandes, E., Bradshaw, T., & Loaiza-Perez, A. (2020). New treatments in renal cancer: The AhR ligands. *International Journal of Molecular Science*, 21(10) Retrieved from <https://www.mdpi.com/1422-0067/21/10/3551>
- Jacobs, K. M., Bhave, S. R., Ferraro, D. J., Jaboin, J. J., Hallahan, D. E., & Thotala, D. (2012). GSK-3 β : A bifunctional role in cell death pathways. *International Journal of Cell Biology*, 2012, e930710. doi:10.1155/2012/930710
- Jain, A. K., & Jaiswal, A. K. (2007a). GSK-3 β acts upstream of fyn kinase in regulation of nuclear export and degradation of NF-E2 related factor 2*. *Journal of Biological Chemistry*, 282(22), 16502-16510. doi:10.1074/jbc.M611336200
- Jain, A. K., & Jaiswal, A. K. (2007b). GSK-3 β acts upstream of fyn kinase in regulation of nuclear export and degradation of NF-E2 related factor 2*. *Journal of Biological Chemistry*, 282(22), 16502-16510. doi:10.1074/jbc.M611336200
- Jaramillo, M. C., & Zhang, D. D. (2013). The emerging role of the Nrf2–Keap1 signaling pathway in cancer . *Genes & Development*, , 2179-2191. Retrieved from <http://genesdev.cshlp.org/content/27/20/2179.short>
- Jessen, C., Kreß, J. K. C., Baluapuri, A., Hufnagel, A., Schmitz, W., Kneitz, S., . . . Meierjohann, S. (2020). The transcription factor NRF2 enhances melanoma malignancy by blocking differentiation and inducing COX2 expression. *Oncogene*, 39(44), 6841-6855. doi:10.1038/s41388-020-01477-8
- Jones, D. R., Moussaud, S., & McLean, P. (2014). Targeting heat shock proteins to modulate α -synuclein toxicity. *Therapeutic Advances in Neurological Disorders*, 7(1), 33-51. doi:10.1177/1756285613493469

- Joo, H., Choi, J., Moon, H., Lee, C. Y., Yoo, K., Kim, S. W., & Hwang, K. (2018). Protective effects of kenpaullone on cardiomyocytes following H₂O₂-induced oxidative stress are attributed to inhibition of connexin 43 degradation by SGSM3. *Biochemical and Biophysical Research Communications*, 499(2), 368-373. doi:10.1016/j.bbrc.2018.03.166
- Juge, N., Mithen, R. F., & Traka, M. (2007). Molecular basis for chemoprevention by sulforaphane: A comprehensive review. *Cellular and Molecular Life Sciences* : *CMLS*, 64(9), 1105-1127. doi:10.1007/s00018-007-6484-5
- Kalimuthu, S., & Se-Kwon, K. (2013). Cell survival and apoptosis signaling as therapeutic target for cancer: Marine bioactive compounds. *International Journal of Molecular Sciences*, 14(2), 2334-2354. doi:10.3390/ijms14022334
- Kalkavan, H., & Green, D. R. (2018). MOMP, cell suicide as a BCL-2 family business. *Cell Death and Differentiation*, 25(1), 46-55. doi:10.1038/cdd.2017.179
- Kalthoff, S., Ehmer, U., Freiberg, N., Manns, M. P., & Strassburg, C. P. (2010). Interaction between oxidative stress sensor Nrf2 and xenobiotic-activated aryl hydrocarbon receptor in the regulation of the human phase II detoxifying UDP-glucuronosyltransferase 1A10. *The Journal of Biological Chemistry*, 285(9), 5993-6002. doi:10.1074/jbc.M109.075770
- Kanninen, K., White, A. R., Koistinaho, J., & Malm, T. (2011). Targeting glycogen synthase kinase-3 β for therapeutic benefit against oxidative stress in alzheimer's disease: Involvement of the Nrf2-ARE pathway. *International Journal of Alzheimer 's Disease*, 2011, 985085-9. doi:10.4061/2011/985085

- Kapuy, O., Papp, D., Vellai, T., Bánhegyi, G., & Korcsmáros, T. (2018). Systems-level feedbacks of NRF2 controlling autophagy upon oxidative stress response. *Antioxidants*, 7(3), 39. doi:10.3390/antiox7030039
- Kennedy, D., Jäger, R., Mosser, D. D., & Samali, A. (2014). Regulation of apoptosis by heat shock proteins. *IUBMB Life*, 66(5), 327-338. doi:10.1002/iub.1274
- Kensler, T. W., Wakabayashi, N., & Biswal, S. (2007). Cell survival responses to environmental stresses via the Keap1-Nrf2-ARE pathway. *Annual Review of Pharmacology and Toxicology*, 47, 89-116. doi:10.1146/annurev.pharmtox.46.120604.141046
- Kitabayashi, T., Dong, Y., Furuta, T., Sabit, H., Jiapaer, S., Zhang, J., . . . Nakada, M. (2019). Identification of GSK3 β inhibitor kenpaullone as a temozolomide enhancer against glioblastoma. *Scientific Reports*, 9(1), 1-12. doi:10.1038/s41598-019-46454-8
- Kochhar, A., Kopelovich, L., Sue, E., Guttenplan, J. B., Herbert, B., Dannenberg, A. J., & Subbaramaiah, K. (2014). p53 modulates Hsp90 ATPase activity and regulates aryl hydrocarbon receptor signaling. *Cancer Prevention Research (Philadelphia, Pa.)*, 7(6), 596-606. doi:10.1158/1940-6207.CAPR-14-0051
- Kumar Palai, T., & Ranjan Mishra, S. (2015). Caspases: An apoptosis mediator. *Journal of Advanced Veterinary and Animal Research*, 2(1) Retrieved from https://www.researchgate.net/publication/286670707_Caspases_An_Apoptosis_Mediator
- Kumar, S., Moniruzzaman, M., Chakraborty, A., Sarbajna, A., & Chakraborty, S. B. (2021). Crosstalk between heat shock proteins, NRF2, NF- κ B and different endogenous antioxidants

- during lead-induced hepatotoxicity in *puntius ticto*. *Aquatic Toxicology (Amsterdam, Netherlands)*, 233, 105771. doi:10.1016/j.aquatox.2021.105771
- Kwee, J. K. (2014). A paradoxical chemoresistance and tumor suppressive role of antioxidant in solid cancer cells: A strange case of dr. jekyll and mr. hyde. *BioMed Research International*, 2014, e209845. doi:10.1155/2014/209845
- Lanneau, D., Brunet, M., Frisan, E., Solary, E., Fontenay, M., & Garrido, C. (2008). Heat shock proteins: Essential proteins for apoptosis regulation. *Journal of Cellular and Molecular Medicine*, 12(3), 743-761. doi:10.1111/j.1582-4934.2008.00273.x
- Lazaro, I., Oguiza, A., Recio, C., Lopez-Sanz, L., Bernal, S., Egido, J., & Gomez-Guerrero, C. (2017). Interplay between HSP90 and Nrf2 pathways in diabetes-associated atherosclerosis. *Clinica E Investigacion En Arteriosclerosis: Publicacion Oficial De La Sociedad Espanola De Arteriosclerosis*, 29(2), 51-59. doi:10.1016/j.arteri.2016.10.003
- Lee, Y., Lee, D. M., & Lee, a. S. (2015). Nrf2 expression and apoptosis in quercetin-treated malignant mesothelioma cells. *Molecules and Cells*, 38(5), 416-425. doi:10.14348/molcells.2015.2268
- Leost, M., Schultz, C., Link, A., Wu, Y., Biernat, J., Mandelkow, E., . . . Meijer, L. (2000). Paullones are potent inhibitors of glycogen synthase kinase-3 β and cyclin-dependent kinase 5/p25. *European Journal of Biochemistry*, 267(19), 5983-5994. doi:10.1046/j.1432-1327.2000.01673.x
- Levine, A. J. (1997). *p53, the cellular gatekeeper for growth and division*. United States: Elsevier Inc. doi:10.1016/S0092-8674(00)81871-1

- Li, C., Liu, C., Tsai, C., Peng, Y., Yang, Y., Liao, P., . . . Kang, J. (2017). Cytoplasmic aryl hydrocarbon receptor regulates glycogen synthase kinase 3 beta, accelerates vimentin degradation, and suppresses epithelial-mesenchymal transition in non-small cell lung cancer cells. *Archives of Toxicology*, *91*(5), 2165-2178. doi:10.1007/s00204-016-1870-0
- Li, R., Jia, Z., & Zhu, H. (2019). Regulation of Nrf2 signaling. *Reactive Oxygen Species (Apex, N.C.)*, *8*(24), 312-322. Retrieved from <https://www.ncbi.nlm.nih.gov/pmc/articles/PMC6830569/>
- Liguori, I., Russo, G., Curcio, F., Bulli, G., Aran, L., Della-Morte, D., . . . Abete, P. (2018). Oxidative stress, aging, and diseases. *Clinical Interventions in Aging*, *13*, 757-772. doi:10.2147/CIA.S158513
- Lu, M., Wang, P., Qiao, Y., Jiang, C., Ge, Y., Flickinger, B., . . . Gong, R. (2019). GSK3 β -mediated Keap1-independent regulation of Nrf2 antioxidant response: A molecular rheostat of acute kidney injury to chronic kidney disease transition. *Redox Biology*, *26*, 101275. doi:10.1016/j.redox.2019.101275
- Lv, Y., Jiang, H., Li, S., Han, B., Liu, Y., Yang, D., . . . Zhang, Z. (2020). Sulforaphane prevents chromium-induced lung injury in rats via activation of the akt/GSK-3 β /fyn pathway. *Environmental Pollution*, *259*, 113812. doi:10.1016/j.envpol.2019.113812
- Lynn Kysh. (2018a). *Review articles* Nature Publishing Group. Retrieved from <http://norris.usc.libguides.com/reviewarticles>
- Lynn Kysh. (2018b). *Review articles* Nature Publishing Group. Retrieved from <http://norris.usc.libguides.com/reviewarticles>

- Ma, Q. (2013). Role of nrf2 in oxidative stress and toxicity. *Annual Review of Pharmacology and Toxicology*, 53, 401-426. doi:10.1146/annurev-pharmtox-011112-140320
- Maheo, K., Morel, F., Langouet, S., Kramer, H., Le Ferrec, E., Ketterer, B., & Guillouzo, A. (1997). Inhibition of cytochromes P-450 and induction of glutathione S-transferases by sulforaphane in primary human and rat hepatocytes. *Cancer Research*, 57(17), 3649-3652. Retrieved from <http://cancerres.aacrjournals.org/cgi/content/abstract/57/17/3649>
- Massaad, C. A., & Klann, E. (2011). Reactive oxygen species in the regulation of synaptic plasticity and memory. *Antioxidants & Redox Signaling*, 14(10), 2013-2054. doi:10.1089/ars.2010.3208
- Matsuoka, T., & Yashiro, M. (2014). The role of PI3K/akt/mTOR signaling in gastric carcinoma. *Cancers*, 6(3), 1441-1463. doi:10.3390/cancers6031441
- Menegon, S., Columbano, A., & Giordano, S. (2016). The dual roles of NRF2 in cancer. *Trends in Molecular Medicine*, 22(7), 578-593. doi:10.1016/j.molmed.2016.05.002
- Meriin, A., Yaglom, J., Gabai, V., Mosser, D., Zon, L., & Sherman, M. (1999). Protein-damaging stresses activate c-jun N-terminal kinase via inhibition of its dephosphorylation: A novel pathway controlled by HSP72. *Molecular and Cellular Biology*, 19(4) Retrieved from <https://europepmc.org/article/PMC/84047>
- Merlin, J. P. J., Rupasinghe, H. P. V., Dellaire, G., & Murphy, K. (2021). Role of dietary antioxidants in p53-mediated cancer chemoprevention and tumor suppression. *Oxidative Medicine and Cellular Longevity*, 2021, e9924328. doi:10.1155/2021/9924328

Mitogen-activated protein kinase (MAPK) modules containing three sequentially activated protein kinases are key components of a series of vital signal transduction pathways that regulate processes such as cell proliferation, cell differentiation, and cell death in eukaryotes from yeast to humans (Fig. 1) (Qi and Elion 2005; Raman 2007; . . . vates the MAPKK, which, in turn, activates the MAPK. (2012). *MAP kinase pathways* doi:10.1101/cshperspect.a011254

Morimoto, R. I. (1998). Regulation of the heat shock transcriptional response: Cross talk between a family of heat shock factors, molecular chaperones, and negative regulators. *Genes & Development*, 12(24), 3788-3796. doi:10.1101/gad.12.24.3788

Mosser, D. D., Caron, A. W., Bourget, L., Meriin, A. B., Sherman, M. Y., Morimoto, R. I., & Massie, B. (2000). The chaperone function of hsp70 is required for protection against stress-induced apoptosis. *Molecular and Cellular Biology*, 20(19), 7146-7159. Retrieved from <https://www.ncbi.nlm.nih.gov/pmc/articles/PMC86268/>

Nanda, N. (2016). Oxidative stress in hypothyroidism. *International Journal of Clinical and Experimental Physiology*, 3, 4. doi:10.4103/2348-8093.180013

Nandini, D. B., Rao, R. S., Deepak, B. S., & Reddy, P. B. (2020). Sulforaphane in broccoli: The green chemoprevention!! role in cancer prevention and therapy. *Journal of Oral and Maxillofacial Pathology : JOMFP*, 24(2), 405. doi:10.4103/jomfp.JOMFP_126_19

Nannelli, A., Rossignolo, F., Tolando, R., Rossato, P., Longo, V., & Gervasi, P. G. (2009). Effect of β -naphthoflavone on AhR-regulated genes (CYP1A1, 1A2, 1B1, 2S1, Nrf2, and GST) and antioxidant enzymes in various brain regions of pig. *Toxicology (Amsterdam)*, 265(3), 69-79. doi:10.1016/j.tox.2009.09.010

- Nicholls, D. G., & Budd, S. L. (2000). Mitochondria and neuronal survival. *Physiological Reviews*, 80(1), 315-360. doi:10.1152/physrev.2000.80.1.315
- Oh, Y. S., & Jun, H. (2017). Effects of glucagon-like peptide-1 on oxidative stress and Nrf2 signaling. *International Journal of Molecular Sciences*, 19(1) doi:10.3390/ijms19010026
- Paladino, S., Conte, A., Caggiano, R., Pierantoni, G., & Faraonio, R. (2018). Nrf2 pathway in age-related neurological disorders: Insights into MicroRNAs. *Cellular Physiology and Biochemistry*, 47(5), 1951-1976. doi:10.1159/000491465
- Paul, S., Ghosh, S., Mandal, S., Sau, S., & Pal, M. (2018). NRF2 transcriptionally activates the heat shock factor 1 promoter under oxidative stress and affects survival and migration potential of MCF7 cells. *The Journal of Biological Chemistry*, 293(50), 19303-19316. doi:10.1074/jbc.RA118.003376
- Percário, S., da Silva Barbosa, A., Varela, E. L. P., Gomes, A. R. Q., Ferreira, M. E. S., de Nazaré Araújo Moreira, T., & Dolabela, M. F. (2020). Oxidative stress in parkinson's disease: Potential benefits of antioxidant supplementation. *Oxidative Medicine and Cellular Longevity*, 2020 doi:10.1155/2020/2360872
- Perez-Leal, O., Barrero, C. A., & Merali, S. (2017). Pharmacological stimulation of nuclear factor (erythroid-derived 2)-like 2 translation activates antioxidant responses. *The Journal of Biological Chemistry*, 292(34), 14108-14121. doi:10.1074/jbc.M116.770925
- Phiel, C. J., Wilson, C. A., Lee, V. M. -, & Klein, P. S. (2003). GSK-3 α regulates production of alzheimer's disease amyloid- β peptides. *Nature*, 423(6938), 435-439. doi:10.1038/nature01640

- Pizzino, G., Irrera, N., Cucinotta, M., Pallio, G., Mannino, F., Arcoraci, V., . . . Bitto, A. (2017). Oxidative stress: Harms and benefits for human health. *Oxidative Medicine and Cellular Longevity*, 2017 doi:10.1155/2017/8416763
- Pluquet, O., Qu, L., Baltzis, D., & Koromilas, A. E. (2005). Endoplasmic reticulum stress accelerates p53 degradation by the cooperative actions of Hdm2 and glycogen synthase kinase 3 β . *Molecular and Cellular Biology*, 25(21), 9392-9405. doi:10.1128/MCB.25.21.9392-9405.2005
- Pollet, M., Shaik, S., Mescher, M., Frauenstein, K., Tigges, J., Braun, S. A., . . . Haarmann-Stemmann, T. (2018). The AHR represses nucleotide excision repair and apoptosis and contributes to UV-induced skin carcinogenesis. *Cell Death and Differentiation*, 25(10), 1823-1836. doi:10.1038/s41418-018-0160-1
- Pru, J. K., Kaneko-Tarui, T., Jurisicova, A., Kashiwagi, A., Selesniemi, K., & Tilly, J. L. (2009). Induction of proapoptotic gene expression and recruitment of p53 herald ovarian follicle loss caused by polycyclic aromatic hydrocarbons. *Reproductive Sciences (Thousand Oaks, Calif.)*, 16(4), 347-356. doi:10.1177/1933719108327596
- Rai, N. K., Tripathi, K., Sharma, D., & Shukla, V. K. (2005). Apoptosis: A basic physiologic process in wound healing. *The International Journal of Lower Extremity Wounds*, 4(3), 138-144. doi:10.1177/1534734605280018
- Rampal, G., Khanna, N., Thind, T. S., Arora, S., & Pal Vig, A. (2012). Role of isothiocyanates as anticancer agents and their contributing molecular and cellular mechanisms. *Medicinal Chemistry & Drug Discovery*, , 79-93. Retrieved

from <https://www.researchgate.net/publication/266508172> Role of isothiocyanates as anticancer agents and their contributing molecular and cellular mechanisms

Rinaldi Tosi, M. E., Bocanegra, V., Manucha, W., Gil Lorenzo, A., & Vallés, P. G. (2011). The Nrf2-Keap1 cellular defense pathway and heat shock protein 70 (Hsp70) response. role in protection against oxidative stress in early neonatal unilateral ureteral obstruction (UUO). *Cell Stress & Chaperones*, 16(1), 57-68. doi:10.1007/s12192-010-0221-y

Romorini, L., Garate, X., Neiman, G., Luzzani, C., Furmento, V. A., Guberman, A. S., . . . Miriuka, S. G. (2016). AKT/GSK3 β signaling pathway is critically involved in human pluripotent stem cell survival. *Scientific Reports*, 6(1), 35660. doi:10.1038/srep35660

Roos, D. (2019). Chronic granulomatous disease. *Methods in Molecular Biology (Clifton, N.J.)*, 1982, 531-542. doi:10.1007/978-1-4939-9424-3_32

Rotblat, B., Melino, G., & Knight, R. A. (2012). NRF2 and p53: Januses in cancer? *Oncotarget*, 3(11), 1272-1283. doi:10.18632/oncotarget.754

Rudolf, E., & Cervinka, M. (2011). Sulforaphane induces cytotoxicity and lysosome- and mitochondria-dependent cell death in colon cancer cells with deleted p53. *Toxicology in Vitro: An International Journal Published in Association with BIBRA*, 25(7), 1302-1309. doi:10.1016/j.tiv.2011.04.019

Satoh, T., Stalder, R., McKercher, S. R., Williamson, R. E., Roth, G. P., & Lipton, S. A. (2015). Nrf2 and HSF-1 pathway activation via hydroquinone-based proelectrophilic small molecules is regulated by electrochemical oxidation potential. *Asn Neuro*, 7(4) doi:10.1177/1759091415593294

Selvaraj, S., & Perlingeiro, R. C. R. (2019). Induced pluripotent stem cells for neuromuscular diseases: Potential for disease modeling, drug screening, and regenerative medicine. In R. L. Reis (Ed.), *Encyclopedia of tissue engineering and regenerative medicine* (pp. 471-481). Oxford: Academic Press. Retrieved from <https://www.sciencedirect.com/science/article/pii/B9780128012383655046>

Shang, G., Tang, X., Gao, P., Guo, F., Liu, H., Zhao, Z., . . . Li, H. (2015). Sulforaphane attenuation of experimental diabetic nephropathy involves GSK-3 beta/fyn/Nrf2 signaling pathway. *The Journal of Nutritional Biochemistry*, 26(6), 596-606.
doi:10.1016/j.jnutbio.2014.12.008

Sherman, M. Y., & Goldberg, A. L. (2001). Cellular defenses against unfolded proteins: A cell biologist thinks about neurodegenerative diseases. *Neuron*, 29(1), 15-32.
doi:10.1016/S0896-6273(01)00177-5

Shi, Y., Mosser, D. D., & Morimoto, R. I. (1998). Molecular chaperones as HSF1-specific transcriptional repressors. *Genes & Development*, 12(5), 654-666. Retrieved from <https://www.ncbi.nlm.nih.gov/pmc/articles/PMC316571/>

Shields, H. J., Traa, A., & Van Raamsdonk, J. M. (2021a). Beneficial and detrimental effects of reactive oxygen species on lifespan: A comprehensive review of comparative and experimental studies. *Frontiers in Cell and Developmental Biology*, 9, 628157.
doi:10.3389/fcell.2021.628157

Shields, H. J., Traa, A., & Van Raamsdonk, J. M. (2021b). Beneficial and detrimental effects of reactive oxygen species on lifespan: A comprehensive review of comparative and

experimental studies. *Frontiers in Cell and Developmental Biology*, 0 doi:10.3389/fcell.2021.628157

Shin, S., Wakabayashi, N., Misra, V., Biswal, S., Hwa Lee, G., Agoston, E., . . . Kensler, T. (2007). NRF2 modulates aryl hydrocarbon receptor signaling: Influence on adipogenesis. Retrieved from <https://journals.asm.org/doi/abs/10.1128/MCB.00915-07>

Singh, A. V., Xiao, D., Lew, K. L., Dhir, R., & Singh, S. V. (2004). Sulforaphane induces caspase-mediated apoptosis in cultured PC-3 human prostate cancer cells and retards growth of PC-3 xenografts in vivo. *Carcinogenesis*, 25(1), 83-90. doi:10.1093/carcin/bgg178

Sporn, M. B., & Liby, K. T. (2012). NRF2 and cancer: The good, the bad and the importance of context. *Nature Reviews. Cancer*, 12(8), 564-571. doi:10.1038/nrc3278

Srivastava, R. K., Mi, Q. S., Hardwick, J. M., & Longo, D. L. (1999). Deletion of the loop region of bcl-2 completely blocks paclitaxel-induced apoptosis. *Proceedings of the National Academy of Sciences of the United States of America*, 96(7), 3775-3780. doi:10.1073/pnas.96.7.3775

Sulforaphane attenuation of experimental diabetic nephropathy involves GSK-3 beta/fyn/Nrf2 signaling pathway | elsevier enhanced reader. Retrieved from <https://reader.elsevier.com/reader/sd/pii/S0955286315000248?token=81913750102CC7ECA257DFF26FBEE6173C2313A6C12A9A23E05014462CB11A50CD43B6083054E2D8E74A0C62EBF56A29&originRegion=us-east-1&originCreation=20210726203223>

Tastan, B., Arioiz, B. I., & Genc, S. (2017). Targeting NLRP3 inflammasome with Nrf2 inducers in central nervous system disorders. *Frontiers in Immunology*, 13(14), 1011-2. doi:10.3389/fimmu.2022.865772

- Tayyem, R. F., Heath, D. D., Al-Delaimy, W. K., & Rock, C. L. (2006). Curcumin content of turmeric and curry powders. *Nutrition and Cancer*, 55(2), 126-131.
doi:10.1207/s15327914nc5502_2
- Tischkau, S. A. (2020). Mechanisms of circadian clock interactions with aryl hydrocarbon receptor signalling. *European Journal of Neuroscience*, 51(1), 379-395.
doi:10.1111/ejn.14361
- Tonelli, C., Chio, I. I. C., & Tuveson, D. A. (2018). Transcriptional regulation by Nrf2. *Antioxidants & Redox Signaling*, 29(17), 1727-1745. doi:10.1089/ars.2017.7342
- Tsujii, M., & DuBois, R. N. (1995). Alterations in cellular adhesion and apoptosis in epithelial cells overexpressing prostaglandin endoperoxide synthase 2. *Cell*, 83(3), 493-501.
doi:10.1016/0092-8674(95)90127-2
- Tsujimoto, Y. (1998). Role of bcl-2 family proteins in apoptosis: Apoptosomes or mitochondria? *Genes to Cells*, 3(11), 697-707. doi:10.1046/j.1365-2443.1998.00223.x
- Uchi, Hiroshi, MD, PhD, Yasumatsu, M., Morino-Koga, S., PhD, Mitoma, Chikage, MD, PhD, & Furue, Masutaka, MD, PhD. (2016). Inhibition of aryl hydrocarbon receptor signaling and induction of NRF2-mediated antioxidant activity by cinnamaldehyde in human keratinocytes. *Journal of Dermatological Science*, 85(1), 36-43.
doi:10.1016/j.jdermsci.2016.10.003
- Varman, D. R., Jayanthi, L. D., & Ramamoorthy, S. (2021). Glycogen synthase kinase-3 β supports serotonin transporter function and trafficking in a phosphorylation-dependent manner. *Journal of Neurochemistry*, 156(4), 445-464. doi:10.1111/jnc.15152

- Watcharasit, P., Bijur, G., Zmijewski, J., Song, L., Zmijewska, A., Chen, X., . . . Jope, R. (2002). Direct, activating interaction between glycogen synthase kinase-3 β and p53 after DNA damage. *Proceedings of the National Academy of Sciences of the United States of America*, 99(12), 7951-7955. Retrieved from <https://www.pnas.org/content/99/12/7951>
- Westerheide, S. D., & Morimoto, R. I. (2005). Heat shock response modulators as therapeutic tools for diseases of protein conformation. *The Journal of Biological Chemistry*, 280(39), 33097-33100. doi:10.1074/jbc.R500010200
- Xu, Y., Liu, H., & Song, L. (2020). Novel drug delivery systems targeting oxidative stress in chronic obstructive pulmonary disease: A review. *Journal of Nanobiotechnology*, 18 doi:10.1186/s12951-020-00703-5
- Yang, H., Xiang, S., Kazi, A., & Sebti, S. M. (2020). The GTPase KRAS suppresses the p53 tumor suppressor by activating the NRF2-regulated antioxidant defense system in cancer cells. *The Journal of Biological Chemistry*, 295(10), 3055-3063. doi:10.1074/jbc.RA119.011930
- Yang, Y., & Chan, W. K. (2021). Glycogen synthase kinase 3 beta regulates the human aryl hydrocarbon receptor cellular content and activity. *International Journal of Molecular Sciences*, 22(11) doi:10.3390/ijms22116097
- Yao, E. F., & Denison, M. S. (1992). DNA sequence determinants for binding of transformed ah receptor to a dioxin-responsive enhancer. *Biochemistry (Easton)*, 31(21), 5060-5067. doi:10.1021/bi00136a019
- Ye, R., Dai, N., He, Q., Guo, P., Xiang, Y., Zhang, Q., . . . Zhang, Q. (2018). Comprehensive anti-tumor effect of brusatol through inhibition of cell viability and promotion of apoptosis

caused by autophagy via the PI3K/akt/mTOR pathway in hepatocellular carcinoma. *Biomedicine & Pharmacotherapy*, 105, 962-973.

doi:10.1016/j.biopha.2018.06.065

Yin, T., Wang, M., Qing, Y., Lin, Y., & Wu, D. (2016). Research progress on chemopreventive effects of phytochemicals on colorectal cancer and their mechanisms. *World Journal of Gastroenterology*, 22(31), 7058-7068. doi:10.3748/wjg.v22.i31.7058

Yu, J., & Zhang, L. (2008). PUMA, a potent killer with or without p53. *Oncogene*, 27(S1), S71-S83. doi:10.1038/onc.2009.45

Yu, X., Shang, X., Huang, X., Yao, G., & Song, S. (2020). Brusatol: A potential anti-tumor quassinoid from *Brucea javanica*. *Chinese Herbal Medicines*, 12(4), 359-366.

doi:10.1016/j.chmed.2020.05.007

Zenkov, N. K., Kozhin, P. M., Chechushkov, A. V., Martinovich, G. G., Kandalintseva, N. V., & Menshchikova, E. B. (2017). Mazes of Nrf2 regulation. *Biochemistry. Biokhimiia*, 82(5), 556-564. doi:10.1134/S0006297917050030

Zhang, C., Su, Z., Khor, T. O., Shu, L., & Kong, A. T. (2013). Sulforaphane enhances Nrf2 expression in prostate cancer TRAMP C1 cells through epigenetic regulation. *Biochemical Pharmacology*, 85(9), 1398-1404. doi:10.1016/j.bcp.2013.02.010

Zhang, N. (2011). The role of endogenous aryl hydrocarbon receptor signaling in cardiovascular physiology. *Journal of Cardiovascular Disease Research*, 2(2), 91-95. doi:10.4103/0975-3583.83033

- Zhang, Y., Ahn, Y., Benjamin, I. J., Honda, T., Hicks, R. J., Calabrese, V., . . . Dinkova-Kostova, A. T. (2011). HSF1-dependent upregulation of Hsp70 by sulfhydryl-reactive inducers of the KEAP1/NRF2/ARE pathway. *Chemistry & Biology*, *18*(11), 1355-1361. doi:10.1016/j.chembiol.2011.09.008
- Zhong, M., Lynch, A., Jehle, S., Luo, L., Hall, D. R., Iwase, R., . . . Whitty, A. (2020). Interaction energetics and druggability of the protein-protein interaction between kelch-like ECH-associated protein 1 (KEAP1) and nuclear factor, erythroid 2 like 2 (Nrf2). *Biochemistry*, *59*(4), 563-581. doi:10.1021/acs.biochem.9b00943
- Zhou, C., Poulton, E., Grün, F., Bammler, T. K., Blumberg, B., Thummel, K. E., & Eaton, D. L. (2007). The dietary isothiocyanate sulforaphane is an antagonist of the human steroid and xenobiotic nuclear receptor. *Molecular Pharmacology*, *71*(1), 220-229. doi:10.1124/mol.106.029264
- Zhou, J., Wang, M., Sun, N., Qing, Y., Yin, T., Li, C., & Wu, D. (2019). Sulforaphane-induced epigenetic regulation of Nrf2 expression by DNA methyltransferase in human caco-2 cells. *Oncology Letters*, *18*(3), 2639-2647. doi:10.3892/ol.2019.10569
- Zhu, S., Liu, S., Wang, L., Ding, W., Sha, J., Qian, H., & Lu, Y. (2020). Brusatol protects HepG2 cells against oxygen-glucose deprivation-induced injury via inhibiting mitochondrial reactive oxygen species-induced oxidative stress. *Pharmacology*, *105*(7-8), 416-423. doi:10.1159/000504482
- Zilfou, J. T., Spector, M. S., & Lowe, S. W. (2005). Slugging it out: Fine tuning the p53-PUMA death connection. *Cell*, *123*(4), 545-548. doi:10.1016/j.cell.2005.11.003

